NIH Public Access
Author Manuscript
J Micromech Microeng. Author manuscript; available in PMC 2010 March 4.

Published in final edited form as:
J Micromech Microeng. 2009 July 8; 19(8): . doi:10.1088/0960-1317/19/8/083001.

Self-assembly from milli- to nanoscales: methods and applications

M Mastrangeli[1,2], **S Abbasi**[3], **C Varel**[3], **C Van Hoof**[2], **J-P Celis**[1], and **K F Böhringer**[3]

[1] IMEC, Kapeldreef 75, 3001 Leuven, Belgium

[2] MTM Department, Katholieke Universiteit Leuven, Kasteelpark Arenberg 44, 3001 Leuven, Belgium

[3] Electrical Engineering Department, University of Washington, Box 352500, Seattle, WA 98195, USA

Abstract

The design and fabrication techniques for microelectromechanical systems (MEMS) and nanodevices are progressing rapidly. However, due to material and process flow incompatibilities in the fabrication of sensors, actuators and electronic circuitry, a final packaging step is often necessary to integrate all components of a heterogeneous microsystem on a common substrate. Robotic pick-and-place, although accurate and reliable at larger scales, is a serial process that downscales unfavorably due to stiction problems, fragility and sheer number of components. Self-assembly, on the other hand, is parallel and can be used for device sizes ranging from millimeters to nanometers. In this review, the state-of-the-art in methods and applications for self-assembly is reviewed. Methods for assembling three-dimensional (3D) MEMS structures out of two-dimensional (2D) ones are described. The use of capillary forces for folding 2D plates into 3D structures, as well as assembling parts onto a common substrate or aggregating parts to each other into 2D or 3D structures, is discussed. Shape matching and guided assembly by magnetic forces and electric fields are also reviewed. Finally, colloidal self-assembly and DNA-based self-assembly, mainly used at the nanoscale, are surveyed, and aspects of theoretical modeling of stochastic assembly processes are discussed.

1. Introduction

The packaging and integration of micro- and nanoscale modules, such as sensors, actuators and transceivers, and data processing, microfluidic, power management, electromechanical and optoelectronic devices, into heterogeneous multifunctional systems is one of the big challenges in the field of microelectromechanical systems (MEMS) and nanotechnology. Indeed, the fabrication processes and the material prerequisites for the components are usually incompatible; hence, it is not possible to fabricate them all on a common substrate, as it would be done in a monolithic approach. Consequently, in a heterogeneous approach the components of a system are fabricated separately under optimal conditions before being assembled to construct a functioning system.

The common method used for assembly and packaging in microelectronic manufacturing is robotic pick-and-place. This technique has proven accurate and reliable for large component scales, and its throughput is satisfying for consumer electronic applications [1]. However, pick-

© 2009 IOP Publishing Ltd Printed in the UK
karlb@u.washington.edu and mastran@imec.be

NIH-PA Author Manuscript NIH-PA Author Manuscript NIH-PA Author Manuscript

NIH-PA Author Manuscript NIH-PA Author Manuscript NIH-PA Author Manuscript

and-place is confronted with a trade-off between throughput and component placement accuracy. Moreover, this method is serial, it requires closed-loop control and it becomes more expensive as device dimensions shrink to smaller scales and registration constraints become more stringent. Also, stiction problems [2,3] become inevitable for device sizes smaller than 300 μm[1].

Self-assembly (SA), defined as the autonomous organization of components into ordered patterns or structures without human intervention [4], provides a promising packaging alternative. SA is parallel in nature and can be applied to a wide size range, from millimeter to nanometer scales. It may avoid direct contact manipulation of components, thus overcoming the stiction issue. Initial SA attempts were applicable for only one part type [5-7], which was a disadvantage of SA in comparison to pick-and-place robots. However, recent advances in programmable SA have made the construction of heterogeneous microelectronic systems feasible [8-11]. SA can achieve yield and throughput comparable to those of pick-and-place techniques. Moreover, it can be used to build small, complex standalone structures.

This article presents an overview over the state-of-the-art in methods and techniques adopted for SA purposes. The realization of complex, three-dimensional (3D) microelectromechanical structures through the lifting and out-of-plane rotation of movable two-dimensional (2D) plates is covered in section 2. Several actuation mechanisms have been introduced to allow the fully functional exploitation of the third spatial dimension for devices fabricated by essentially planar processes. In section 3, SA with the aid of capillary forces is reviewed. As we transition to smaller and smaller scales, the surface tension force, increasingly dominating over inertial forces, can be employed in various SA schemes. Section 4 covers shape matching for SA. In this approach, parts and receptor sites are designed and fabricated with geometrically complementary shapes in order to enhance the selective capture and localization of the parts in the correct position within the assembled system. This method can be used to assemble different types of parts within one single assembly step. SA using magnetic forces is reviewed in section 5. Magnetic forces are non-contact forces, and they can be controlled to be both attractive and repulsive, which makes them a good candidate for integration applications. Section 6 surveys usage of electric fields in carrying out assembly. Electrostatic and electrodynamic fields can be used to cause motion in fluids of charged and non-charged particles, and thus to guide them to the desired assembly locations. Methods of assembly for colloidal particles, with sizes ranging from 1 μm to 10 nm, into two- and three-dimensional structures for a wide range of technological applications, are discussed and investigated in section 7. DNA hybridization is also widely used in SA applications. In section 8, DNA is studied both as a structural material and in DNA-mediated SA. Considerations about the theoretical modeling of the dynamics of passive stochastic self-assembling systems are exposed in section 9. Finally, further discussion and perspectives are provided in section 10.

1.1. Metrics for self-assembly

SA techniques can be used for two main purposes. The first is to accomplish manufacturing tasks—such as the heterogeneous integration of devices—that are nowadays commonly performed by standard techniques, such as robotic pick-and-place, in alternative and more advantageous ways. The second purpose is to accomplish tasks that cannot be achieved otherwise.

In the first setting, the industrial success of SA could be affirmed upon an in-the-field comparison with the performance of established techniques. Consequently, besides the advantages carried by the intrinsic features of SA mentioned at the beginning of this section, convenient metrics to evaluate SA methods in this perspective can be mechanical yield (i.e. concerning only the physical binding), electrical yield, throughput, duration of the assembly process, registration and/or alignment accuracy, additional processing load, material and

NIH-PA Author Manuscript

NIH-PA Author Manuscript

NIH-PA Author Manuscript

processing compatibility with established fabrication processes. Depending on specific applications, some types of metrics will be more or less important and pertinent than others.

The second setting mainly refers to the construction of 3D structures—e.g. 3D MEMS, multi-bodies objects, folding and wrapping of planar structures—and to the assembly performed at scales or in environments which are not easily reachable by standard tools. Nanoscale assembly and computation are the prototypical examples. Almost all work in this framework is exploratory, often constituting the only way to achieve a desired goal or even proving a goal achievable in the first place. Therefore, in the absence of an established standard of reference, these works are probably going to set the standard themselves, and consequent adequate metrics.

In both cases, most of the techniques that will be reviewed in the following sections—with the remarkable exception of the fluidic self-assembly process commercialized by Alien Technology Inc. (see section 4)—are presently at a stage of on-going development, if not at a proof-of-concept level. Therefore, the performance of the methods we will exemplify is most probably not yet definitive, and susceptible to further improvement and optimization. In the case of proof of concepts, statistics are also normally absent due to insufficient data sets available.

Table 1 provides a synoptic overview and discussion of the general methodologies hereby reviewed.

1.2. Material issues

Some techniques of system integration by SA make use of materials which are not yet standard for the electronic manufacturing industry.

The most evident example in the literature is the utilization of self-assembled monolayers (SAMs) [12] to condition the wetting properties of surfaces e.g. in capillary SA applications. Their use for this purpose was first introduced by the Whitesides Group at Harvard University. Thiol-ended SAMs [13] are particularly useful, as they selectively adsorb onto several metal surfaces (notably onto gold and copper) and make them hydrophilic or hydrophobic according to their functional end group. This in turn allows the selective deposition of fluid drops on them (see section 3.2). SAMs can be deposited both from the vapor and liquid phase, the second method being the most common in the literature. While full monolayer assembly and crystallization may take hours, such a level of structural integrity is not mandatory for the applications considered here; hence, the preparation time can be much shorter. Interestingly, SAMs are an elegant way to exploit nanoscale supramolecular SA to enable SA at larger scales (from micro- to millimeter).

In the magnetic SA domain, magnetic actuation of MEMS structures and magnetic part-to-substrate assembly requires soft and/or hard magnetic materials (e.g. NdFeB, CoNiP and SmCo alloys). These materials can be deposited as films by sputtering, or manually as powders. While intense research is dedicated to the enhancement of such materials, the compatibility of magnetic effects with device functionalities and fabrication needs to be fully ascertained.

SA driven by (di)electrophoretic forces requires the fabrication of local field sources on the target substrates (see sections 6.1 and 6.2). These sources may coincide with the same electrodes that will later be used to drive the assembled devices (as in the case of e.g. LEDs, transistors, nanotubes and nanowires); otherwise, a fraction of the substrate will be needed to host similar structures that will normally be active only during the assembly process.

NIH-PA Author Manuscript

NIH-PA Author Manuscript

NIH-PA Author Manuscript

The assembly environment is an important parameter to consider. As opposed to early attempts, many SA methods investigated nowadays at micro-to-milli scales, and all of those at nanoscale, operate in a liquid environment (most commonly water-based solutions and ethylene glycol). This is done to avoid the deleterious effects of friction and stiction, and to provide efficient mass transport and mixing to the parts of the system. SA in liquid has achieved many remarkable results. However, it may pose tight constraints on the kind of materials and devices that can be assembled. For example, MEMS structures can be very sensitive to liquids, while device passivating materials like oxides are water-retaining (i.e. hygroscopic). Also, perfect device sealing may be mandatory to limit the effects of humidity and moisture on the performance and reliability of electrical devices. In view of this, dry (i.e. in air) approaches to SA have re-emerged recently. They achieve part-to-template SA by performing stochastic part feeding on geometrically organized and physically preconditioned templates. Mobility is provided to the parts by the externally induced vibration of the template. These methods can also be easily extended to large substrate sizes.

2. Self-assembly of microelectromechanical structures

The complex microelectromechanical structures fabricated by surface micromachining are only partially 3D, since they are built by stacking 2D thin films. The full development or exploitation of three dimensionality can be achieved by folding and rotating movable parts out of the wafer plane and locking them into predesigned positions. Folding manipulations can be accomplished through a micro-manipulator under a microscope, but this approach is normally serial, time consuming, expensive and may damage the structures. Therefore, several alternative batch actuation mechanisms were devised for the purpose. Compared to most of the examples reviewed in the following sections, the folding of 3D structures is a form of *deterministic* assembly, as the trajectory described by the parts composing the system is completely specified before the actual assembly takes place.

Pister noted that, after release, mechanical structures not stuck to the substrate were quite susceptible to the hydraulic forces induced during rinsing [14]. He exploited these forces to assemble hinged polysilicon structures into 3D configurations. He designed springs which could lock the structures in place, vertically or at an angle, once they rotated beyond a critical angle with respect to the substrate. The assembly yield was low because of the randomness of the process. Stiction during drying after wet release of sacrificial structures was also exploited by Isamoto *et al* to induce an out-of-plane offset positioning of a vertical comb drive actuator, significantly simplifying its fabrication [15]. Agache *et al* investigated stiction-controlled locking systems for 3D microstructures such as scratch drive actuators [16]. Rose *et al* reported on the application of stiction and capillary forces to the precise lateral displacement, alignment, suspension and locking of microcantilevers for atomic force microscopy applications [17].

Folding of structures with small radii of bending by thermal SA was investigated by Ebefors *et al* [18]. They deposited polyimide inside V-grooves etched at the edge of released plates. Thermal shrinking of the polyimide due to curing induced the deployment of the structures out of plane. By controlling the curing temperature, a wide range of bending angles could be chosen without the need of locking structures, and process variations could be compensated. The technique also did not affect aluminum conductors crossing the grooves.

Kaajakari and Lal used triboelectricity to assemble arrays of flaps, retroreflectors and plates with retaining springs [19]. They used a piezoelectric actuator to ultrasonically vibrate hinged polysilicon plates over silicon nitride or polysilicon substrates. Reciprocal rubbing between the surfaces induced charges by contact electrification, which vertically stabilized the plates on the substrates. Triboelectrification was also considered the cause of the memory effect, by

NIH-PA Author Manuscript NIH-PA Author Manuscript NIH-PA Author Manuscript

which out-of-plane actuation occurred even without further ultrasonic vibration after the initial ultrasonic assembly.

Lai *et al* assembled 3D microstructures fabricated by a multi-user MEMS process by means of centrifugal forces [20]. They devised an experimental set-up which could provide steady angular velocity to the substrates and reduce the effects of airflow. They demonstrated the successful assembly of hinged structures by applying inertial forces which could overcome friction and surface forces while still avoiding disruptive stresses on the hinges. Latching features were designed to lock the structures after assembly.

Magnetic forces can also be exploited to actuate microstructures with available degrees of freedom. Shimoyama *et al* designed movable structures which could be actuated by the Lorentz force [21]. The structures could carry a current and were anchored to the substrate through elastic joints. When immersed in an external magnetic field, the current induced the Lorentz force on the structures, whose out-of-plane deflection could be controlled by changing the magnitude of the current and the direction of the magnetic field. Iwase and Shimoyama devised a sequential batch actuation mechanism to lift ferromagnetic structures out of plane by applying an external magnetic field in the direction perpendicular to the substrate [22]. They controlled the stiffness of the elastic hinges attaching the structures to the substrate by designing the number of hinge beams and their length. By increasing the magnitude of the magnetic field, the structures with softer hinges were lifted first, so that the sequence of assembly steps could be specified (figure 1). The assembly of complex structures, such as regular tetrahedrons, was demonstrated.

The use of capillary forces for the SA of 3D micromechanical structures is reviewed in section 3.1.

3. Self-assembly using capillary forces

Surface tension dominates inertial forces and gravity as we approach sub-millimeter scales. Indeed, the surface tension force scales with length, while gravity scales with length cubed. Hence, it can be used as an effective driving force for SA of parts at micro- and nanoscales [23]. The surface tension force is mainly used in two approaches: deterministic folding of planar structures into three-dimensional structures, and stochastic aggregation of components to each other or to an assembly template.

3.1. Folding 3D structures

In this approach, a planar structure is usually fabricated through surface micromachining with hinges covered with solder [24], glass [25] or photoresist [26]. Heating up of the system melts the solder and reflows the glass or the photoresist, and surface energy minimization causes the hinges to bend, resulting in the controlled deployment of a 3D structure. The initial application of such techniques was the construction of optomechanical micromachined devices, such as scanning micromirrors, which could be deployed out of plane, thus overcoming fabrication limitations in micromaching [26]. The final angle of the rotated out-of-plane structures depends on the global energy minimum of the system; it can be accurately predicted by finite element simulations of the movable joints [27]. Mechanical stopping structures can be used to lock the plates at the desired angles (figure 2). For a comprehensive overview of the state-of-the-art in this field, see the review paper by Syms *et al* [28]. This method was also used to construct 100–300 μm sized 3D building blocks featuring electronic components on their faces (figure 3(I)) [29]. Finite element simulations showed that these 3D blocks could be constructed with a variety of materials, and sizes could range from the millimeter scale down to the nanometer scale. A size range of 2–15 μm has been demonstrated in the experiments (figure 3(II)) [30]. Cho *et al* used the self-folding mechanism to fabricate an orthogonal three-axis sensor.

NIH-PA Author Manuscript
NIH-PA Author Manuscript
NIH-PA Author Manuscript

Cantilevers were built on the six faces of a cubic structure (figure 3(III)), having different sizes and thus different resonance frequencies. This 3D sensor could be used to gain angular and orientational information about a chemical or biological analyte, including the direction in which it is approaching the sensor [31].

3.2. Self-assembly and part integration

Conformal part-to-template and part-to-part SA are examples of *stochastic* assemblies: while the parts and the template contribute to determine the overall configuration of the assembled structure, the actual correspondence between binding sites and individual parts is not determined in advance. The trajectories described by the parts to reach their target assembly sites during the assembly process are random and not predefined.

3.2.1. Part-to-template assembly—In the capillary approach to part-to-template assembly, receptor sites on the assembly template are covered with a liquid adhesive or with molten solder. As the parts get introduced to the assembly template, they attach to the adhesive-coated receptor sites. Then the parts self-align over the sites to minimize the interfacial energies. Different adhesive liquids require surfaces with different wetting properties or coatings for the receptor sites. For an acrylate-based adhesive or hydrocarbon liquids, receptor sites should be hydrophobic for aqueous assembly environments, and hydrophilic using water-based fluids for air assembly environments. For low-temperature melting solder, receptor sites should be coated with thin metal films with good solder-wetting capability, e.g. copper and gold [32]. This type of SA is particularly effective for very high precision registration and alignment of parts, which makes the technique the more interesting the smaller the pitch of the interconnections between parts and substrates.

Srinivasan *et al* demonstrated a prototypical fluidic capillary SA technique [6]. They patterned a substrate with an array of hydrophobic, SAM-coated Au binding sites. When the substrate was inserted into water through a film of hydrophobic adhesive floating on the water surface, the adhesive covered only the hydrophobic binding sites. Then they introduced microparts fabricated from silicon-on-insulator wafers through a pipette toward the substrate in the water. When the hydrophobic pattern on the microparts came in contact with the adhesive, shape matching and self-alignment occurred spontaneously due to interfacial energy minimization. Finally, the adhesive was polymerized by heat or UV light depending on the type of the adhesive, so that the bonding became permanent. Binding sites of shapes with in-plane rotational symmetries such as squares gave alignment yields up to 100% (figure 4(*a*)). The translational and rotational misalignments were less than 0.2 μm and within 0.3°, respectively. Binding sites without in-plane rotational symmetries (aimed at a uniquely-oriented alignment) such as semicircles and commas gave alignment yields of approximately 30–40% (figure 4 (*b*)) [33]. The technique was later adapted to assemble and electrically interconnect micromirrors [34], LEDs [8] and micromachined inductors [35] onto pre-processed substrates.

Low-temperature melting solder can be used to assemble microcomponents with both electrical and mechanical connections on a substrate. Jacobs *et al* developed a SA process exploiting low-temperature melting solder to mount LED arrays on flexible cylindrical templates [7]. The assembly template was patterned with copper squares, and a simple dip-coating process left molten solder on these copper squares, since copper has very good wetting capability for solder. The dip-coating process was performed in an acidic aqueous environment to avoid oxidation of the solder surface. Since an LED has electrical polarity, the two electrodes of the flat LEDs, located on the top and bottom faces, were distinguished by being covered with gold bonding pads of different areas; this tailored the capillary force exerted on each face upon contact with the molten solder. Hundreds of LEDs and a flexible assembly template were placed inside a vial; the vial was filled with water heated at a temperature above the melting point of the solder.

NIH-PA Author Manuscript NIH-PA Author Manuscript NIH-PA Author Manuscript

The LEDs were tumbled inside the vial, so to be attracted, aligned and bonded to the receptor sites on the template by the surface tension forces of the molten solder. By controlling the agitation intensity, the LED components self-assembled with unique face orientation. After this step, the gold pads on the top surfaces of the bonded LEDs were coated with solder by another dip-coating process. As a final assembly step, a flexible transparent film patterned with electrical circuits and metal interconnection lines was manually aligned to the assembly template, i.e. a wafer-level flip-chip bonding process was combined with the capillary action of the molten solder to align the film with high accuracy to the assembly template. Thus, the electrical connections to the top electrodes of the LED segments were established. Assembly was successful by testing, with a low defect rate of approximately 2% (figure 5)[33].

Capillary force-driven SA can also proceed in an air environment, as long as the receptor sites are coated with liquid droplets that act as a medium to attach flat microcomponents. Fang *et al* demonstrated a capillarity-driven SA method to surface mount lead zirconate titanate (PZT) actuators for microfluidic devices [36]. The hydrophilic receptor sites were precisely recessed wells with an opening smaller than the PZT actuators, and the bonding face of each PZT actuator had a hydrophilic area of identical size at the center as the recess' opening. All the surfaces except the receptor wells and the bonding areas on the PZT actuators were hydrophobic. A simple dip-coating process left adhesive droplets only in receptor wells. When PZT actuators were attached to these adhesive droplets, they self-aligned to minimize interfacial energies. Then, the aligned PZT actuators were pressed down such that their rims touched the substrate with excess adhesive squeezed out, and the electrically insulated adhesive was polymerized by heating to form permanent bonds. Electrical and mechanical connections were established at the rim and at the center, respectively, of the PZT actuators.

Fang and Böhringer devised a SA method to be performed in an air environment, which used a two-step assembly consisting of a shape-matching step and a capillary force-driven step [37]. First the 790 μm^2 silicon parts were trapped vertically in cavities, which only had space for one part. Then the parts were transferred to a substrate with an array of receptor sites covered with water drops. The parts had only one hydrophobic face, and the other faces were hydrophilic. After transferring them to the second substrate and removing the substrate with cavities, parts turned down to face the substrate with their hydrophilic face (figure 6). This process assembled microparts to 1000 densely packed receptor sites in about 2 min with a defect rate of approximately 1%. Higher part density could be achieved by transferring two or more batches of parts to the same pre-patterned substrate. This also allowed the integration of different components. The assembly template could be re-used for further assembly runs.

Fukushima *et al* introduced a capillary self-aligning step into a 3D integration process flow [38]. They dispensed a controlled amount of diluted hydrofluoric acid onto extruded, hydrophilic receptor sites etched onto a temporary silicon carrier wafer. Dies of various dimensions in the millimeter scale were collectively picked up and dropped onto the receptor sites, where they quickly self-oriented and aligned to the receptor edges. An accuracy of less than half micron was claimed for this alignment step [39]. As the liquid drops evaporated, the dies strongly adhered to the receptor sites. Then the carrier wafer was turned upside down and aligned to a pre-processed target wafer, where the dies were subsequently transferred for further processing. The process could be repeated a number of consecutive times; the group used it to fabricate multi-layered multifunctional devices, artificial retinas and memory chips.

Physical modeling and binding site design: Numerical simulations of the physics underlying the capillary part-to-template SA can be suitably performed through Surface Evolver, freeware, finite-element mathematical software developed by K Brakke at Susquehanna University [40]. The software specifically aims at the calculation of minimal-energy configurations of the surface of bodies satisfying user-defined physical and geometrical constraints and

NIH-PA Author Manuscript NIH-PA Author Manuscript NIH-PA Author Manuscript

specifications, including surface tension, volume, density, wetting boundaries and contact angles. The software can handle multiple bodies at the same time; however, simulations have so far addressed only single part assembly and no collective phenomena.

Given the focus on energy minimization, dynamic simulations can be performed by SE only in the limit of their quasi-static approximations. Within this limit, the behavior of a part floating over a fluid drop sitting on a binding site can be likened to that of an anisotropic spring, whose constant has tensorial nature. A theoretical model of a similar fluid joint was proposed by van Veen [41]. The components of the spring constant can be derived after calculating the relationships of energy and force versus lateral displacements and rotations (see e.g. figure 7 for the case of a square part over a square binding site), which was first shown by Greiner *et al* [42]. A consistent comparison between numerical predictions and experimental measurements of capillary restoring forces acting on small assembled dies was reported by Zhang *et al*, who used an optically encoded micromachined force sensor for the task [43].

Both theoretical and simulative results lead to some general observations:

- The restoring forces acting on the part are proportional to the surface tension of the fluid drop, and inversely proportional to its volume. Accurate choice of the fluid interfacial energy and its volume is required to control the forces.
- The restoring forces deriving from displacements of the part along the vertical direction are about one order of magnitude larger than those consequent to comparable lateral displacements. This implies a separation of time scales for vertical and lateral movements.
- The lateral restoring forces are anisotropic and depend on the design of the binding sites. In the case of asymmetric part/binding site designs, restoring forces are larger for lateral displacement along shorter sides.

Lienemann *et al* extended the simulations including the effects of surface defects present on the binding site and of fluid volume shrinking (due e.g. to polymerization of the adhesive) on the self-aligning performance of capillary SA [44]. Tay *et al* investigated the influence of fluid wetting on restoring torques, concluding that, for small enough contact angles of the fluid on the binding site, the maximum restoring torques are insensitive to the variations of such angles [45]. Lu *et al* used the previous results to develop an algorithm to model the dynamics of capillary SA [46]. They conclude that, for masses of parts and volumes of fluid drops within specified limits, the assembly times do not show significant variations.

The performance and yield of capillary part-to-template SA are strongly dependent on the characteristics of the binding sites. Both their geometrical design and physical optimization were addressed.

On the theoretical side, Böhringer *et al* developed a first-order numerical model predicting the energy landscape associated with a specific binding site design [47]. The model takes into account the energy of each significant interface of the system. The physical tendency of the system to minimize its free energy is reflected in the model by the maximization of the geometrical overlap between the binding sites of the part and of the substrate. Given this, the energy landscape can be calculated by the 2D convolution of the pattern(s) of the sites. The predictions of the models are consistent with those obtainable by Surface Evolver for relative displacements between the part and the substrate site larger than the thickness of the intervening fluid drop. This model has been the base for the attempts of the same group to derive geometrical conditions and constraints for the design of patterns which could lead to the unique in-plane orientation of the parts [48]. This is particularly relevant for the assembly of polarity-dependent devices. The general problem of finding patterns capable of inducing a pre-specified

NIH-PA Author Manuscript

NIH-PA Author Manuscript

NIH-PA Author Manuscript

capillary assembly dynamics—or more simply, of originating a pre-specified energy landscape —is so far without a solution [49].

On the physical side, Mastrangeli *et al* introduced a simple technique to achieve perfectly conformal dip-coating of arbitrary binding sites patterned on surfaces [50]. By surrounding the sites with a relatively thin wetting sidewall, the shape of the fluid drop was constrained to adhere to all geometrical features of the sites. Moreover, the technique significantly enhances the reproducibility of the dip-coating process and its insensitivity to accidental surface defects, which are relevant parameters to extend this type of assembly to large substrates.

3.2.2. Part-to-part assembly—This assembly approach is used for the aggregation of parts to each other, and for the construction of 2D or 3D mechanical structures and electrical networks. 2D structures are mainly constructed by floating the parts at a liquid–air or liquid–liquid interface and using the capillary action of the liquid menisci forming among the parts to induce reciprocal attraction or repulsion. Hosokawa *et al* configured the geometry of the parts to tailor the attraction forces between them [51]. Their parts, formed by polyimide–polysilicon bilayers, floated on top of water due to the hydrophobicity of polyimide. The sharp edge of one set of parts caused large attractive forces, and thus the parts were assembled in controlled configurations (figure 8). Since parts at the same height on the water surface attract each other, while parts at different heights repel each other, another set of parts with the sharp edge curled upward was introduced to produce a wider variety of controlled part configurations by the interplay of attracting and repelling interactions.

Bowden *et al* performed a 2D assembly of millimeter scale poly(dimethylsiloxane) (PDMS) parts placed at the perfluorodecalin/water interface [52]. The assembly was controlled by tailoring the shape of interacting menisci between the parts. The interaction between the part faces was strong and attractive when the profiles of the menisci matched, while it was weak when they did not match. The surface energy properties of the vertical edges of the parts, which determined the menisci profile, were systematically controlled to achieve the desired assembly configuration: hydrophobic vertical stripes were patterned on the selected part edges, and chiral designs were also introduced; the shape of the edges was modified, and the density of the parts was changed to control the height of the parts relative to the fluid interface. A wide variety of assembled structures were obtained and cataloged according to structural and symmetrical properties. Based on the physics of lateral capillary forces acting between particles floating at a liquid interface [53], Klavins developed a Lagrangian model of a tile-based capillary assembly [54]. His basic structure is a water bug with 4 feet of controllable wettability. He introduced algorithms to avoid defects and aggregate desired terminating structures. Rothemund exploited capillary SA of tiles as a universal Turing machine to elaborate complex tile patterns and simulate a one-dimensional cellular automaton [55].

It is possible to exploit capillary forces for building 3D structures [56]. Breen *et al* used low melting point alloy in aqueous potassium bromide to arrange mesoscale (i.e. millimeter to centimeter scale) parts into 3D structures [57]. The parts were 3D objects molded in polyurethane. Depending on the final desired structure, the selected faces of the parts were first covered with copper foil, and subsequently with low melting point alloy by dip-coating. External agitation was then applied on the parts floating on a potassium bromide solution, and the parts attached to each other at the solder-coated faces due to surface energy minimization. This method was used to construct crystalline structures (figure 9(*a*)), and even more complex features such as helices [58]. A similar approach was used to construct 3D electrical networks [59]. The basic unit of the assembly was a polyhedron (a truncated octahedron), which had printed electrical circuits and LEDs on its faces. The printed wires on the polyhedron faces connected the LEDs to patterns of solder dots. These solder patterns attached the parts to each

other after melting in a liquid environment, thus completing the electrical circuits and constructing a functioning 3D electrical circuit (figure 9(*b*)).

Clark *et al* self-assembled 3D structures using 2D microcomponents consisting of polyhedral metal plates [60]. The surface energy of the plates was altered using SAMs, and the assembly was carried out in water. The hydrophobic sides were covered with a thin layer of hydrophobic liquid; hence, these faces attached to each other to minimize the surface energy in the hosting fluid. A similar method was used to construct 3D structures from metal or polyurethane rods with a size range of millimeter to nanometer [61,62]. Morris *et al* studied different methods of putting the hydrophobic adhesive on the treated faces of microparts in an aqueous medium [63].

3.3. Programmable self-assembly

A challenge for stochastic SA methods is the integration of heterogeneous microelectronic systems composed of more than one type of components. While all methods discussed previously for capillarity-based part-to-template SA deal only with identical components and do not contemplate the possibility of selecting the type or batch of parts to be bound to the assembly sites, it is worthwhile to consider techniques which permit to integrate multiple, different types of components on the same template.

Xiong *et al* first demonstrated a method for controlled multibatch capillary SA of microparts [8]. It was based on the fluidic SA technique developed by Srinivasan *et al*, described in section 3.2.1 [6]. They patterned an oxidized silicon substrate with an array of gold binding sites, and these normally hydrophilic sites became hydrophobic after adsorbing a thiol SAM. To be active, i.e. to adsorb an adhesive lubricant droplet for later anchoring of parts, a binding site should be hydrophobic. They adopted an electrochemical method to controllably desorb the hydrophobic SAM from the gold binding sites; this was achieved by applying an appropriate electrical potential between the gold binding sites and the aqueous environment [64]. Before the first batch assembly step, some binding sites were selectively deactivated by SAM desorption, to be then reactivated for the next batch assembly steps. An array of commercial LED components was assembled on the substrate with a heat-polymerizable adhesive, and the electrical connections between the substrate and the LED components were later established by solder electroplating.

Chung *et al* proposed a method for solder-based programmable and reconfigurable SA based on the electronically controlled activation of solder-based binding sites [9]. This assembly method is similar to that of Jacobs *et al* discussed in section 3.2.1 [7]. However, in this work the assembly template was fabricated so that a copper electronic heater was embedded under each solder-coated binding site. By heating up the binding sites the solder melted, thus activating the sites, and the introduced parts with metal pads wettable by solder could assemble on them. Since electronic heaters were individually addressable, each binding site could be heated up and thus activated separately (figure 10(*a*)). Consequently, different types of parts could be assembled by introducing each type after activating the corresponding binding sites. Numerical simulations were used to calculate the minimum power needed to melt the solder, and the corresponding minimum distance between binding sites that prevented thermal crosstalk. Using this method, three different kinds of LEDs (yellow, green and red) were assembled to the substrate (figure 10(*b*)).

Solders with different melting points were used by Liu *et al* to assemble different types of parts in a multibatch-wise manner [11]. Two solders with different melting points, e.g. 70 °C for solder A and 47 °C for solder B, were deposited on selected binding sites by covering the rest of the sites with resist. The hosting liquid, i.e. the liquid in which the assembly was performed, was then heated up to the melting point of solder B, and the first batch of parts was introduced

NIH-PA Author Manuscript
NIH-PA Author Manuscript
NIH-PA Author Manuscript

and assembled. After the first part of the assembly was concluded, the temperature of the liquid environment was increased until it reached the melting point of solder A; at this point the second batch of parts was introduced and assembled. Using a larger number of solders with different melting points, a larger number of batches of parts could be assembled.

Sharma utilized the thermally induced gelling behavior of a properly chosen hosting fluid to selectively assemble several types of parts on a target template [10]. Hydrophobic sites were fabricated on the parts and on the assembly template, and the template sites were covered with hexadecane. The hosting fluid formed a gel around the sites when they were heated up; this prevented the assembly of parts onto undesired sites. Consequently, by individually heating up the sites and so deactivating them, several part types could be assembled on a single template.

4. Self-assembly using shape matching

This class of methods is inspired by multiple biological examples of selective lock-and-key processes. It exploits the three-dimensional, geometric shape matching and complementarity for selective binding between microparts and recessed receptor sites, and is aided by fluidic transport and gravity. In a typical scheme, the parts are randomly distributed on the assembly template, and an external agitation or force is used to move them around until they fall by gravity into the matching shape recesses on the template. The parts are then kept in the recessed binding sites by capillary or van der Waals forces.

The first implementation of a technique of this kind, commonly called fluidic self-assembly (FSA), was proposed by Yeh and Smith and aimed at the integration of GaAs devices on silicon substrates [5,65]. Parts and substrates were processed separately with complementary geometrical features. The parts, whose size could range from few microns to millimeters, had the shape of truncated trapezoidal pyramids which fit inside receptors embossed or etched into the substrates. This allowed for the unique vertical orientation of the parts while helping their lateral alignment. The parts were dispensed through an inert carrier fluid across the substrate and allowed to reach available complementary receptor sites. Parts that did not bind were recycled for other assembly runs. After assembly, the substrate was extracted from the fluid, dried and further processed for planarization and fabrication of electrical interconnections. The technique was later applied also to the integration of silicon microstructures [66], vertical cavity surface emitting lasers (VCSELs) [67] and enhanced electron mobility transistors (HEMTs) on a ceramic substrate [68]. Alien Technology Inc.[4] is currently using this assembly approach to manufacture radio frequency identification (RFID) tags. They claimed a throughput of about 2 million assembled parts per hour. To date, FSA represents probably the most successful application of SA techniques to electronic manufacturing.

Soga *et al* used shape-matching-based fluidic self-assembly to integrate GaAs blocks on a silicon substrate [69,70]. They enhanced the process yield with what they called the fluid dynamic assembly (FDA) [70]. This method employed fluid dynamic effects to get face control for the parts to be assembled. Round GaAs parts were assembled in circular recessed binding sites on the silicon substrate. In most of the assembly applications, the parts are flat and only one of their two main faces is functional (e.g. it bears electrical interconnections to the substrate); this is normally the face required to match and attach to the receptor site. However, it is usually hard to control the vertical orientation of the parts, because in their geometry there is no distinction between the top and bottom faces. It was shown, using both simulations and experiments, that by fabricating specially shaped structures on the parts, the face with which they approached the recessed binding sites could be controlled. Two polyimide structures, O-

[4]Alien Technology Corporation. Available online: http://www.alientechnology.com

NIH-PA Author Manuscript NIH-PA Author Manuscript NIH-PA Author Manuscript

NIH-PA Author Manuscript NIH-PA Author Manuscript NIH-PA Author Manuscript

type and C-type, were used on the circular GaAs parts, which gave 87% and 96% face selectivity yield, respectively (figure 11).

The assembly of heterogeneous silicon circuit parts on a flexible plastic substrate was demonstrated by Stauth and Parviz using shape matching [71]. Electronic components such as single-crystal silicon field-effect transistors and diffusion resistors, with sizes in the range of 100 μm, were introduced to a template submerged in liquid, and fluid flow was used to move the components on the template. Cr/Au contact pads were fabricated both on the parts and in the receptor sites for electrical connection. The contact pads on the substrate were coated with solder using dip-coating prior to the assembly. By using different shapes for the parts, such as circular, triangular and rectangular, and using complementary-shaped receptor site wells, components were selectively assembled over the template. In the next step, solder reflow was performed to bond the parts to the binding site due to capillary force, and also to establish electrical connections between the parts and the template (figure 12(I)). The authors also modeled the forces acting on the parts due to fluidic drag and surface tension of molten solder by numerical finite element methods. The mechanical yield of this SA process was 97% for substrates containing 10 000 binding sites. A similar approach was used to assemble AlGaAs-based light emitting diodes (LEDs) on silicon and glass substrates (figure 12(II)). The reported electrical yield was 62%; such lower yield was mainly dependent on the degradation of the solder bumps in the hot acidic assembly environment [72]. Zheng *et al* used this method for encapsulation of AlGaN/GaN LEDs [73]. They reported SA of 200 LEDs with 380 μm × 330 μm size with a yield of 95% in 2 min.

Chung *et al* used a shape-matching method to guide and assemble microstructures inside fluidic channels [74]. Grooves were fabricated on top of the microchannels, and complementarily shaped structures were fabricated on the parts. Using this method, they demonstrated the heterogeneous assembly of polymeric microstructures and living cells, as well as the integration of silicon chips.

Zheng *et al* used sequential shape-matching-based SA to fabricate three-dimensional circuits [75,76]. 200 μm size LEDs were assembled onto device carriers using shape recognition and solder bonding, and then encapsulation units were assembled onto LED-carrier assemblies, thus forming a 3D circuit path. The assembly for 600 LEDs was performed in 2 min with no defects. The overall assembly yield is currently 97% (figure 13).

Fang *et al* used a combination of capillary forces and shape matching to assemble silicon parts on the substrate [77]. As opposed to all work reviewed above on shape-matching-based SA, fluid flow was not used as a part delivery method in their approach. Two methods of self-organizing parallel assembly (SPASS) were introduced: a semidry uniquely orienting process (semi-DUO-SPASS) and a dry uniquely orienting process (DUO-SPASS). Both assembly processes consisted of the following steps. First the parts were spread in a single layer and uniquely face-oriented; this was achieved by surface energy modification in a semi-DUO-SPASS, and by geometrical modification in a DUO-SPASS. Then the parts were transferred to the assembly template, and external agitation was used to move them over the template and have them assembled to the binding sites due to shape matching. In this step, the alignment of the parts was rough due to the tolerances in the shape-matching features. In the next step, a finer alignment of the parts was introduced, using capillary forces in the semi-DUO-SPASS, and shape matching with finer alignment features in the DUO-SPASS. In the final step, aligned parts were transferred to a chip carrier template via wafer-level flip-chip bonding (figure 14). The part size was 2 mm × 2 mm, and the assembly was completed for 164 binding sites within 3 min with 1% defect. Ong *et al* adopted a very similar dry assembly approach, and extended it by exploiting the features of the parts for the establishment of solder interconnects as well [78,79]. Park *et al* also introduced a fully dry shape-matching-based SA method of silicon parts

NIH-PA Author Manuscript NIH-PA Author Manuscript NIH-PA Author Manuscript

with 95% yield within 1 min [80]. Two sets of complementary features were used on the parts and substrate to achieve proper in-plane orientation, aided by substrate agitation.

5. Magnetic self-assembly

Magnetic interactions are being exploited in a wide range of micromechanic applications, including valve pumps, relays, micromirrors, actuators, RF switches, magnetic storage, magnetic field sensing and biomedical applications [81]. Potential advantages of magnetic interactions are non-contact, long-distance action; insensitivity to the surrounding medium; independence on the details of surface chemistry; high energy density and their favorable downscaling properties [82,83]. Magnetic interactions can be both attractive and repulsive depending on polarization, and can be tailored by magnet geometry and materials. All these remarkable features make magnetic forces very interesting and are indeed sustaining the emergence of the magnetic MEMS field. Magnetic interactions have been utilized as driving forces for micro- and nanoscale SA in a variety of settings, which are reviewed below.

The first embodiment of a magnetic SA technique can be traced back to the 1969 US patent of Yando [84]. It describes an apparatus composed of an array of magnets made up of laminated sheets of magnetic alloys, stacked inside a supporting substrate in the direction perpendicular to its surface. According to the patent, particles, intended to represent microdevices, were prepared with magnetic coatings and spread over the substrate. A gradually attenuated mechanical vibration was applied to the substrate. The particles consequently moved across the substrate and assembled so to match the position of the trapping magnetic array.

More recently, the application of magnetic forces for SA purposes was reproposed by Fonstad [85]. The approach he put forward, called magnetically assisted statistical assembly (MASA), was envisioned as a variation of the fluidic SA approach to address the integration of III–V heterostructure devices onto pre-processed electronic substrates. The main novelty stems from the introduction of a strong, short-ranged magnetic retentive force to keep the devices in place after being assembled into the shallow cavities of the target substrate. The substrate can be an integrated circuit or a temporary carrier wafer. The process is shown in figure 15. A thick dielectric layer was patterned over the substrate with highly symmetrical recesses having roughly the same dimensions and shapes as the devices, called nanopills, to be thereby assembled. A high-coercivity magnetic material, such as CoPt, was patterned at the bottom of the recesses and magnetized in the direction normal to the substrate. The nanopills, epitaxially grown on a separate wafer and released by selective etching, were coated with a thin, soft magnetic film of e.g. nickel. The assembly consisted in flooding a fluid containing an excess number of nanopills over the substrate, which was tilted and vibrated over a stage. As the nanopills stochastically settled inside the recesses, their magnetic film was saturated by the magnetic field, whose strength decayed exponentially with distance. Consequently, a retentive force prevented the nanopills from being removed by gravity, fluidic drag or other components. Alternatively, in the ‘snow globe’ way, the nanopills sedimented on the substrate by gravity, then the substrate was tilted to remove excess unassembled pills and the process repeated until all recesses were filled. After assembly, the devices were fixed in place by a polymer, which filled the voids and planarized the substrate. Standard lithographic processing was then performed to further complete the integration of the devices. The method was not pursued beyond an initial process and technology development [86].

Shet *et al* [87] extended the technique proposed by Fonstad by introducing an external, long-ranged magnetic field source at the backside of the target substrate during the assembly process. Such an external field enhanced and extended the range of the attraction felt toward the recesses of the substrate by the nanopills. The locking of the nanopills was again aided by the strong, short-ranged force produced by magnets patterned at the bottom of the recesses. The same

NIH-PA Author Manuscript NIH-PA Author Manuscript NIH-PA Author Manuscript

group also proposed a non-stochastic assembly approach based on a feed tape [88]. The feed tape was slid above and parallel to a target substrate. Pills of equal shape and size as the recesses realized in the substrate were attached to the bottom side of the tape, and their exposed side was coated with a thin film of high magnetic permeability. The magnetic field created by an external moving magnet magnetized the coating, and the consequent attractive force pulled the pills off the tape and into the recesses of the substrate. This method should help reducing frustration (e.g. the presence of multiple devices impinging on the same recess, or recesses left unoccupied because of blocks created by agglomerated devices).

A dry SA technique combining magnetic attraction force, shape matching and mechanical vibration was devised by Ramadan *et al* (figure 16) [89]. A host substrate, featuring physical recesses, was superposed to a master array comprising embedded NdFeB magnets, whose position exactly matched that of the recesses. Target chips, bearing a CoNiP soft magnetic film on their non-functional side, were seeded over the substrate, which was mechanically vibrated and tilted. This motion caused the chips fluctuate across the substrate until being trapped in the recesses, aided by the attractive magnetic force ensued by the underlying magnets. The amplitude of the substrate vibration and the chip thickness were tailored so that the only stable configuration possible for the chips was the one having the functional side facing upward. The horizontal alignment of the chips was controlled by shape matching between the chips and the recesses of the host substrate. After assembly, the master array could be removed and reutilized, while the chips could be further processed by wire bonding or flip-chip techniques. An assembly of 2500 chips in 5 min with 97% yield was claimed with this technique.

In the dry SA approach of Shetye *et al* [90], powder-based permanent SmCo micromagnets were embedded both in the chips to be assembled and in the binding sites of the target substrate, which featured no other guiding template (figure 17). The substrate was set upside-down 10 mm above the base of a glass container, which was connected to an electromechanical shaker. Five times as many chips as the binding sites were placed on the glass substrate, and were pushed upward toward the target substrate by the shaker action. The magnets of all the chips were equally polarized in the direction normal to the surface, so that mutual clamping between chips was avoided. The assembly of the chips on the substrate took place when the overlap between chips and binding sites was such that the consequent attractive magnetic force was superior to gravity. Assembly defects might include stacking of chips on the substrate, due to excessive magnetic attraction, and chip angular misalignment, due to friction between chips and the surface of the substrate. Misalignment could be alleviated by vibrating the substrate after the assembly. Assembly yield close to 100% was claimed.

Boncheva *et al* exploited competition between magnetic and mechanical interactions to induce the spontaneous folding of flat elastomeric sheets into free-standing, centimeter-sized three-dimensional objects [91]. The sheets had the shape of 3D compact objects unfolded and projected into a plane. Magnetic dipoles were properly patterned and arranged on the sheets so to advantageously exploit their tendency to form stable closed loops. The minimization of the total system energy, which included both magnetic and elastic components, drove the self-folding of the sheets into approximately spherical shells. The SA was normally achieved after agitation of the structures in water. This fabrication technique was used to assemble simple working electrical circuits surrounding spherical cavities.

Golosowsky *et al* reported the formation of stable ordered arrays of millimeter-sized magnetic particles floating on a liquid surface [92]. The particles were composed of permanent Nd–Tb magnets encapsulated into styrofoam disks, which floated on a liquid surface with the magnetization direction perpendicular to the surface. The particles interacted via short-ranged, repulsive lateral magnetic interactions rather than via capillary interactions. Two-dimensional hexagonal lattices, whose lattice constant could be tuned by the application of an external

NIH-PA Author Manuscript

NIH-PA Author Manuscript

NIH-PA Author Manuscript

magnetic field, formed spontaneously. Array symmetry varied with particle shapes, magnets and magnet position inside the particles. By stacking several of these lattices, out-of-plane attractive magnetic interactions led to the formation of ordered three-dimensional crystals.

Grzybowski *et al* used competition between magnetic and hydrodynamic interactions to build a dynamically self-assembling system [93]. In their experimental set-up, a set of magnetite-doped PDMS disks were placed at liquid–air or liquid–liquid interface in a beaker, subject to the magnetic field produced by a rotating permanent magnet positioned at the bottom of the beaker (figure 18(*a*)). The disks spun around their axis at the same frequency of the rotating bar; due to their motion, they repelled each other, but at the same time they were attracted to the axis of rotation of the magnet. The interplay between attractive and repulsive interactions led to the formation of a wide variety of spatial patterns, which behaved as dissipative structures and, once organized, were stable for days (figures 18(*b*) and (*c*)). The properties and morphology of the patterns depended on the number, size and shape of the disks and on the rotation speed of the permanent magnet. The observed behavior of the disks in such setting was likened to that of classical artificial atoms and molecules [94]. The group conducted several experiments using variants of the experimental set-up to further investigate the phenomena associated with dissipative structures, vortex interactions and dynamic SA [95-99].

Yellen and Friedman demonstrated the magnetically controlled, programmable SA of two types of colloidal particles [100]. In their set-up, Co micromagnets were patterned on and magnetized parallel to a substrate, and an array of square photoresist microwells were defined at the poles of the magnets. The substrate was immersed in water, where superparamagnetic colloidal beads were injected. The combination of the local magnetic fields with an externally applied magnetic field was used to selectively and controllably attract or repel the beads from predefined wells, which could accommodate for only one bead each. Once assembled, the assembled beads would remain trapped in the wells during washing for removal of excess beads and subsequent assembly steps. No cross-contamination was observed between the assemblies of different beads. The technique could be extended to assembly of multiple types of particles by thermomagnetic programming of the soft magnets.

When an external magnetic field is applied to a suspension of magnetic particles, they tend to assemble into linear aggregates, with their magnetic dipoles aligned in a head-to-tail fashion and parallel to the magnetic field. Tanase *et al* controlled the aggregation of Ni nanowires, permanently magnetized along their long axis, by applying a small external magnetic field to their suspension [101]. Because of the aligning effect of the field and the competition between magnetic dipole–dipole interactions and fluid drag effects, the wires formed extended head-to-tail chains aligned to the direction of the field. Their morphology was governed by the strength of the external field: at higher field intensity the chains straightened and lost the tendency to form branched structures [102]. The chains were stable after removal of the field, and retained their shape during slow evaporation of the solvent. The same group also demonstrated magnetic trapping of composite Pt–Ni–Pt nanowires between a pair of permanently magnetized Ni electrodes (figure 19) [102]. The assembly was enhanced by the application of an external magnetic field which aligned the nanowires along the long axis of the electrodes. The inclusion of Pt caps at the edges of the nanowires helped the formation of low-resistance metal contacts with the gold-coated electrodes. With a similar technique, Ye *et al* aligned and assembled ferromagnetic composite Au–Ni–Au nanowires between pairs of solder-coated, magnetic contact pads [103]. Permanent bonding and ohmic contacts between the nanowires and the contact pads were realized by solder reflow. They supported the utility of the assembly strategy by fabricating a functional, nanowire-based integrator.

Love *et al* [104] demonstrated the use of magnetic interactions between ferromagnetic objects to direct and stabilize the lateral SA of ordered 3D structures in the absence of any external

NIH-PA Author Manuscript

NIH-PA Author Manuscript

NIH-PA Author Manuscript

field (figure 20). They electroplated few-micrometer-long rods of submicrometer diameter inside membranes of porous alumina by alternating gold (diamagnetic) sections and nickel (ferromagnetic) disks. The disks' thickness was smaller than their diameter. Thus, upon magnetization by an external field the rods had their axis of magnetization perpendicular to their long physical axis. The rods were suspended in a solution and, upon ultrasonication, they laterally self-assembled into hexagonally close-packed bundles, composed of few tens of units. The rods were oriented side-by-side, their long axis parallel and had their ferromagnetic sections aligned. According to a macroscale model, the energy-minimizing, most stable configuration of defect-free bundles has the rods arranged in head-to-tail rings, forming concentric loops aligned in the same direction. The bundles had insignificant global magnetic dipole, which justified the absence of coalescence into larger assemblies.

6. Electric-field-mediated self-assembly

Early work regarding levitation, holding and orientation of particles and cells showed that electric fields could be successfully applied to perform microassembly tasks in fluid environments [105,106]. Indeed, the use of electric fields may afford non-contact handling of components [107]. Moreover, electric fields can be produced by trapping electrodes which can be fabricated in a massively parallel way, thanks to VLSI technology and the abundant knowledge about electrical properties of materials gained in MEMS research. Conversely, the use of such planar technology may confine this set of techniques to two-dimensional assembly only.

6.1. Electrophoretic self-assembly

An electrostatic field can be used to induce motion in charged particles in liquids of moderate viscosity: this phenomenon is called electrophoresis (EP). EP is largely employed in biology and microfluidics to discriminate among homologous molecules, and has been also applied to assemble microscopic devices over patterned planar arrays. Edman *et al* used a variant of EP called electroosmosis to assemble a 20 μm diameter InGaAs LED onto a pair of Sn/Pb-coated electrodes designed over silicon substrates [108]. A negative current was applied to the electrodes, which induced bulk fluid movement in a buffer fluid of low conductivity. The fluid movement attracted the LED toward the electrodes. Once the LED was on the electrodes, the current was briefly reversed to force the LED onto the electrode surface. LED and substrate were then extracted from the solution and reflowed for the bonding. The process was self-aligning and exhibited micrometer-scale precision. A programmable array of electrodes producing an electrostatic field with switchable configurations was used by O'Riordan *et al* to drive by EP both deterministic and stochastic assembly of mesoscale devices [109]. By switching field configurations, GaAs-based LEDs could be manipulated, transported across the electrodes and precisely located at selected receptor electrodes (figure 21). The assembly was completed by evaporating the transport medium and establishing metal contacts to the electrodes by solder reflow. The electrophoretic assembly approach was extended by Esener *et al* by functionalizing with DNA strands both assembling parts and electrode binding sites [110]. This is done to provide a strong coulombic attraction, due to the DNA charge, between devices and field sources, while at the same time exploiting the highly selective hybridization of complementary DNA strands to allow for transient bonding of the devices to the electrodes. The technique was intended for the assembly of optoelectronic devices on silicon substrates. No bonding was demonstrated after assembly, though solutions were advanced. Lee *et al* used a similar process, involving the functionalization of Au films with charged organic species, to direct the transport and positioning of generic silicon-based, micron-sized islands across interdigitated electrodes [111].

NIH-PA Author Manuscript
NIH-PA Author Manuscript
NIH-PA Author Manuscript

6.2. Dielectrophoretic self-assembly

Dielectrophoresis (DEP) is possibly a more compelling means to achieve micro- and particularly nano-SA. Compared to electrophoresis, where a static, uniform electric field induces a force exclusively on charged bodies, DEP affects both charged and uncharged ones. When an object has different conductivities and dielectric constants compared to the surrounding fluid medium, charges accumulate on its interfacial regions, and the object appears externally as an electric dipole. Upon application of a spatially non-uniform, dynamic electric field in that region, the object experiences a force which is not dependent on the direction of the field, being instead proportional to the gradient of the square of the electric field. In this non-uniform field, the components of the force acting on the object do not balance out, and movement is induced. The object is attracted toward the regions of higher field intensities, which are distributed in proximity of the driving electrodes, if its polarizability is higher than that of the surrounding medium (positive DEP); otherwise, it is repelled because the maxima of the field would preferentially attract the medium (negative DEP) [112]. A high-frequency rotating electric field can also induce rotation of the objects. At the same time, the power generated by the electric fields may heat up the medium and give rise to convection flows, electrothermal forces and other electrohydrodynamic effects, which for high field intensities can be competitive with dielectrophoretic forces and thus should be accounted for [113]. AC electrokinetic phenomena are frequently employed in biotechnology [114]. They can be induced and ingeniously tailored by proper 2D or 3D electrode designs to produce the required electric traps. The approach may be successfully scaled down to handle sub-micrometer-sized parts for nanotechnology applications [112]. In the specific assembly perspective, the difference in behavior displayed by positive and negative DEP has an energetic counterpart. In positive DEP the field's energy maxima represent potential minima for the assembling particles, but non-contact manipulation requires closed-loop control, whose implementation may be impractical for micron-scale electrode arrays. Conversely, open-loop non-contact operations are possible with negative DEP, but the particles must overcome potential barriers to set into the traps, which are moreover metastable in the best case.

Negative DEP and electrothermal effects were exploited by Bashir's group to direct the assembly of 10 μm sized silicon resistors between pairs of Au/Cr-coated electrodes [115]. After assembly, the electric field was maintained so to keep the resistors in the correct positions during reflow while the liquid solution evaporated. In another application involving micron-sized, three-terminal MOSFETs, the same group chemically improved the stability of the final assembly [116]. In this case, the substrate electrodes were functionalized with thiol-ended SAMs, which created a bridging bond to the Au-coated device electrodes once they assembled in place over the binding sites (figure 22). A subsequent thermal annealing helped reduce the contact resistance between the electrical terminals of the MOSFETs and the electrodes.

Cohn tried to combine the advantages of both positive and negative DEP introducing the so-called bipolar dielectrophoresis (BiDEP), in which a long-range attractive force gave way to a repulsive force at short range, as with molecular bonds [117]. In a first attempt, compound dummy devices were built with an inner core of higher dielectric constant than the outer thin shell, that of the medium being intermediate. At large distances a lumped permittivity higher than that of the medium appeared to the field sources, while the situation reversed in near field. The balance of attractive and repulsive force components resulted in a stable equilibrium at a fixed distance from the electrodes. In a second, more successful approach, the fluid medium was made out of a mixture of two liquids of different dielectric constants, respectively higher and lower than that of the devices. As the microstructures approached the driving electrodes, the field gradient induced the liquids to de-mix, the component of higher polarizability segregating into the high-field-intensity region between the parts and the electrodes, creating a dielectric gradient. The DEP force cancelled out at the iso-dielectric points, where the parts

NIH-PA Author Manuscript

NIH-PA Author Manuscript

NIH-PA Author Manuscript

levitated in stable equilibrium. Actual electrical contact could be progressively achieved by changing the voltage and the relative composition of the mixture.

DEP was also applied to the directed fabrication, assembly and integration of nanoparticles. Bhatt *et al* demonstrated the formation of gold fibrillar nanowires out of dielectrophoretic agglomeration of nanometer-sized gold particles [118]. By applying an ac polarization to pairs of planar electrodes covered by an aqueous suspension of particles, microwires began assembling at the electrode surface by aggregation of particles, and continued to grow at the edges until they bridged the millimeter- to centimeter-long gap between the electrodes, creating a short circuit. By controlling the process parameters, both straight single wires and massively parallel arrays of wires with good ohmic properties could be produced. With a similar dielectrophoretic technique, Lumsdon *et al* fabricated one- and two-dimensional crystals of latex or silica particles between the gap of planar electrodes on a surface [119]. The crystals were specifically oriented without the need for patterned templates. The transition from order to disorder of the crystals could be induced in a few seconds by switching on and off the alternating electric field. Several works reported successful use of DEP for the manipulation and assembly of nanowires [120-124] and nanotubes [125,126] from suspensions placed between pairs or arrays of ac-polarized electrodes.

6.3. Dry electrostatic self-assembly

In a dry setting, Böhringer *et al* demonstrated the use of mechanic vibration and electrostatic fields to sort and position millimeter-sized parts on a planar substrate [127]. The top aluminum plate of a piezoelectric actuator was used as the bottom armature of a parallel-plate capacitor, whose dielectric was a glass plate whose top side was coated with gold and lithographically patterned with arrayed apertures. When a voltage difference was applied between the armatures of such an actuator, fringing electrostatic fields were created by those apertures in the upper electrode. Electrically neutral parts were polarized by the fields and were attracted toward the minima of the electrostatic potential, i.e. toward the center of the apertures. Their motion was driven by the ultrasonic vibration of the plate, which helped to overcome friction and adhesion forces. Once the parts got stuck in the electrostatic traps, they would reduce the local amplitude of the fringing fields, thus preventing other parts from sticking in the same locations. The measured assembly rate showed an exponential-like distribution.

Highly ordered and defect-free crystals of millimetersized spheres were self-assembled by Grzybowski *et al* exploiting mutual interactions arising from contact electrification [128]. Two types of spheres of equal size but different, insulating materials were randomly set into a polystyrene dish, whose walls were coated with a thin gold film. When the dish was vibrated by a linear magnetic motor, the spheres wandered randomly around the entire container. While rolling along the surface of the dish, the spheres separated and accumulated charge triboelectrically; the sign of the charge depended on the type of material. Disordered aggregates formed when the charges had the same polarity on both types of spheres; if the polarity was opposite, regular and closed arrays assembled upon a sequence of gentle and then vigorous vibration. The resulting lattices were steady-state products of SA, insensitive to ambient conditions, to the electrical bias applied to the container and to the order in which the spheres were added. The type of lattice produced depended only on the relative number of spheres and the interplay between attractive and repulsive electrostatic interactions among them.

7. Colloidal self-assembly

Colloidal particles are small objects with at least one characteristic dimension comprised between 1 nm and 1 μm, their range of sizes being defined by the importance of the Brownian motion. They include slurries, clays, sols and aerosols, foams, proteins, viruses, bacteria and cells [129]. The most experimentally studied and used examples of colloidal particles are silica

NIH-PA Author Manuscript NIH-PA Author Manuscript NIH-PA Author Manuscript

colloids and polymer latexes. In the past decades, the formation of highly ordered structures of colloidal particles with sufficiently large domain sizes has attracted a wide research interest, also given the ample range of possible applications for this novel class of materials. Two-dimensional assemblies have been used as arrays of microlenses in imaging [130] and as physical masks in microlithography (also called nanosphere lithography) [129,131-134]; three-dimensional assemblies, also called synthetic opals [135], have been used as precursors in producing high-strength ceramics [136], as templates for porous silica membranes [137,138] and as diffractive elements in the fabrication of optical components [139,140] and photonic bandgap (PBG) structures [141,142]. Several self-organizing techniques have been devised to assemble high-quality arrays of monodispersed colloidal particles. Notably, the availability of colloids of highly uniform size and shape is very important for the SA of crystalline arrays of large sizes, since uniformity and order affect the electronic, optical, magnetic and electrokinetic properties of the resulting aggregates [129].

7.1. Two-dimensional films of colloidal particles

2D thin films or even monolayer arrays of spheres can be assembled on solid supports or at air–liquid interfaces. In the Langmuir method (figure 23(*a*)), the colloidal spheres are spread at a liquid–air interface through a spreading agent. The spheres need to be modified so to be only partially immersed into the surface of the liquid. As a consequence, strong attractive capillary interactions, possibly coupled with electrostatic ones, lead to the spontaneous formation of two-dimensional aggregates at the fluid interface. The aggregates can be subsequently transferred onto a variety of solid substrates [131, 132, 143]. The morphology of the aggregate is dependent on many parameters such as size and concentration of particles, surface hydrophobicity and charge density of the colloid, and the electrolytic properties of the solvent [144, 145]. The formation of an ordered colloidal monolayer requires that the interparticle attraction be sufficiently weak to allow the formation of ordered domains which can deform during drying [143].

In the method of solvent evaporation or convective assembly (figure 23(*b*)), a liquid dispersion of colloidal spheres is spread onto the surface of a solid substrate. Under controlled evaporation of the solvent, the spheres self-assemble into a close-packed hexagonal array. Flat, clean and homogeneous substrate surfaces are required to generate highly ordered arrays of large domain sizes; glass slides and silicon wafers have been used directly. Direct microscopic observation revealed that the crystalline ordering of a core array nucleus starts when the thickness of the evaporating liquid layer becomes equal to the diameter of the spheres, i.e. when the spheres start to protrude from the liquid surface. The attractive lateral capillary forces, due to the menisci formed around the particles, and the convective transport, due to the inward liquid flux that tends to compensate for the evaporation from the nucleus surface, bring the particles toward the periphery of the ordered region and, overcoming Brownian motion, progressively pack the assembly and drive the self-organization [146, 147]. Particles order first in the evaporating liquid surface, then in successively formed layers. Neither electrostatic repulsion nor van der Waals attraction among particles plays a significant role in this case. Using polydisperse colloidal suspension, size-dependent segregation leads to the formation of polycrystalline monolayers with grains composed of particles of the same size; the process is strongly dependent on the evaporation rate of the liquid, and thus on temperature [148]. The evaporation of the solvent can also be controlled by spin-coating the colloidal dispersion on a solid substrate [134]. In such a case, to obtain a uniform monolayer the dispersion must completely wet the substrate surface, and there should be repulsion between the colloid particles and the solid substrate [149].

A related method, proposed by Jiang *et al* [150], involved immersing a planar substrate nearly vertically in a colloidal suspension. Under proper conditions, the solvent evaporation led to

NIH-PA Author Manuscript
NIH-PA Author Manuscript
NIH-PA Author Manuscript

the deposition of a highly ordered multilayered array of particles of quite uniform thickness on the substrate, starting from a position below the initial level of the substrate–solvent–air contact line. After the opaline film was dried, the adhesion of the particles to each other and to the substrate was sufficient to handle the film without damage. The thickness of the film could be controlled by properly choosing particle size and concentration, and it could be linearly increased by subsequent coating steps.

An interesting variant of the solvent evaporation method, referred to as controlled plate withdrawal, was devised by Dimitrov and Nagayama and is illustrated in figure 24 [151]. A clean, flat wettable solid plate was dipped vertically into a suspension of colloidal particles. When the plate was kept stationary, monolayers of particle arrays spontaneously started to form at the plate–suspension–air triple line down to the bulk suspension. By vertically withdrawing the plate, together with the already formed particle arrays, from the suspension (in the direction opposite to that of the array growth) at a rate equal to that of array formation, a linear, continuous array growth was achieved. The ordered array growth process could be split into two main stages: first, the convective fluid motion due to the evaporation of water from the wetting thin film surface brought the colloidal particles from the bulk of the suspension to the film; second, the interactions between the particles confined in the thin film, mainly lateral capillary and electrostatic forces, produced the specific textures of the array. The film thickness was independent of the evaporation rate. The method could be used with a wide range of substrates and suspensions, provided that the substrate was completely wettable by the suspension, so that a film of thickness close to but less than the diameter of the spheres was formed; the particles were able to slide on the substrate—adsorbing particles would form an amorphous aggregate; aggregation of particles at the suspension surface was prevented by restricting the water evaporation near the particle film; water evaporation from the particle arrays was slow enough; and the suspension and the plate were free from impurities. The technique may be likened to the Langmuir–Blodgett technique, the main difference being that the latter case requires the particle film to be initially formed on the suspension surface to be then transferred onto the substrate, while in the former case the film is directly formed on the substrate from the bulk suspension.

The evaporative method devised by Micheletto *et al* [152] involved the deposition of a drop of colloidal suspension on a carefully cleaned glass substrate connected to a Peltier cell for the accurate control of humidity and temperature stability. The substrate was inserted in an airtight box, to slow down the evaporation of the solvent and protect from external air flow. The whole system was tilted by 9°, so that the evaporation started from the upper edge of the sample and gradually reached the bottom until the substrate was dry. The evaporation speed and the quality of the resulting aggregate depended on this tilt angle. With this technique, ordered arrays of 42 nm sized latex spheres were successfully assembled.

In the method based on (di)electrophoretic deposition (figure 23(*c*)), a liquid dispersion of colloidal spheres is confined between two parallel electrodes. Upon application of a sufficiently high electric field, the particles start to move toward each other and to organize from their original random distribution on the anode to form a stable 2D hexagonal array. The process can be modulated by changing the strength or the frequency of the applied electric field. Indeed the long-range attraction forces are generated by electrohydrodynamic fluid flows, which overcome the electrical repulsion among the equally charged particles. The flows are induced by distortions in the electric field (owing to the inhomogeneities in the double layer of ions and counterions at the electrode surface) [153], and by the ionic current flowing through the solution [154]. Once the particles are close to the anode surface, where they remain mobile, electrohydrodynamic and electrokinetic processes assemble them into arrays. Increasing the attractive force between the particles and the electrode, the particles can be permanently attached to the surface. Hayward *et al* combined electric-field-directed colloidal assembly with

NIH-PA Author Manuscript

NIH-PA Author Manuscript

NIH-PA Author Manuscript

UV-induced, controllable photochemical activity at an indium–tin–oxide semiconducting electrode to produce tunable patterns of ordered, micrometer-sized colloidal arrays [155]. Externally masked UV illumination locally altered the current density pattern at the anode, so that the particles in suspension were swept from the darkened areas to the lighted regions. Illumination assisted the immobilization of the particles at the electrode. Light modulation of colloidal assembly was not observed when the semiconducting electrode was replaced by a conducting one.

All the methods presented above produce close-packed crystals of spheres, with packing density close to 74%. Optical approaches can be used to create lattices of colloidal particles where the interparticle distance could be varied independently of particle size. For example, optical standing waves having a regular pattern of intensity antinodes were created inside the solvent; optical forces organized the dielectric particles into ordered 2D structures by transporting them to the antinode maxima [156]. Alternatively, the external optical fields could induce interactions between dielectric objects that could also result in the creation of complex structures [157].

7.2. Three-dimensional colloidal structures

For the realization of 3D arrays of colloidal particles, gravitational sedimentation is probably the simplest approach. It is controlled by the size and density of the particles and by the sedimentation rate; it relies on gravitational settling, Brownian motion and crystallization. The formation of an ordered, typically polycrystalline lattice by this method is only possible at specific volume fractions of colloids and when the sedimentation rate is slow enough: this allows the particles deposited at the bottom of a container to undergo a hard-sphere disorder-to-order phase transition. Large particles form amorphous sediments because their rate of accumulation at the bottom is higher than the maximum crystal growth rate [158]. Major disadvantages of the method are the formation of numerous defects, the low control over the morphology of the top surface and over the number of layers in the 3D structure and its slowness when dealing with submicron particles: full suspension sedimentation can take up to weeks. The process can be accelerated and the quality of the assembly can be improved by centrifugation or filtration [159]. Dinsmore *et al* demonstrated manipulation, ordering and control of colloidal particles by local entropic forces produced by passive structures etched into the walls of a container [160]. Van Blaanderen *et al*'s colloidal epitaxy used lithographically defined template surfaces to tailor the lattice structure, orientation and size of defectless 3D crystalline array growth by slow colloidal sedimentation [161].

A more convenient strategy for the SA of large-scale 3D crystalline arrays of colloidal particles exploits the minimization of electrostatic repulsive interactions among highly charged colloidal particles suspended in a liquid medium. Under appropriate conditions, this leads to the spontaneous organization of the particles into a variety of crystalline structures, referred to as colloidal crystals [162]. When the electric screening length is shorter than the center-to-center distance between two spheres, the colloidal spheres will behave as hard spheres and will not influence each other until they are in physical contact; otherwise, they will behave as soft spheres [163]. In both cases, the resulting crystalline structures have the spheres separated by a distance of the order of their size (packing density less than 50%) due to the mutual electrical repulsion. The method requires stringent experimental constraints on temperature, size monodispersity, superficial charge density of the spheres, sphere density and counterion concentration in the solvent.

Kim *et al* produced complex 2D and 3D structures of ordered monodisperse lattices by the micromolding in capillaries (MIMIC) technique [164]. An elastomeric mold patterned with micron-sized, open-ended channels was put into conformal contact with a clean support substrate, and a drop of particle suspension was placed on the substrate at one end of the mold.

NIH-PA Author Manuscript NIH-PA Author Manuscript NIH-PA Author Manuscript

The suspension filled the network of channels by capillary action. After solvent evaporation and mold peel-off, a pattern complementary to that of the mold was formed of structures of crystallized particles. The order of the lattice varied across the channels, progressively improving toward the exit end. This was consistent with the unidirectional liquid flow inside the channels. At the exit end, evaporation of water and attractive capillary forces between particles caused aggregation and nucleation of particles into a crystal. The water lost by evaporation induced a flow influx toward the open end which transported particles from the bulk fluid to the lattice, which thus kept growing. No ordered arrays were produced when channel filling started from both ends.

Park *et al* used the tendency of monodisperse colloidal spheres to organize themselves into ordered 3D structures when subjected to physical confinement to produce arrays of spheres with domain sizes as large as 1 cm^2 [165]. Their experimental set-up, shown in figure 25, comprised a cell composed of a layer of photoresist of variable thickness included between two glass substrates. The photoresist layer was patterned with shallow channels, while a small tube was attached to a hole in the top substrate. An aqueous dispersion of monodisperse beads was injected in the cell through the tube, and then a positive pressure was applied to force the solvent to flow through the channels. Continuous sonication forced the beads to adopt their most thermodynamically stable states. The beads accumulated at the bottom of the cell and, retained by the channels, assembled into a close-packed hexagonal lattice. The rate of packing was proportional to the applied pressure, while at fixed pressure the rate decreased with decreasing bead dimensions. Free-standing films could be produced by injecting curable polymers in the cell after solvent evaporation; being confined by the cell walls, the colloidal lattice was not deformed by the injection. The number of layers in the assembly could be precisely controlled by changing the ratio between the thickness of the cell and the diameter of the beads. The technique has also tight control over the surface morphology. It is fast, it works for colloidal particles of broad size range (from 50 nm to 50 μm) and it is independent of chemical composition and surface properties of the particles [142].

Shear forces were used by Amos *et al* to induce large-scale reorganization in colloidal crystals [166]. A suspension of 790 nm diameter particles was confined between two parallel glass slides placed at a normal distance of 10 μm. Capillary action caused the suspension to fill the entire cell in minutes, and a polycrystalline structure with small domains formed. To increase the domain size, a shear force was applied by slightly oscillating laterally the bottom slide with respect to the top one. This caused melting of the crystal. Upon removal of the shear, recrystallization rapidly reoccurred characterized by larger domain sizes. Vickreva *et al* used controlled oscillatory shear to enhance the packing of sedimenting latex microspheres [167].

Ordered 3D opaline arrays of colloidal particles can be used as templates for the fabrication of porous materials with precisely controlled pore sizes and highly ordered 3D porous structures (figure 26) [129]. This class of materials is called inverse or inverted opals, and could find application as PBG crystals, catalysts, membranes and low-k dielectric materials. The mechanism of production is in principle straightforward. After the original opaline array has been dried, the void spaces among the colloidal spheres are fully infiltrated via capillary action with a liquid precursor such as an UV- or thermally curable prepolymer, an organic monomer plus an initiator or a sol–gel precursor to a ceramic material; interstitial filling can also be accomplished with gaseous precursors or by electrodeposition. Subsequent solidification of the precursor and removal of colloidal spheres give the final, highly regular 3D porous structure. The possible pore dimensions span a range from tens of nanometers to tens of microns. The fidelity of the process is mainly determined by van der Waals interactions, wetting of the template surface, filling of the void spaces and shrinking of the precursor during solidification. Such templating procedure has been applied to a variety of materials, including organic polymers [168], ceramic materials [137, 138], semiconductors [169, 170], oxides

NIH-PA Author Manuscript NIH-PA Author Manuscript NIH-PA Author Manuscript

[171-173] and metals [174-176], the only limitation apparently being the availability of a precursor able to infiltrate among the colloidal spheres without significantly swelling or dissolving the template.

8. DNA self-assembly

DNA is a chain polymer that self-assembles into a double helix of base pairs. DNA plays a key role in living creatures by digitally encoding the genetic information required for protein synthesis through assembly of amino acids. Digitization and parallel synthesis in DNA have inspired programmable SA in nanotechnology. DNA is becoming the main building block for the bottom-up approach in nanotechnology. It attracts much attention since it is programmable and easy to replicate. As a building block, it is also easy to find in nature or synthesize under laboratory conditions. One can classify the work done in this field into two main groups: DNA as a structural material and DNA-mediated SA.

8.1. DNA as a structural material

Work with DNA as a structural material initially focused on building single structures, but has shifted toward more complex 2D and 3D periodic or aperiodic arrays in the last 5–6 years. Sticky ends, double crossovers (DX), Holliday junctions and hairpins are some of the motifs used for this purpose [177]. They all consist of DNA strands that connect or intertwine in a predictable fashion. Chen and Seeman demonstrated the first closed polyhedron [178]. They first assembled faces of a cube and then formed the cube through ligation. However, this cube was not a rigid structure. Since then, Seeman and co-workers have fabricated a truncated octahedron [179], Borromean rings [180], 2D arrays [181] and 8 and 12 arm junctions [182] using aforementioned motifs. They overcame the rigidity problem using the DX motif in their truncated octahedron [179]. However, a stepwise assembly method is used in those assemblies —assembling building blocks and using those building blocks to assemble bigger structures —requiring time-consuming intermediate processes. As building blocks are assembled through ligation, it is difficult to replicate those structures. Two problems, time-consuming processes and replication, were eliminated using single strand DNA (ssDNA) to construct nanostructures by Shih *et al* [183]. They folded a 1.7 kilobase ssDNA into a nanoscale octahedron using helping strands. In 2006, Rothemund introduced the term ‘DNA origami’ using a similar method to Shih's [184]. He used a ssDNA and short helping strands to fold it into an arbitrary 2D shape. He constructed smiling faces, equilateral triangles and stars to demonstrate the achievable complexity (figure 27). He employed a five-step design approach including approximating the desired shape, rasterizing, synthesis and assembly. He extended these 2D arrays as displays by adding hairpin structures similar to the ‘DNA barcode’ demonstrated by Yan *et al* [185]. Yan *et al* coded bit strings on DNA with the presence of a hairpin denoting ‘1’ and the absence denoting ‘0’. The bit string was coded on DX tiles and read using an atomic force microscope (AFM). Recently, Zhang *et al* constructed DNA icosahedra having 20 triangular faces using five-point star motifs [186]. After the construction, stars were no longer planar and bent 32° showing structural flexibility of DNA tiles.

In order to control DNA assembly, one should identify four elements of SA: components, driving force, binding force and environment. Components can be nucleotides, DNA strands or 2D and 3D structures made of DNA. Base–base hybridization is the binding force in DNA SA. This binding force is very specific with respect to base pair sequences and provides programmability in DNA assembly through arrangement of base sequences. Programmed or arranged sequences have very high affinity to conjugate sequences, leading to assembly of DNA strands or particles attached to DNA strands. Thermal vibration and Brownian motion can be taken as the driving force. This leads to the control of assembly rates through temperature. The environment is usually a solution and it may also include patterned substrates. DNA assembly suffers from local energy minima more than other assemblies. The first cube

structure demonstrated by Chen and Seeman had a very low yield, so as the truncated octahedron. However, this could be increased by controlling the temperature as shown by Goodman *et al* [187]. Goodman and co-workers used four ssDNA to form a tetrahedron. Their process started at 95 °C and the temperature was dropped to 4 °C while DNA strands assembled in a hierarchical way with a yield as high as 95%.

8.2. DNA-mediated self-assembly

DNA-mediated SA explores the potential of DNA scaffolds to assemble nanoscale circuits, sensors and assembly of microscale components through DNA hybridization. DNA SA offers precise assembly of nanoscale circuit components since it is programmable. However, electrical connection between those components has been a primary challenge. It is known that a DNA molecule has a very low conductance, exhibiting insulator characteristics. Thus, most work focused on enhancing electrical conductivity of DNA by metallization. Braun *et al* demonstrated a 12 μm long, 100 nm wide conductive silver wire formed by DNA metallization [188]. Their method included stretching of DNA between electrodes, localization of silver ions on DNA bases through ion exchange and further development of those ions. The resulting wire had an electrical resistance of several megaohms. Other groups working in that field reported metallization of DNA using palladium [189-192], platinum [193], silver [194-196], nickel [197], copper [198] and gold [199]. The lowest resistance reported in those studies is 200 Ω for a silver wire corresponding to a bulk resistivity of 2.4×10^{-6} Ω m [194], still much higher than a polycrystalline bulk resistivity of 1.6×10^{-8} Ω m. Linear double stranded DNA (dsDNA) was used in early studies on metallization. LaBean and co-workers demonstrated metallization of 4 × 4 nanoribbons [194] and triple crossover nanotubes [195] with silver, showing that metallization could be extended to potential scaffolds for nanoscale circuits. In the same year, Deng and Mao reported a DNA-assisted nanofabrication method for 2D metallic arrays on glass or mica surface [190]. Their method included unidirectional alignment and stretching of DNA chains on a solid surface, which may be a gateway to incorporate nanoscale structures with microscale chips. They reported construction of ordered 1D and 2D arrays by directed motion of a liquid drop as illustrated in figure 28. An alternative DNA stretching method is electrostretching: aligning DNA along the electric field [200]. Another regular 2D array which was envisioned to be a part of a memory system was designed by Le *et al* [199]. They assembled DNA–Au nanocomponents on a pre-assembled scaffold on a solid surface by hybridization.

DNA metallization methods presented up to now have good DNA-to-substrate metallization selectivity: metallization on the substrate is very low or does not occur. However, they are not selective to different bases, limiting the ability to pattern metal. Keren *et al* faced the problem introducing a DNA sequence-specific molecular lithography method on DNA chains [201]. They polymerized the RecA protein obtained from *Escherichia coli* on an ssDNA molecule as illustrated in figure 29(i). ssDNA bound to a dsDNA carrying a homologous sequence and served as a mask during metallization (figures 29(ii)–(iii)). They managed to build a gold wire with 25 Ω resistance demonstrating ohmic characteristics up to 200 nA. Carell and co-workers reported a method similar to molecular lithography in [202,203], where they used aldehyde to address non-metalized locations and perform two-layer metallization. Using molecular lithography, Karen *et al* self-assembled a carbon nanotube field-effect transistor [204]. They again used the RecA protein and homologous recombination. After recombination, biotin bound to RecA through anti-RecA, so did a streptavidin-functionalized carbon nanotube. Segments unprotected by RecA were then metalized. This work promoted DNA SA for carbon nanotube electronics. However, low yield and irreproducibility were still a problem. Recently, Wang *et al* constructed a nanostructure by functionalizing carbon nanotubes with ssDNA and metallization [205]. They argued that it could be used as a diode depending on the amount of metallization.

NIH-PA Author Manuscript NIH-PA Author Manuscript NIH-PA Author Manuscript

NIH-PA Author Manuscript NIH-PA Author Manuscript NIH-PA Author Manuscript

DNA is not only used as a scaffold in SA but also as a linking material. Bashir and co-workers demonstrated electrophoretic SA of 4 μm × 4 μm silicon components carrying a Au layer using charged ssDNA to link molecules [111]. Extending their work, they later assembled microscale polystyrene beads, nanoscale gold particles and microscale silicon islands [206]. They offered three strategies for assembly. The first method used hybridization between ssDNA attached to substrate and components. The second method employed biotin-avidin binding with avidin-coated particles and biotinylated DNA on the substrate. The last one employed biotinylated dsDNA on both surfaces and used avidin as a linking material. Using the last method, they presented SA of microscale silicon islands with a yield of 82%. Another study using both DNA hybridization and avidin-biotin binding was reported by Wang *et al.* They proposed [207] and later demonstrated [208] DNA-mediated SA of a quantum dot waveguide. The proposed method started with formation and patterning of SAM on silicon oxide to which the ssDNA bound. A biotinylated complementary strand hybridized with the strand bound to the substrate. SA was completed when streptavidin-linked quantum dots were assembled using streptavidin-biotin binding. Recently, Kusakabe *et al* proposed a sequential assembly method using ssDNA-attached micro/nanoparticles [209]. The proposed method employed DNA strands of different lengths corresponding to different hybridization temperatures to achieve a layer-by-layer assembly. The assembly method had promising results for nanoparticles while the results were not satisfactory for microscale components. This is a common problem faced by many DNA-mediated self-assemblies, since it is still unclear whether the DNA hybridization force is sufficient to overcome gravity, capillary and fluidic drag forces experienced by microscale particles.

8.3. Nanorobots and DNA computing

Besides self-assembled structures and DNA-mediated SA, DNA nanorobots and computers can be identified as the third mainstream in DNA studies. DNA computers can be constructed using a set of cleverly designed ‘DNA tiles’. DNA tiles are rigid supermolecular structures formed using double crossover molecules. DNA computers based on tiles can be used for universal computation, since Turing machines are known to be universal computers and Wang tiles are equivalent to Turing machines.

Adleman and Winfree showed that DNA computation can be used to solve combinatorial problems [210] and arithmetic calculations [211]. Adleman encoded a graph to solve the Hamiltonian path problem [210], while Winfree performed arithmetic calculations using input tiles and specific binding between tiles [211]. Fraulhammer expanded the field to RNA computation by solving a chess problem using RNA strands [212]. Later, Winfree and co-workers built a cellular automaton which updated itself using the XOR function and built DNA Sierpinski triangles [213]. They had error rates varying from 1% to 10%. Winfree and Bekbolatov proposed an error correcting method using proofreading tiles which halted assembly when an assembly error occurred till another error [214]. This provided some time for disassembly of the faulty state. Error correction efforts resulted in error-free [215] and error-tolerant systems [216]. Reif *et al* presented error-resilient DNA tiling assembly after a proofreading tiles method [217]. They reported compact error-resilient tiling methods without increasing the size of the tiling assembly. In contrast to that, Winfree and Bekbolatov's approach results in a structure four times bigger than the original size. DNA computation is a parallel process and has high data density, but it suffers from a long preparation process and lack of interface with larger scale objects for practical uses. Thus, it is likely that DNA computation will not replace electronic computers in the near future. However, it can serve as a platform to develop algorithmic SA methods. Experience and knowledge gained in the field of DNA computation can be used to build DNA nanostructures using cleverly designed DNA tiles. This may result in higher yield, precise control of growth using control tiles and error correction applications.

NIH-PA Author Manuscript

NIH-PA Author Manuscript

NIH-PA Author Manuscript

Another emerging field is DNA nanorobots that use DNA SA for building robots or mechanical structures in the nanoscale. DNA nanorobots make use of hybridization between DNA strands to create motion or direct transportation of materials. Yurke *et al* introduced molecular tweezers that open and close according to addition of strands carrying those commands (figure 30) [218]. Yin *et al* designed a track made of DNA that could carry a walker DNA [219]. The walker DNA was transported along the track by a series of enzyme-controlled hybridization and dehybridization events occurring between track DNA strands and the walker strand. Shin and Pierce developed a similar method where they employed linking strands that bound the walker to the anchor on the track [220]. This linking strand was removed using a complementary strand when the walker was moving to the next anchor. Ding and Seeman reported a robotic arm attached to a 2D DNA array for precise placement of molecules [221]. Robot arm movement was controlled by set strands.

DNA SA is a promising candidate to build nanoscale structures, circuits and nanorobots. As mentioned in the previous paragraph, DNA can be used to build molecular scale rigid structures that can be used to form superstructures. Superstructures can be programmed to assemble nanoscale electronic components and carbon nanotubes. After a selective metallization process, the superstructure can be turned into a nanoscale circuit. In order to reach that near future aim, DNA assembly yield should be improved demonstrating large-scale assemblies. Assemblies to form large structures will be critical to fill the gap between established microscale technology and emerging DNA assembly applications. DNA-mediated SA is also a powerful tool for fabrication of nanodevices. However, it is yet unclear whether it will expand to the microscale since hydrogen bonds do not scale up at the same rate as competing forces such as gravity. DNA-mediated assembly can be used for assembling larger components in a two-step process where DNA is used for recognition of assembly sites and an aiding material is used to supply larger binding force. Fine tuning of forward and reverse reaction rates is also required. DNA assemblies are promising overall, but they still experience a major problem: precise visualization. AFM and gel electrophoresis are the two methods used to monitor experimental results. The AFM is a contact measurement technique and is reported to damage DNA nanostructures [184]. This monitoring problem will be more critical in the near future when practical applications of DNA SA are ready for use in industry and scientific research.

9. Modeling of stochastic assembly dynamics

Vast literature is available on the modeling of the dynamics of various stochastic assembly processes. Models based on rate equations, in analogy with chemical kinetics, were introduced by Hosokawa *et al* to describe the time evolution of the discrete aggregates emerging in passive self-assembling systems [51,222]. Adleman *et al* developed a model for the SA of linear polymers out of molecular units [223]. The model is based on difference and differential equations with initial conditions, and allows the characterization of the resulting equilibria of the systems. Dehon *et al* described a stochastic model of a self-assembled nanowire-based address decoder [224]. White *et al* proposed a model for self-reconfigurable cellular robots based on passive stochastic self-organization [225]. Klavins introduced a graph grammar-based approach to model active reconfigurable assembly of programmable units [226].

Probabilistic approaches are common for the theoretical modeling of the dynamics of stochastic SA. Of pre-eminent interest are models which allow us to mathematically relate control and environmental parameters (e.g. shape and number of parts and binding sites, volumes, parts mobility, duration of experiments) to process requirements (e.g. expected time to achieve a predefined yield, throughput). SA proceeds by discrete stochastic assembly events, each taking place with non-null probabilities and error rates. Discrete mathematics and difference equations would be the natural setting for its description. However, discrete-time models quickly become exceedingly complex. Besides being easier and more intelligible, continuous-time models

NIH-PA Author Manuscript

NIH-PA Author Manuscript

NIH-PA Author Manuscript

based on differential equations can be thought as the limit of discrete models for large numbers of interacting parts and for high frequency of binding events.

In sections 9.1 and 9.2, we generalize and discuss two models—originally proposed by Verma *et al* [66] and by Zheng *et al* [75], respectively—describing the dynamics of part-to-template and part-to-part passive self-assembling systems.

For ease of modeling, we hereby assume that (1) part mobility and mixing is so that the parts can efficiently explore the entire physical assembly space; (2) the binding (i.e. assembly) and breaking (i.e. disassembly) probabilities are time-invariant and independent on the number of parts and binding sites present; (3) only two-body events are possible, both for assembly (i.e. the result of each single assembly event is a dimer) and disassembly processes. These simplifying assumptions will be critically assessed in section 9.3.

We first define the parameters used in the following models:

$N_P \equiv$ number of parts

$N_S \equiv$ number of binding sites (for 2D assembly) or target carriers (for 3D assembly)

$x(t) \equiv$ number of assembled parts $\equiv$ number of filled binding sites. The time dependence of x will be assumed throughout, but will not be shown in the following formulas for conciseness.

The above three parameters satisfy the inequality $0 \le x \le N_S \le N_P$.

$R_A \equiv$ rate of assembly

$R_D \equiv$ rate of disassembly.

9.1. Steady-state model

This modeling approach is based on an estimation of the rates of assembly and of disassembly processes acting in the system under consideration. It does not consider the time evolution of the system. According to the steady-state hypothesis, the asymptotic result of the assembly process is set by the equilibrium of the two concurrent tendencies. Applied to part-to-template SA, the result of the model resembles that of a first-order superficial adsorption process.

We first assume phenomenologically that the rate of assembly is proportional to the number of unassembled parts ($N_P - x$) and to the number of unfilled sites ($N_S - x$), i.e. $R_A = k_A (N_P - x)(N_S - x)$, where k_A is the assembly rate constant. The rate of disassembly is assumed to be proportional to the number of filled sites, i.e. $R_D = k_{D1}x$. This is a form of self-disassembly which may take place in noisy environments, e.g. when excessive vibration is induced on the template and consequently on the assembled parts.

To achieve the steady state, we require that

$$\frac{\mathrm{d}x}{\mathrm{d}t} = R_A - R_D = 0 \quad \Rightarrow \quad R_A\big|_{x\mathrm{eq}} = R_D\big|_{x\mathrm{eq}}. \tag{1}$$

Solving this quadratic equation for x_{eq} and defining $C_1 \equiv k_{D1}/k_A$, the filling ratio (or yield) $\theta \equiv x_{\mathrm{eq}}/N_S$ is obtained from the only possible equilibrium solution:

$$\theta = \frac{1}{2} + \frac{N_P + C_1}{2N_S} - \sqrt{\left(\frac{1}{2} + \frac{N_P + C_1}{2N_S}\right)^2 - \frac{N_P}{N_S}}. \quad (2)$$

The model suggests that a high assembly yield can be achieved by using redundant parts (i.e. a large part-to-binding site ratio; this is indeed commonly done in the literature [5,71,76,90]); by increasing the constant k_A representing the probability of assembly (e.g. by enhancing shape matching and selectivity between the parts and the sites; by improving part mobility and avoiding the obstruction of binding sites); and by decreasing the probability of disassembly represented by k_{D1} (e.g. by designing the system so that the desired assembly configuration is robust against noise, turbulent flow and other interferences).

Alternatively, disassembly of assembled parts may be caused by the number of residual parts present in the assembly space. The corresponding disassembly rate is $R_D = k_{D2}x(N_P - x)$. Since assembly proceeds by collisions, this disassembly process may be reasonably common in systems where the parts need to have enough kinetic energy to wander in space, and by hitting already assembled parts they may disassemble them. For $C_2 \equiv k_{D2}/k_A$, the filling ratio derived from equation (1) in this case becomes

$$\theta = \frac{1}{1 + C_2}. \quad (3)$$

Finally, both self-disassembly of assembled parts and concurrent disassembly induced by residual parts can be described in a single model. By putting $R_D = k_{D1}x + k_{D2}x(N_P - x)$ in equation (1), the general result for the filling ratio is

$$\theta = \frac{N_S + (1+C_2)N_P + C_1}{2(1+C_2)N_S} - \sqrt{\left(\frac{N_S + (1+C_2)N_P + C_1}{2(1+C_2)N_S}\right)^2 - \frac{N_P}{(1+C_2)N_S}}, \quad (4)$$

which includes equations (2) and (3) as special cases for $C_2 = 0$ and $C_1 = 0$, respectively.

9.2. Nonlinear time-continuous model

The time evolution of self-assembling systems is in general nonlinear, due to the collective behavior of the ensemble of parts. This is best described by a time-continuous model based on differential equations. For clarity, it is convenient in this setting to express the assembly and disassembly probability constants, introduced in the previous section, as inverse of time constants. We therefore define the average time-to-assembly $T_A \equiv 1/k_A$ and the average time-to-disassembly $T_D \equiv 1/k_D$. These are, in principle, the phenomenological parameter characteristics of the assembly system which could be experimentally estimated during multiple assembly runs. We define a self-assembly system *efficient* if $0 < T_A < T_D$, i.e. parts have time to assemble before some type of disassembly takes place.

As in the steady-state model, we assume that the assembly rate is proportional to the number of residual parts and to the number of unfilled sites, i.e. $R_A = [(N_P - x)(N_S - x)]/T_A$. We also introduce a general disassembly term D, which is a function of the number of filled sites x. Hence, we can derive a general first-order differential equation for the time evolution of the number of filled sites:

NIH-PA Author Manuscript NIH-PA Author Manuscript NIH-PA Author Manuscript

NIH-PA Author Manuscript

NIH-PA Author Manuscript

NIH-PA Author Manuscript

$$\frac{\mathrm{d}x}{\mathrm{d}t}=\frac{(N_P-x)(N_S-x)}{T_A}-\frac{D(x)}{T_D}. \tag{5}$$

The hypothesis of considering only two-body events has the mathematical consequence of making $D(x)$ of order 2 in x at the maximum. This in turns allows a closed-form analytical solution of equation (5), whose details depend on the specific form of $D(x)$.

Using the initial condition $x(t = 0) = 0$, the solution to equation (5) can be put in the form

$$x(t)=x_2\frac{\mathrm{e}^{(x_1-x_2)\frac{t}{T_A}}-1}{\mathrm{e}^{(x_1-x_2)\frac{t}{T_A}}-\frac{x_2}{x_1}}, \tag{6}$$

, where $x_1 \geq x_2 > 0$ are the roots of the second-order polynomial in x which appears during the solution of equation (5); they depend on N_P, N_S, T_A, T_D and on the coefficients of $D(x)$. According to equation (6), $x(t)$ shows an exponentially increasing trend with assembly time. In the limit of long assembly times, we get

$$\lim_{t\to\infty} x(t)=x_2. \tag{7}$$

Furthermore, by inverting equation (6) the assembly time required to achieve a desired assembly yield can be predicted.

The number of parts assembled at a certain time is thus dependent on the duration of the assembly process, on the number of parts, on the number of sites and on the time constants of the system. We now look at particular cases.

(1) *No disassembly possible*. This is the case for $T_D \to \infty$, valid for systems whose assembled state is very stable. For this value of T_D, we get $x_1 = N_P$ and $x_2 = N_S$. Hence, in the absence of disassembling forces, according to equation (7), the model predicts the asymptotic filling of all binding sites in time. This means that, in principle (i.e. excluding defects and damage to parts), stochastic SA can achieve 100% assembly yield. However, the assembly procedure may need to terminate within a predetermined time, so that the maximal assembly yield may be out of reach in practice.

Case (1) is the particular case originally considered by Zheng *et al* [75]. In their experimental work, they reported the exponentially increasing yield of the assembly for a linear increase of assembly time. They also estimated the time-to-assembly constant T_A by measuring the mean capture time for a single part and a single target carrier in the assembly space. Exponential increase of assembly yield as a function of time was also demonstrated by Stauth and Parviz [71].

(2) *Disassembly proportional to residual parts and filled sites.* In this case, typical of part-to-template assembly with no substrate vibration, the disassembly term of equation (5) has the form $D(x) = x[N_P - x]/T_D$, which leads to $x_1 = N_P$ and $x_2 = N_S/(1 + T_A/T_D)$. Thus, according to the model a finite time-to-disassembly constant implies an asymptotical yield always lower than 100%. In analogy to the work of Zheng *et al*, T_D could be estimated as the mean time-to-disassembly of single assembled parts.

(3) *Disassembly in part-to-part assembly*. For a general treatment of disassembly events in this setting, all possible collision events between assembled parts on one side and

assembled parts, unassembled parts and residual target carriers on the other need to be considered—because each of these events can in principle induce disassembly. The disassembly term of equation (5) then assumes the form

$$D(x)=\frac{x\left[(N_S-x)+(N_P-x)+\frac{x-1}{2}\right]}{T_D}.$$

The closed-form solution of equation (5) for this case, though not handy, can nonetheless be interpreted along similar lines as those discussed in the previous scenarios.

9.3. Limits of the models

The constants that were introduced in the models lump many interacting factors. Some of them may be experimentally determined (e.g. mean time-to-(dis)assembly). Nonetheless, a complete theoretical model should be able to derive such parameters from first principles, e.g. from the equations describing the physics of the interactions driving the assembly.

Multi-body collision events were not considered. These are less and less probable the larger the number of parts involved. Still, they may take place and influence the history of the assembly. For example, in capillary SA more than one part can impinge on the same binding site, and the removal of one of them may alter the integrity of the fluid coating.

As seen above, enhanced assembly speed and yield may be achieved using a large parts-to-sites ratio. This can be done without significant consequences on the processing costs when the excess parts can be retrieved after the assembly and recycled. There could be a limit on the maximum number of parts present in the environment during assembly runs. A high part density may increase the chance of collision and damage, which could irreversibly decrease the yield. It may also impair the transport and mixing of the parts themselves: this would alter the assembly rates, making them density-dependent. Thus the assumptions of the models presented above are valid for ensembles containing not-too-many parts, or parts whose occupied (e.g. excluded) volume is reasonably smaller than the total volume. This is in analogy with models of ideal solutions and much diluted gases. In this setting, though, the discrete nature of assembly events may not be neglected. For example, assembly events may be interpreted as transitions between the reachable discrete states of the system. The system could then be described by an oriented graph governed by probabilistic transition rules. The theories of Markov chains and graph grammars could constitute solid foundations for similar approaches.

Finally, we treated the assembly processes as reaction-limited, by assuming all parts sufficiently mobile to reach all binding sites. This requires ideal mixing and transport mechanisms. The more common diffusion-limited assembly processes [227], where parts can practically have access only to a limited number of binding sites, require different mathematical models to be described, possibly involving spatially-dependent diffusion and transport terms.

10. Conclusions

'More than Moore' is one of the main ascending trends in current microelectronics. It focuses on the realization of new, powerful devices borne from the integration of different functional modules into standalone systems. It is thus to be expected that, as the dimensions of components and modules downscale, and as the market for multifunctional devices expands, the need will arise for an efficient packaging technology which can be adopted to efficiently assemble heterogeneous microsystems.

NIH-PA Author Manuscript
NIH-PA Author Manuscript
NIH-PA Author Manuscript

NIH-PA Author Manuscript NIH-PA Author Manuscript NIH-PA Author Manuscript

SA constitutes a viable packaging paradigm to meet such a challenge. In this review we have discussed its main embodiments, which exploit a diverse set of driving forces (gravitational, capillary, electric, magnetic, chemical) and span a wide range of physical sizes (from milli- to nanoscale). Compared to robotic pick-and-place, SA techniques are parallel in nature, and can avoid the direct contact between manipulators and components, two features that can boost their throughput and efficiency.

Only a few of the techniques and applications we have presented have so far reached such a stage of development as to be ready for industrial adoption. Further experimental and theoretical work is needed to enhance the yield of SA and deepen our knowledge of its working principles.

Particularly, we believe that the algorithmic and programming aspects of SA should be thoroughly explored. We need a more systematic theory of SA. The fundamental relationship between SA and (universal) computation has been substantiated by groundbreaking and far-reaching work on DNA computing and graph grammars, which combine formal programming concepts and tools with structural chemistry. Nonetheless, the modeling of SA remains far from straightforward, given its multi-disciplinary nature and the broad spectrum of effects and aspects it involves.

Acknowledgments

MM was supported by a Fonds Wetenschappelijk Onderzoek (FWO) grant for this work. SA, CV, and KFB were supported in part by National Science Foundation grant ECS-05-1628, Intel Corporation contract 30412 and the DARPA Center for Interfacial Engineering of Microelectromechanical Systems (CIEMS).

References

1. Morris CJ, Stauth SA, Parviz BA. Self-assembly for microscale and nanoscale packaging: steps toward self-packaging. IEEE Trans. Adv. Packag 2005;28:600–11.
2. Fearing, RS. Survey of sticking effects for micro parts handling; IEEE/RSJ Int. Workshop on Intelligent Robots and Systems (IROS); Pittsburgh, PA. 1995.
3. Arai, F.; Ando, D.; Fukuda, T. Adhesion forces reduction for micro manipulation based on micro physics; IEEE Conf. on MEMS; 1996.
4. Whitesides GM, Grzybowski B. Self-assembly at all scales. Science 2002;295:2418–21. [PubMed: 11923529]
5. Yeh HJ, Smith JS. Fluidic self-assembly for the integration of GaAs light-emitting diodes on Si substrates. IEEE Photonics Technol. Lett 1994;6:706–8.
6. Srinivasan U, Liepmann D, Howe RT. Microstructure to substrate self-assembly using capillary forces. J. Microelectromech. Syst 2001;10:17–24.
7. Jacobs HO, Tao AR, Schwartz A, Gracias DH, Whitesides GM. Fabrication of a cylindrical display by patterned assembly. Science 2002;296:323–5. [PubMed: 11951039]
8. Xiong X, Hanein Y, Fang J, Wang Y, Wang W, Schwartz DT, Böhringer KF. Controlled multibatch self-assembly of microdevices. J. Microelectromech. Syst 2003;12:117–27.
9. Chung J, Zheng W, Hatch TJ, Jacobs HO. Programmable reconfigurable self-assembly: parallel heterogeneous integration of chip-scale components on planar and nonplanar surfaces. J. Microelectromech. Syst 2006;15:457–64.
10. Sharma R. Thermally controlled fluidic self-assembly. Langmuir 2007;23:6843–9. [PubMed: 17497901]
11. Liu M, Lau WM, Yang J. On-demand multi-batch self-assembly of hybrid MEMS by patterning solders of different melting points. J. Micromech. Microeng 2007;17:2163–8.
12. Schreiber F. Structure and growth of self-assembling monolayers. Prog. Surf. Sci 2000;65:106.
13. Love JC, Estroff LA, Kriebel JK, Nuzzo RG, Whitesides GM. Self-assembled monolayers of thiolates on metals as a form of nanotechnology. Chem. Rev 2005;105:68.

NIH-PA Author Manuscript NIH-PA Author Manuscript NIH-PA Author Manuscript

14. Pister, KSJ. Hinged polysilicon structures with integrated CMOS TFTs; 5th Solid-State Sensor and Actuator Workshop; Hilton Head Island, SC. 1992.
15. Isamoto K, Makino T, Moroswa A, Chong C, Fujita H, Toshiyoshi H. Self-assembly technique for MEMS vertical comb electrostatic actuator. IEICE Electron. Express 2005;2:311–5.
16. Agache V, Quévy E, Collard D, Buchaillot L. Stiction-controlled locking system for three-dimensional self-assembled microstructures: theory and experimental validation. Appl. Phys. Lett 2001;79:3869–71.
17. Rose F, Hattori M, Kobayashi D, Toshiyoshi H, Fujita H, Kawakatsu H. Application of capillary forces and stiction for lateral displacement, alignment, suspension and locking of self-assembled microcantilevers. J. Micromech. Microeng 2006;16:2077–85.
18. Ebefors T, Kalvesten E, Stemme G. New small radius joints based on thermal shrinkage of polyimide in V-grooves for robust self-assembly 3D microstructures. J. Micromech. Microeng 1998;8:188–94.
19. Kaajakari, V.; Lal, A. Electrostatic batch assembly of surface MEMS using ultrasonic triboelectricity; 14th Int. Conf. on Micro Electro Mechanical Systems; 2001.
20. Lai, KWC.; Hui, AP.; Li, WJ. IEEE MEMS. Las Vegas, NV: 2002. Non-contact batch micro-assembly by centrifugal force.
21. Shimoyama, I.; Kano, O.; Miura, H. 3D micro-structures folded by Lorentz force; Proc. 11th Ann. Workshop on Micro Electro Mechanical Systems; Heidelberg, Germany. 1998.
22. Iwase E, Shimoyama I. Multistep sequential batch assembly of three-dimensional ferromagnetic microstructures with elastic hinges. IEEE J. Microelectromech. Syst 2005;14:1265–71.
23. Harsh, KF.; Bright, VM.; Lee, YC. Study of micro-scale limits of solder self-assembly for MEMS; 50th Electronic Components and Technology Conf; Las Vegas, NV. 2000.
24. Syms RRA. Equilibrium of hinged and hingeless structures rotated using surface tension forces. IEEE J. MEMS 1995;4:177–84.
25. Syms RRA. Rotational self-assembly of complex microstructures by the surface tension of glass. *Sensors Actuators* A 1998;65:238–43.
26. Syms RRA. Surface tension powered self-assembly of 3-D micro-optomechanical structures. J. Microelectromech. Syst 1999;8:448–55.
27. Harsh, K.; Lee, YC. Modeling of solder self-assembled MEMS; Conf. on Micro-Optics Integration and Assemblies; San Jose, CA. 1998.
28. Syms RRA, Yeatman EM, Bright VM, Whitesides GM. Surface tension-powered self-assembly of microstructures—the state-of-the-art. J. Microelectromech. Syst 2003;12:387–417.
29. Gracias DH, Kavthekar V, Love JC, Paul KE, Whitesides GM. Fabrication of micrometer-scale, patterned polyhedra by self-assembly. Adv. Mater 2002;14:235–8.
30. Leong TG, Lester PA, Koh TL, Call EK, Gracias DH. Surface tension-driven self-folding polyhedra. Langmuir 2007;23:8747–51. [PubMed: 17608507]
31. Cho JH, Hu S, Gracias DH. Self-assembly of orthogonal three-axis sensors. Appl. Phys. Lett 2008;93:043505.
32. Saeedi S, Abbasi S, Böhringer KF, Parviz BA. Molten-alloy driven self-assembly for nano and micro scale system integration. Fluid Dyn. Mater. Process 2006;2:221–45.
33. Fang, J.; Bohringer, KF. Self-assembly. In: Gianchandani, YB.; Tabata, O.; Zappe, H., editors. Comprehensive Microsystems. Amsterdam: Elsevier: 2008. p. 403-27.
34. Srinivasan U, Helmbrecht MA, Rembe C, Muller RS, Howe RT. Fluidic self-assembly of micromirrors onto microactuators using capillary forces. IEEE J. Sel. Top. Quantum Electron 2002;8:4–11.
35. Scott KL, Hirano T, Yang H, Singh H, Howe RT, Niknejad AM. High-performance inductors using capillary based fluidic self-assembly. J. Microelectromech. Syst 2004;13:300–9.
36. Fang J, Wang K, Böhringer KF. Self-assembly of PZT actuators for micropumps with high process repeatability. J. Microelectromech. Syst 2006;15:871–8.
37. Fang J, Böhringer KF. Parallel micro component-to-substrate assembly with controlled poses and high surface coverage. J. Micromech. Microeng 2006;16:721–30.

NIH-PA Author Manuscript NIH-PA Author Manuscript NIH-PA Author Manuscript

38. Fukushima, T.; Yamada, Y.; Kikuchi, H.; Tanaka, T.; Koyanagi, M. Self-assembly process for chip-to-wafer three-dimensional integration; Electronic Components and Technology Conf; Reno, NV. 2007.
39. Fukushima, T.; Kikuchi, H.; Yamada, Y.; Konno, T.; Liang, J.; Sasaki, K.; Inamura, K.; Tanaka, T.; Koyanagi, M. New three-dimensional integration technology based on reconfigured wafer-on-wafer bonding technique; IEEE Int. Electron Devices Meeting; Washington, DC. 2007.
40. Brakke KA. The surface evolver. Exp. Math 1992;1:141–65.
41. Van Veen N. Analytical derivation of the self-alignment motion of flip chip soldered components. J. Electron. Packag 1999;121:6.
42. Greiner, A.; Lienemann, J.; Korvink, JG.; Xiong, X.; Hanein, Y.; Bohringer, KF. Capillary forces in micro-fluidic self-assembly; 5th Int. Conf. Modeling and Simulations of Microsystems; San Juan, Puerto Rico. 2002.
43. Zhang X, Chen C-C, Bernstein RW, Zappe S, Scott MP, Solgaard O. Microoptical characterization and modeling of positioning forces on Drosophila embryos self-assembled in two-dimensional arrays. IEEE J. Microelectromech. Syst 2005;14:11.
44. Lienemann J, Greiner A, Kornink JG, Xiong X, Hanein Y, Bohringer KF. Modeling, simulation and experimentation of a promising new packaging technology—parallel fluidic self-assembly of micro devices. Sensors Update 2003;13:41.
45. Tay, AAO.; Li, H.; Gao, X.; Chen, J.; Kripesh, V. Simulation of forces acting on tiny chips during fluidic self-assembly; Electronic Packaging Technology Conf; 2006.
46. Lu, Y.; Xia, S.; Liu, M.; Zhang, J. Dynamic simulation of MEMS self-assembly using capillary force; IEEE Int. Conf. on Nano/Micro Engineered and Molecular Systems; Zhuhai, China. 2006.
47. Bohringer, KF.; Srinivasan, U.; Howe, RT. Modelling of capillary forces and binding sites for fluidic self-assembly; IEEE Int. Conf. on Micro Electro Mechanical Systems; 2001.
48. Xiong, X.; Liang, S-H.; Bohringer, KF. Geometric binding site design for surface-tension driven self-assembly; IEEE Int. Conf. on Robotics and Automation; 2004.
49. Xiong, X.; Hanein, Y.; Wang, W.; Schwartz, DT.; Bohringer, KF. Multi-batch micro-selfassembly via controlled capillary forces; IEEE Int. Conf. on Intelligent Robots and Systems; 2001.
50. Mastrangeli M, Ruythooren W, Van Hoof C, Celis J-P. Conformal dip-coating of patterned surfaces for capillary die-to-substrate self-assembly. J. Micromech. Microeng 2009;19:045015.
51. Hosokawa K, Shimoyama I, Miura H. Two-dimensional micro-self-assembly using the surface tension of water. *Sensors Actuators* A 1996;57:117–25.
52. Bowden N, Choi IS, Grzybowski B, Whitesides GM. Mesoscale self-assembly of hexagonal plates using lateral capillary forces: synthesis using the 'capillary bond'. J. Am. Chem. Soc 1999;121:5373–91.
53. Kralchevsky PA, Nagayama K. Capillary forces between colloidal particles. Langmuir 1994;10:14.
54. Klavins, E. Toward the control of self-assembling systems. In: Bicchi, A.; Christensen, H.; Prattichizzo, D., editors. Control Problems in Robotics. Berlin: Springer: 2003. p. 153-68.
55. Rothemund PWK. Using lateral capillary forces to compute by self-assembly. Proc. Natl Acad. Sci 2000;97:984–9. [PubMed: 10655471]
56. Tien J, Breen TL, Whitesides GM. Crystallization of millimeter-scale objects with use of capillary forces. J. Am. Chem. Soc 1998;120:12670–1.
57. Breen TL, Tien J, Oliver SRJ, Hadzic T, Whitesides GM. Design and self-assembly of open, regular, 3D mesostructures. Science 1999;284:948–51. [PubMed: 10320372]
58. Gracias DH, Boncheva M, Omoregie O, Whitesides GM. Biomimetic self-assembly of helical electrical circuits using orthogonal capillary interactions. Appl. Phys. Lett 2002;80:2802–4.
59. Gracias DH, Tien J, Breen TL, Hsu C, Whitesides GM. Forming electrical networks in three dimensions by self-assembly. Science 2000;289:1170–2. [PubMed: 10947979]
60. Clark TD, Tien J, Duffy DC, Paul KE, Whitesides GM. Self-assembly of 10-μm-sized objects into ordered three-dimensional arrays. J. Am. Chem. Soc 2001;123:7677–82. [PubMed: 11480990]
61. Oliver SRJ, Bowden N, Whitesides GM. Self-assembly of hexagonal rod arrays based on capillary forces. J. Colloid Interface Sci 2000;224:425–8. [PubMed: 10727355]

NIH-PA Author Manuscript NIH-PA Author Manuscript NIH-PA Author Manuscript

62. Gu Z, Chen Y, Gracias DH. Surface tension driven self-assembly of bundles and networks of 200 nm diameter rods using a polymerizable adhesive. Langmuir 2004;20:11308–11. [PubMed: 15595750]
63. Morris CJ, Ho H, Parviz BA. Liquid polymer deposition on free-standing microfabricated parts for self-assembly. J. Microelectromech. Syst 2006;15:1795–804.
64. Bohringer KF. Surface modification and modulation in microstructures: controlling protein adsorption, monolayer desorption and micro-self-assembly. J. Micromech. Microeng 2003;13:S1–10.
65. Smith, JS. High density, low parasitic direct integration by fluidic self assembly (FSA); Int. Electron Devices Meeting; 2000.
66. Verma, AK.; Hadley, MA.; Yeh, H-JJ.; Smith, JS. Fluidic self-assembly of silicon microstructures; Electronic Components and Technology Conf; Las Vegas, NV, USA. 1995.
67. Tu JK, Talghader JJ, Hadley MA, Smith JS. Fluidic self-assembly of InGaAs vertical cavity surface emitting lasers onto silicon. IEEE Electron. Lett 1995;31:1448–9.
68. Soga I, Hayashi S, Ohno Y, Kishimoto S, Maezawa K, Mizutani T. Direct integration of GaAs HEMTs on AlN ceramic substrates using fluidic self-assembly. IEEE Electron. Lett 2005;41:1275–6.
69. Soga I, Ohno Y, Kishimoto S, Maezava K, Mizutani T. Fluidic assembly of thin GaAs blocks on Si substrates. Japan. J. Appl. Phys 2003;42:2226–9.
70. Soga I, Ohno Y, Kishimoto S, Maezava K, Mizutani T. Fluid dynamic assembly of semiconductor blocks for heterogeneous integration. Japan. J. Appl. Phys 2004;43:5951–4.
71. Stauth SA, Parviz BA. Self-assembled single-crystal silicon circuits on plastic. Proc. Natl Acad. Sci 2006;103:13922–7. [PubMed: 16968780]
72. Saeedi S, Kim S, Parviz BA. Self-assembled crystalline semiconductor optoelectronics on glass and plastic. J. Micromech. Microeng 2008;18:1–7.
73. Zheng W, Jacobs HO. Shape-and-solder-directed self-assembly to package semiconductor device segments. Appl. Phys. Lett 2004;85:3635–7.
74. Chung SE, Park W, Shin S, Lee SA, Kwon S. Guided and fluidic self-assembly of microstructures using railed microfluidic channels. Nat. Mater 2008;7:581–7. [PubMed: 18552850]
75. Zheng W, Jacobs HO. Fabrication of multicomponent microsystems by directed three-dimensional self-assembly. Adv. Funct. Mater 2005;15:732–8.
76. Zheng W, Chung J, Jacobs HO. Fluidic heterogeneous microsystems assembly and packaging. J. Microelectromech. Syst 2006;15:864–70.
77. Fang J, Böhringer KF. Wafer-level packaging based on uniquely orienting self-assembly (the DUO-SPASS processes). J. Microelectromech. Syst 2006;15:531–40.
78. Ong, YY.; Lim, YL.; Yan, LL.; Vempati, S.; Liao, EB.; Kripesh, V.; Yoon, SU. Self-assembly of components using shape matching; Electronics Packaging Technology Conf; 2007.
79. Ong, YY.; Lim, YL.; Yan, LL.; Liao, EB.; Kripesh, V. Int. Electronic Manufacturing Technology. Putrajaya, Malaysia: 2006. Dry self-assembly and gang bonding of microcomponents from silicon carrier to substrate wafer.
80. Park, S.; Böhringer, KF. IEEE MEMS. Tucson, AZ: 2008. A fully dry self-assembly process with proper in-plane orientation.
81. Niarchos D. Magnetic MEMS: key issues and some applications. *Sensors Actuators* A 2003;109:166–73.
82. Agashe JS, Arnold DP. A study of scaling and geometry effects on the forces between cuboidal and cylindrical magnets using analytical force solutions. J. Phys. D: Appl. Phys 2008;41:105001–9.
83. Cugat O, Delamare J, Reyne G. Magnetic micro-actuators & systems: MAGMAS. IEEE Trans. Magn 2003;39:3607–12.
84. Yando S. Method and apparatus for fabricating an array of discrete elements I. US Patent 1969:3439416.
85. Fonstad CJ. Magnetically-assisted statistical assembly—a new heterogeneous integration technique. MIT Technical Report. 2002
86. Perkins, JM. Magnetically assisted statistical assembly of III-V heterostructures on silicon: initial process and technology development, Department of Electrical Engineering and Computer Science. Massachusetts Institute of Technology; 2002.

NIH-PA Author Manuscript NIH-PA Author Manuscript NIH-PA Author Manuscript

87. Shet S, Mehta VR, Fiory AT, Lepselter MP, Ravindra NM. The magnetic field-assisted assembly of nanoscale semiconductor devices: a new technique. J. Miner. Met. Mater. Soc 2004;56:32–4.

88. Rivero RD, Shet S, Booty MR, Fiory AT, Ravindra NM. Modeling of magnetic-field-assisted assembly of semiconductor devices. J. Electron. Mater 2008;37:374–8.

89. Ramadan Q, Uk YS, Vaidyanathan K. Large scale microcomponents assembly using an external magnetic array. Appl. Phys. Lett 2007;90:172502–1.

90. Shetye SB, Eskinazi I, Arnold DP. Self-assembly of millimeter-scale components using integrated micromagnets. IEEE Trans. Magn 2008;44:4293–6.

91. Boncheva M, Andreev SA, Mahadevan L, Winkleman A, Reichman DR, Prentiss MG, Whitesides S, Whitesides GM. Magnetic self-assembly of three-dimensional surfaces from planar sheets. Proc. Natl Acad. Sci 2005;102:3924–9.

92. Golosowsky M, Saado Y, Davidov D. Self-assembly of floating magnetic particles into ordered structures: a promising route for the fabrication of tunable photonic band gap materials. Appl. Phys. Lett 1999;75:4168–70.

93. Grzybowski BA, Stone HA, Whitesides GM. Dynamic self-assembly of magnetized, millimetre-sized objects rotating at a liquid-air interface. Nature 2000;405:1033–6. [PubMed: 10890439]

94. Grzybowski BA, Jiang X, Stone HA, Whitesides GM. Dynamic, self-assembled aggregates of magnetized, millimeter-sized objects rotating at a liquid-air interface: macroscopic, two-dimensional classical artificial atoms and molecules. Phys. Rev. E 2001;64:011603–1.

95. Grzybowski BA, Whitesides GM. Macroscopic synthesis of self-assembled dissipative structures. *J. Phys. Chem.* B 2001;105:8770–5.

96. Grzybowski BA, Whitesides GM. Directed dynamic self-assembly of objects rotating on two parallel fluid interfaces. J. Chem. Phys 2002;116:8571–7.

97. Ng JMK, Fuerstman MJ, Grzybowski BA, Stone HA, Whitesides GM. Self-assembly of gears at a fluid-air interface. J. Am. Chem. Soc 2003;125:7948–58. [PubMed: 12823016]

98. Grzybowski BA, Radkowski M, Campbell CJ, Lee J, Whitesides GM. Self-assembling fluidic machines. Appl. Phys. Lett 2004;84:1798–800.

99. Grzybowski BA, Campbell CJ. Complexity and dynamic self-assembly. Chem. Eng. Sci 2004;59:1667–76.

100. Yellen BB, Friedman G. Programmable assembly of heterogeneous colloidal particle arrays. Adv. Mater 2004;16:111–5.

101. Tanase M, Bauer LA, Hultgren A, Silevitch DM, Sun L, Reich DH, Searson PC, Meyer GJ. Magnetic alignment of fluorescent nanowires. Nano Lett 2001;1:155–8.

102. Tanase M, Silevitch DM, Hultgren A, Bauer LA, Searson PC, Meyer GJ, Reich DH. Magnetic trapping and self-assembly of multicomponent nanowires. J. Appl. Phys 2002;91:8549–51.

103. Ye H, Gu Z, Yu T, Gracias DH. Integrating nanowires with substrates using directed assembly and nanoscale soldering. IEEE Trans. Nanotech 2006;5:62–6.

104. Love JC, Urbach AR, Prentiss MG, Whitesides GM. Three-dimensional self-assembly of metallic rods with submicron diameters using magnetic interactions. J. Am. Chem. Soc 2003;125:12696–7. [PubMed: 14558803]

105. Jones TB, Kraybill JP. Active feedback-controlled dielectrophoretic levitation. J. Appl. Phys 1986;60:1247–52.

106. Kaler, KVIS.; Tai, AKC. Dynamic (active feedback controlled) dielectrophoretic levitation of Canola protoplasts; IEEE Ann. Int. Conf. Engineering in Medicine and Biology Society; 1998.

107. Van Brussel H, Peirs J, Reynaerts D, Delchambre A, Reinhart G, Roth N, Weck M, Zussman E. Assembly of microsystems. CIRP Ann 2000;49:451–72.

108. Edman CF, Swint RB, Gurtner C, Formosa RE, Roh SD, Lee KE, Swanson PD, Ackley DE, Coleman JJ, Heller MJ. Electric field directed assembly of an InGaAs LED on silicon circuitry. IEEE Photonics Technol. Lett 2000;12:1198–200.

109. O'Riordan A, Delaney P, Redmond G. Field configured assembly: programmed manipulation and self-assembly at the mesoscale. Nano Lett 2004;4:761–5.

NIH-PA Author Manuscript NIH-PA Author Manuscript NIH-PA Author Manuscript

110. Esener, SC.; Hartmann, D.; Heller, MJ.; Cable, JM. DNA assisted micro-assembly: a heterogeneous integration technology for optoelectronics. In: Hussain, A., editor. Critical Review of Optical Science and Technology. San Jose, CA: Photonics West: 1998.
111. Lee SW, McNally HA, Guo D, Pingle M, Bergstrom DE, Bashir R. Electric-field-mediated assembly of silicon islands coated with charged molecules. Langmuir 2002;18:3383–6.
112. Hughes MP. Electric-field-mediated assembly of silicon islands coated with charged molecules. Nanotechnology 2000;11:124–32.
113. Castellanos A, Ramos A, Gonzalez A, Green NG, Morgan H. Electrohydrodynamics and dielectrophoresis in microsystems: scaling law. J. Phys. D: Appl. Phys 2003;36:2584–97.
114. Li H, Bashir R. Dielectrophoretic separation and manipulation of live and heat-treated cells of Listeria on microfabricated devices with interdigitated electrodes. *Sensors Actuators* B 2002;86:215–21.
115. Lee SW, Bashir R. Dielectrophoresis and electrohydrodynamics-mediated fluidic assembly of silicon resistors. Appl. Phys. Lett 2003;83:3833–5.
116. Lee SW, Bashir R. Dielectrophoresis and chemically mediated directed self-assembly of micrometer-scale three-terminal metal oxide semiconductor field-effect transistors. Adv. Mater 2005;17:2671–7.
117. Cohn, MB. Assembly Techniques for Microelectromechanical Systems. Berkley, CA: University of California: 1992.
118. Bhatt KH, Velev OD. Control and modeling of the dielectrophoretic assembly of on-chip nanoparticle wires. Langmuir 2004;20:467–76. [PubMed: 15743092]
119. Lumsdon OS, Kaler EW, Williams JP, Velev OD. Dielectrophoretic assembly of oriented and switchable two-dimensional photonic crystals. Appl. Phys. Lett 2003;82:949–51.
120. Smith PA, Nordquist CD, Jackson TN, Mayer TS, Martin BR, Mbindyo J, Mallouk TE. Electric-field-assisted assembly and alignment of metallic nanowires. Appl. Phys. Lett 2000;77:1399–401.
121. Nagahara LA, Amlani I, Levenstein J, Tsui RK. Directed placement of suspended carbon nanotubes for nanometer-scale assembly. Appl. Phys. Lett 2002;80:3826–8.
122. Boote JJ, Evans SD. Dielectrophoretic manipulation and electrical characterization of gold nanowires. Nanotechnology 2005;16:1500–5.
123. Liu Y, Chung JH, Liu WK, Ruoff RS. Dielectrophoretic assembly of nanowires. *J. Phys. Chem.* B 2006;110:14098–106. [PubMed: 16854106]
124. Papadakis SJ, Gu Z, Gracias DH. Dielectrophoretic assembly of reversible and irreversible metal nanowire networks and vertically aligned arrays. Appl. Phys. Lett 2006;88:233118–20.
125. Evoy S, et al. Dielectrophoretic assembly and integration of nanowire devices with functional CMOS operating circuitry. Microelectron. Eng 2004;75:31–42.
126. Chan RHM, Fung CKM, Li WJ. Rapid assembly of carbon nanotubes for nanosensing by dielectrophoretic force. Nanotechnology 2004;15:S672–7.
127. Bohringer, K-F.; Goldberg, K.; Cohn, M.; Howe, R.; Pisano, A. Parallel microassembly with electrostatic force fields; IEEE Int. Conf. on Robotics & Automation; Leuven, Belgium. 1998.
128. Grzybowski BA, Winkleman A, Wiles JA, Brumer Y, Whitesides GM. Electrostatic self-assembly of macroscopic crystals using contact electrification. Nat. Mater 2003;2:241–5. [PubMed: 12690397]
129. Xia Y, Gates B, Yin Y, Lu Y. Monodispersed colloidal spheres: old materials with new applications. Adv. Mater 2000;12:693–713.
130. Hayashi S, Kumamoto Y, Suzuki T, Hirai T. Imaging by polystyrene latex particles. J. Colloid Interface Sci 1991;144:538–47.
131. Lenzmann F, Li K, Kitai AH, Stover HDH. Thin-film micropatterning using polymer microspheres. Chem. Mater 1994;6:156–9.
132. Burmeister F, Schafle C, Matthes T, Bohmisch M, Boneberg J, Leiderer P. Colloid monolayers as versatile lithographic masks. Langmuir 1997;13:2983–7.
133. Boneberg J, Burmeister F, Schafle C, Leiderer P, Reim D, Fery A, Herminghaus S. The formation of nano-dot and nano-ring structures in colloidal monolayer lithography. Langmuir 1997;13:7080–4.

NIH-PA Author Manuscript NIH-PA Author Manuscript NIH-PA Author Manuscript

134. Hulteen JC, Van Duyne RP. Nanosphere lithography: a materials general fabrication process for periodic particle array surfaces. *J. Vac. Sci. Technol.* A 1995;13:1553–8.
135. Norris DJ, Arlinghaus EG, Meng L, Heiny R, Scriven LE. Opaline photonic crystals: how does self-assembly work? Adv. Mater 2004;16:1393–9.
136. Sacks MD, Tseng T-Y. Preparation of SiO_2 glass from model powder compacts: I. Formation and characterization of powders, suspensions, and green compacts. J. Am. Ceram. Soc 1984;67:526–32.
137. Velev OD, Jede TA, Lobo RF, Lenhoff AM. Porous silica via colloidal crystallization. Nature 1997;389:447–8.
138. Velev OD, Jede TA, Lobo RF, Lenhoff AM. Microstructured porous silica obtained via colloidal crystal templates. Chem. Mater 1998;10:3597–602.
139. Weissman JM, Sunkara HB, Tse AS, Asher SA. Thermally switchable periodicities and diffraction from mesoscopically ordered materials. Science 1996;274:959–63. [PubMed: 8875932]
140. Chang S-Y, Liu L, Asher SA. Preparation and properties of tailored morphology, monodisperse colloidal silica-cadmium sulfide nanocomposites. J. Am. Chem. Soc 1994;116:6739–44.
141. Xia Y, Gates B, Li Z-Y. Self-assembly approaches to three-dimensional photonic crystals. Adv. Mater 2001;13:409–13.
142. Xia Y, Gates B, Park SH. Fabrication of three-dimensional photonic crystals for use in the spectral region from ultraviolet to near-infrared. IEEE J. Lightwave Technol 1999;17:1956–62.
143. Kondo M, Shinozaki K, Bergstrom L, Mizutani N. Preparation of colloidal monolayers of alkoxylated silica particles at the air-liquid interface. Langmuir 1995;11:394–7.
144. Horvolgyi Z, Mate M, Zrinyi M. On the universal growth of two-dimensional aggregates of hydrophobed glass beads formed at the (aqueous solution of electrolyte)—air interfaces. *Colloids Surf.* A 1994;84:207–16.
145. Wickman HH, Korley JN. Colloid crystal self-organization and dynamics at the air/water interface. Nature 1998;393:445–7.
146. Denkov ND, Velev OD, Kralchevsky PA, Ivanov IB, Yoshimura H, Nagayama K. Mechanism of formation of two-dimensional crystals from latex particles on substrates. Langmuir 1992;8:3183–90.
147. Dushkin CD, Nagayama K, Miwa T, Kralchevsky PA. Colored multilayers from transparent submicrometer spheres. Langmuir 1993;9:3695–701.
148. Rakers F, Chi LF, Fuchs H. Influence of the evaporation rate on the packing order of polydisperse latex monofilms. Langmuir 1997;13:7121–4.
149. Deckman HW, Dunsmuir JH, Garoff S, McHenry JA, Peiffer DG. Macromolecular self-organized assemblies. *J. Vac. Sci. Technol.* B 1988;6:333–6.
150. Jiang P, Bertone JF, Hwang KS, Colvin VL. Single-crystal colloidal multilayers of controlled thickness. Chem. Mater 1999;11:2132–40.
151. Dimitrov AS, Nagayama K. Continuous convective assembling of fine particles into two-dimensional arrays on solid surfaces. Langmuir 1996;12:1303–11.
152. Micheletto R, Fukuda H, Ohtsu M. A simple method for the production of a two-dimensional, ordered array of small latex particles. Langmuir 1995;11:3333–6.
153. Yeh S-R, Seul M, Shraiman BI. Assembly of ordered colloidal aggregrates by electric-field-induced fluid flow. Nature 1997;386:57–9.
154. Trau M, Saville DA, Aksay IA. Assembly of colloidal crystals at electrode interfaces. Langmuir 1997;13:6375–81.
155. Hayward RC, Saville DA, Aksay IA. Electrophoretic assembly of colloidal crystals with optically tunablemicropatterns. Nature 2000;404:56–9. [PubMed: 10716438]
156. Hu W, Li H, Cheng B, Yang J, Li Z, Xu J, Zhang D. Planar optical lattice of TiO_2 particles. Opt. Lett 1995;20:964–6. [PubMed: 19859391]
157. Burns MM, Fournier J-M, Golovchenko JA. Optical matter: crystallization and binding in intense optical fields. Nature 1990;249:749–54.
158. Davis KE, Russel WB, Glantschnig WJ. Settling suspensions of colloidal silica: observations and x-ray measurements. J. Chem. Soc. Faraday Trans 1991;87:411–24.

NIH-PA Author Manuscript NIH-PA Author Manuscript NIH-PA Author Manuscript

159. Velev OD, Lenhoff AM. Colloidal crystals as templates for porous materials. Curr. Opin. Colloid Interface Sci 2000;5:56–63.
160. Dinsmore AD, Yodh AG, Pine DJ. Entropic control of particle motion using passive surface microstructures. Nature 1996;383:239–42.
161. Van Blaaderen A, Ruel R, Wiltzius P. Template-directed colloidal crystallization. Nature 1997;385:321–4.
162. Dosho S, et al. Recent study of polymer latex dispersions. Langmuir 1993;9:394–411.
163. Robbins MO, Kremer K, Grest GS. Phase diagram and dynamics of Yukawa systems. J. Chem. Phys 1988;88:3286.
164. Kim E, Xia Y, Whitesides GM. Two- and three-dimensional crystallization of polymeric microspheres by micromolding in capillaries. Adv. Mater 1996;8:245–7.
165. Park SH, Qin D, Xia Y. Crystallization of mesoscale particles over large areas. Adv. Mater 1998;10:1028–32.
166. Amos RM, Rarity JG, Tapster PR, Sheperd TJ. Fabrication of large-area face-centered-cubic hard-sphere colloidal crystals by shear alignment. Phys. Rev. E 2000;61:2929–35.
167. Vickreva O, Kalinina O, Kumacheva E. Colloid crystal growth under oscillatory shear. Adv. Mater 2000;12:110–2.
168. Park SH, Xia Y. Fabrication of three-dimensional macroporous membranes with assemblies of microspheres as templates. Chem. Mater 1998;10:1745–7.
169. Braun PV, Wiltzius P. Microporous materials: electrochemically grown photonic crystals. Nature 1999;402:603–4.
170. Blanco A, et al. Large-scale synthesis of a silicon photonic crystal with a complete three-dimensional bandgap near 1.5 micrometres. Nature 2000;405:437–40. [PubMed: 10839534]
171. Wijnhoven JEGJ, Vos VL. Preparation of photonic crystals made of air spheres in titania. Science 1998;281:802–5. [PubMed: 9694646]
172. Subramanian G, Manoharan VN, Thirne JD, Pine DJ. Ordered macroporous materials by colloidal assembly: a possible route to photonic bandgap materials. Adv. Mater 1999;11:1261–5.
173. Holland BT, Blanford CF, Stein A. Synthesis of macroporous minerals with highly ordered three-dimensional arrays of spheroidal voids. Science 1998;281:538–40. [PubMed: 9677191]
174. Yan H, Blanford CF, Holland BT, Parent M, Smyrl WH, Stein A. A chemical synthesis of periodic macroporous NiO and metallic Ni. Adv. Mater 1999;11:1003–6.
175. Velev OD, Tessier PM, Lenhoff AM, Kaler EW. A class of porous metallic nanostructures. Nature 1999;401:548.
176. Jiang P, Cizeron J, Bertone JF, Colvin VL. Preparation of macroporous metal films from colloidal crystals. J. Am. Chem. Soc 1999;121:7957–8.
177. Seeman NC. DNA nicks and nodes and nanotechnology. Nano Lett 2001;1:22–6.
178. Chen J, Seeman NC. Synthesis from DNA of a molecule with the connectivity of a cube. Nature 1991;350:631–3. [PubMed: 2017259]
179. Zhang Y, Seeman NC. Construction of a DNA-truncated octahedron. J. Am. Chem. Soc 1994;116:1661–9.
180. Mao C, Sun W, Seeman NC. Assembly of Borromean rings from DNA. Nature 1997;386:137–6. [PubMed: 9062186]
181. Garibotti AV, et al. Functional DNAzymes organized into two-dimensional arrays. Nano Lett 2006;6:1505–7. [PubMed: 16834439]
182. Wang X, Seeman NC. Assembly and characterization of 8-Arm and 12-Arm DNA branched junctions. J. Am. Chem. Soc 2007;129:8169–76. [PubMed: 17564446]
183. Shih WM, Quispe JD, Joyce GF. A 1.7-kilobase single-stranded DNA that folds into a nanoscale octahedron. Nature 2004;427:618–21. [PubMed: 14961116]
184. Rothemund PWK. Folding DNA to create nanoscale shapes and patterns. Nature 2006;440:297–302. [PubMed: 16541064]
185. Yan H, et al. Directed nucleation assembly of DNA tile complexes for barcode-patterned lattices. Proc. Natl Acad. Sci. USA 2003;100:8103–8. [PubMed: 12821776]

NIH-PA Author Manuscript NIH-PA Author Manuscript NIH-PA Author Manuscript

186. Zhang C, et al. Conformational flexibility facilitates self-assembly of complex DNA nanostructures. Proc. Natl Acad. Sci 2008;103:10665–9. [PubMed: 18667705]
187. Goodman RP, et al. Rapid chiral assembly of rigid DNA building blocks for molecular nanofabrication. Science 2005;310:1661–5. [PubMed: 16339440]
188. Braun E, et al. DNA-templated assembly and electrode attachment of a conducting silver wire. Nature 1998;391:775–8. [PubMed: 9486645]
189. Richter J, et al. Nanoscale palladium metallization of DNA. Adv. Mater 2000;12:507–10.
190. Deng Z, Mao C. DNA-templated fabrication of 1D parallel and 2D crossed metallic nanowire arrays. Nano Lett 2003;3:1545–8.
191. Lund, J., et al. DNA networks as templates for bottom-up assembly of metal nanowires; 5th IEEE Conf. on Nanotechnology; Nagoya, Japan. 2005.
192. Kudo H, Fujihira M. DNA-templated copper nanowire fabrication by a two-step process involving electroless metallization. IEEE Trans. Nanotechnol 2006;5:90–2.
193. Ford WE, et al. Platinated DNA as precursors to templated chains of metal nanoparticles. Adv. Mater 2001;13:1793–7.
194. Yan H, et al. DNA-templated self-assembly of protein arrays and highly conductive nanowires. Science 2003;301:1882–4. [PubMed: 14512621]
195. Liu D, et al. DNA nanotubes self-assembled from triple-crossover tiles as templates for conductive nanowires. Proc. Natl Acad. Sci 2004;101:717–22. [PubMed: 14709674]
196. Park SH, et al. Optimized fabrication and electrical analysis of silver nanowires templated on DNA molecules. Appl. Phys. Lett 2006;89:033901.
197. Becerril HA, et al. DNA-templated nickel nanostructures and protein assemblies. Langmuir 2006;22:10140–4. [PubMed: 17107012]
198. Monson CF, Woolley AT. DNA-templated construction of copper nanowires. Nano Lett 2003;3:359–63.
199. Le JD, et al. DNA-templated self-assembly of metallic nanocomponent arrays on a surface. Nano Lett 2004;4:2343–7.
200. Namasivayam V, et al. Electrostretching DNA molecules using polymer-enhanced media within microfabricated devices. Anal. Chem 2002;74:3378–85. [PubMed: 12139043]
201. Keren K, et al. Sequence-specific molecular lithography on single DNA molecules. Science 2002;297:72–5. [PubMed: 12098693]
202. Burley GA, et al. Directed DNA metallization. J. Am. Chem. Soc 2006;128:1398–9. [PubMed: 16448080]
203. Fischler M, et al. Formation of bimetallic Ag—Au nanowires by metallization of artificial DNA duplexes. Small 2007;3:1049–55. [PubMed: 17309092]
204. Keren K, et al. DNA-templated carbon nanotube field-effect transistor. Science 2003;302:1380–2. [PubMed: 14631035]
205. Wang X, et al. Carbon nanotube-DNA nanoarchitectures and electronic functionality. Small 2006;2:1356–65. [PubMed: 17192987]
206. McNally H, et al. Self-assembly of micro- and nano-scale particles using bio-inspired events. Appl. Surf. Sci 2003;214:109–19.
207. Wang C-J, Lin LY, Parviz BA. Modeling and simulation for a nano-photonic quantum dot waveguide fabricated by DNA-directed self-assembly. IEEE J. Sel. Top. Quantum Electron 2005;11:500–9.
208. Wang C-J, Parviz BA, Lin LY. Two-dimensional array self-assembled quantum dot sub-diffraction waveguides with low loss and low crosstalk. Nanotechnology 2008;19:1–10. [PubMed: 19436766]
209. Kusakabe, T., et al. MEMS 2008. Tuscan, AZ: 2008. DNA mediated sequential self-assembly of nano/micro components.
210. Adleman LM. Molecular computation of solutions to combinatorial problems. Science 1994;266:1021–4. [PubMed: 7973651]
211. Winfree E. Algorithmic self-assembly of DNA: theoretical motivations and 2D assembly experiments. J. Biomol. Struct. Dyn 2000;11:263–70.
212. Faulhammer D, et al. Molecular computation: RNA solutions to chess problems. Proc. Natl Acad. Sci 2000;97:1385–9. [PubMed: 10677471]

NIH-PA Author Manuscript NIH-PA Author Manuscript NIH-PA Author Manuscript

213. Rothemund PWK, Papadakis N, Winfree E. Algorithmic self-assembly of DNA sierpinski triangles. PLoS Biol 2004;2:2041–53.
214. Winfree, E.; Bekbolatov, R. Lecture Notes in Computer Science. Vol. 2943. Berlin: Springer: 2004. Proofreading tile sets: error correction for algorithmic self-assembly; p. 126-44.
215. Chen, H-L.; Goel, A. Lecture Notes in Computer Science. Vol. 3384. Berlin: Springer: 2005. Error-free self-assembly using error prone tiles; p. 62-75.
216. Ma X, Huang J, Lombardi F. Error tolerant DNA self-assembly using $(2k - 1) \times (2k - 1)$ snake tile sets. IEEE Trans. Nanobiosci 2008;7:56–64.
217. Reif, JH.; Sahu, S.; Yin, P. Lecture Notes in Computer Science. Vol. 3384. Berlin: Springer: 2005. Compact error-resilient computational DNA tiling assemblies; p. 293-307.
218. Yurke B, et al. A DNA-fuelled molecular machine made of DNA. Nature 2000;406:605–8. [PubMed: 10949296]
219. Yin P, et al. A unidirectional DNA walker that moves autonomously along a track. Angew. Chem. Int. Ed 2004;43:4906–11.
220. Shin J-S, Pierce NA. A synthetic DNA walker for molecular transport. J. Am. Chem. Soc 2004;126:10834–5. [PubMed: 15339155]
221. Ding B, Seeman NC. Operation of a DNA robot Arm inserted into a 2D DNA crystalline substrate. Science 2006;314:1583–5. [PubMed: 17158323]
222. Hosokawa K, Shimoyama I, Miura H. Dynamics of self-assembling systems: analogy with chemical kinetics. Artif. Life 1995;1:15.
223. Adleman, L.; Cheng, Q.; Goel, A.; Huang, M-D.; Wasserman, H. Linear self-assemblies: equilibria, entropy and convergence rates; 6th Int. Conf. on Difference Equations; Augsburg, Germany. 2004.
224. DeHon A, Lincoln P, Savage JE. Stochastic assembly of sublithographic nanoscale interfaces. IEEE Trans. Nanotechnol 2003;2:10.
225. White, PJ.; Kopanski, K.; Lipson, H. Stochastic self-reconfigurable cellular robotics; IEEE Int. Conf. Robotics and Automation; 2004.
226. Klavins E, Ghrist R, Lipsky D. A grammatical approach to self-organizing robotic systems. IEEE Trans. Autom. Control 2006;51:14.
227. Sander LM. Diffusion-limited aggregation: a kinetic critical phenomenon? Contemp. Phys 2000;41:203–18.

NIH-PA Author Manuscript

NIH-PA Author Manuscript

NIH-PA Author Manuscript

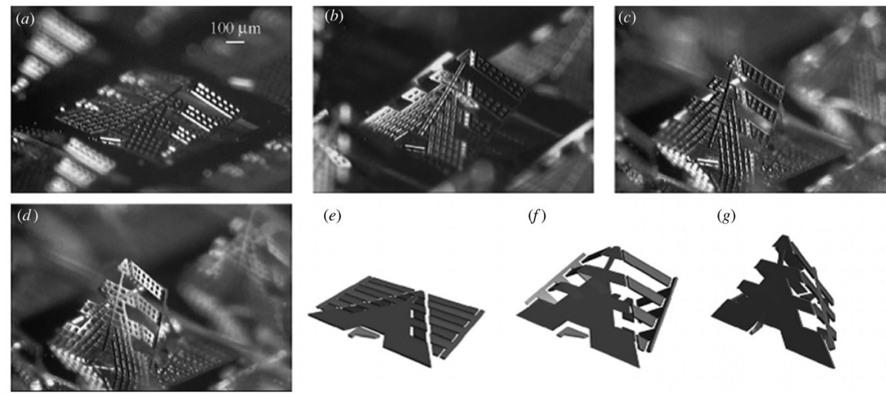

Figure 1.

Steps for magnetically driven assembly of out-of-plane microstructures with inside hinge linkage. (*a*)–(*d*) Microscope photographs of step-by-step assembly under increasing external magnetic field. (*a*) Before magnetic field charge. (*b*) Main part is lifted. (*c*) Main part is erected. (*d*) Lock-in part is lifted. (*e*)–(*g*) Each step in assembly. (Reprinted with permission from [22], © 2005 IEEE.)

NIH-PA Author Manuscript NIH-PA Author Manuscript NIH-PA Author Manuscript

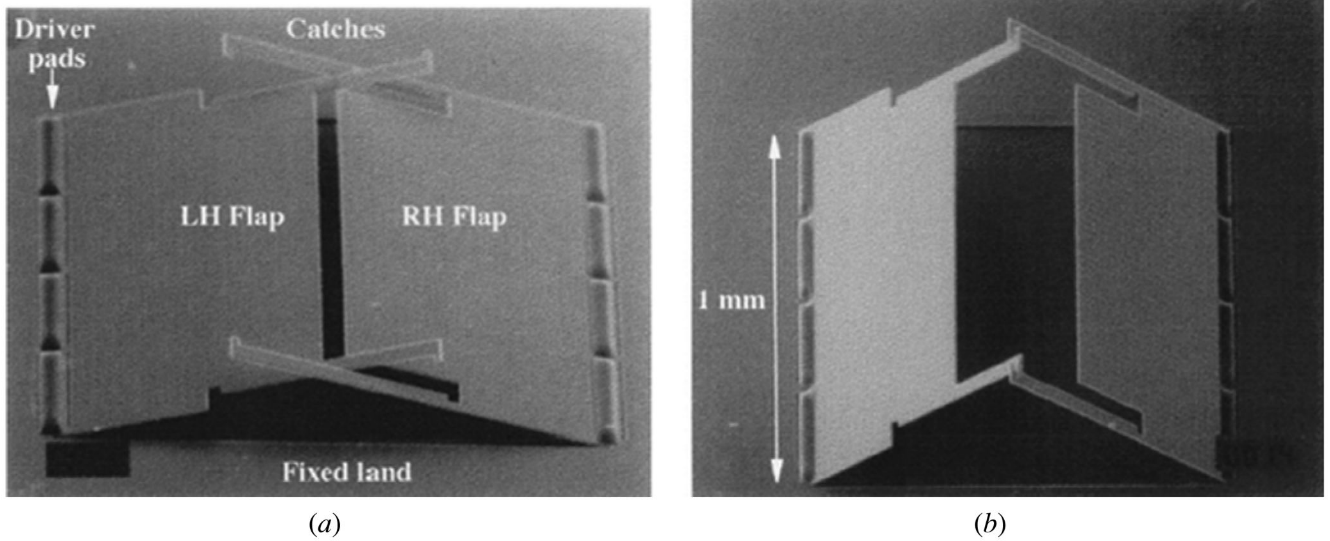

Figure 2.
Self-assembled optomechanical structures based on surface-micromachined, bonded silicon-on-insulator (BSOI) parts and photoresist hinge drivers. (*a*) Symmetric mirror assembly, partly rotated. (*b*) Symmetric mirror assembly, fully rotated. (Reprinted with permission from [26], © 1999 IEEE.)

NIH-PA Author Manuscript

NIH-PA Author Manuscript

NIH-PA Author Manuscript

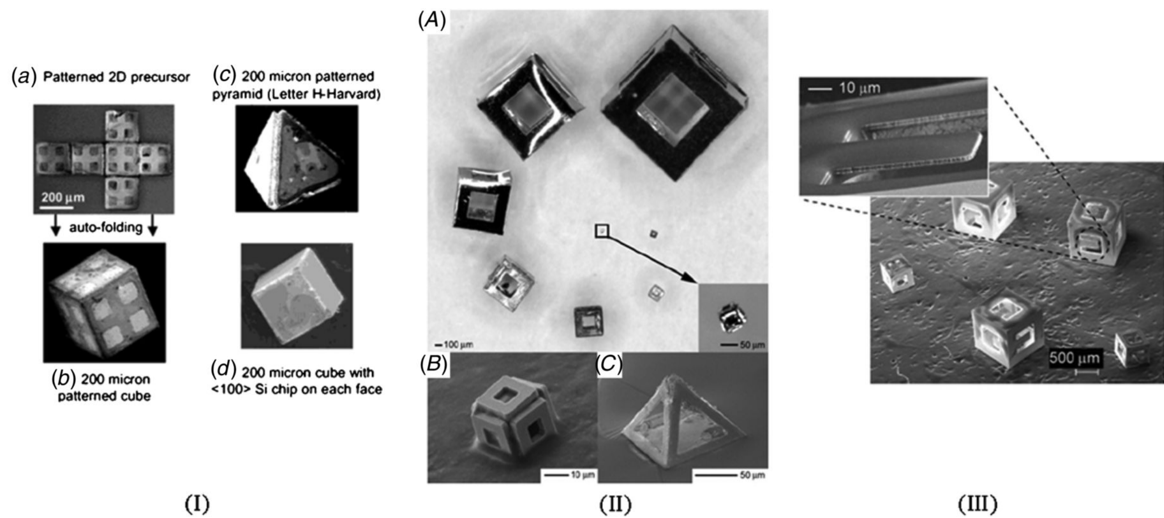

Figure 3.

Capillary self-folding of small building blocks. (I*a*) Optical microscopy image of a 2D cross; the pattern shown is a contrast between Cr and Au. (I*b*) SEM image of a patterned, 200 μm sidelength metallic cube. (I*c*) SEM image of a 200 μm sidelength patterned metallic pyramid. (I*d*) SEM image of a 200 μm sidelength metallic cube containing 340 nm thick ⟨100⟩ silicon chips on each face. (Reprinted from [29], with permission from Wiley.) (II*A*) Optical image showing free-standing polyhedra fabricated with a wide range of sizes all the way from 2 mm to (II*B*) 15 μm and with different shapes (e.g. (II*C*) square pyramid). (Reprinted from [30], with permission from ACS.) (III) Scanning electron microscope image of self-assembled cubic devices with cantilevers along each of the three axes. A single cantilever is also shown in the zoomed inset. (Reprinted with permission from [31], © 2008 American Institute of Physics.)

NIH-PA Author Manuscript

NIH-PA Author Manuscript

NIH-PA Author Manuscript

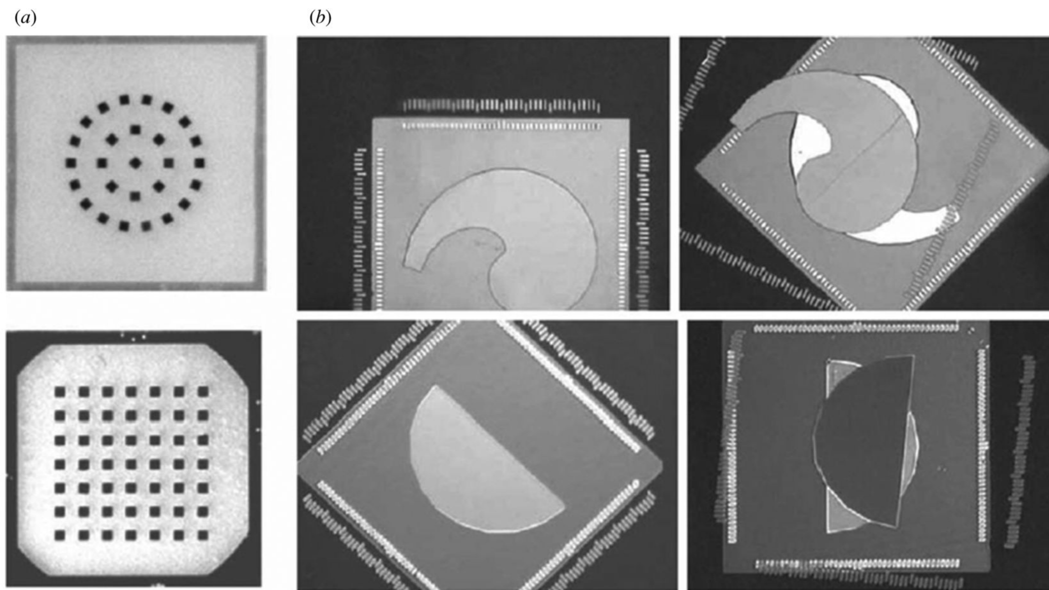

Figure 4.

Optical micrographs of capillary-driven self-assembly of flat microparts, after Srinivasan *et al*: (*a*) square parts on quartz substrates in ring and grid configurations and (*b*) correct and wrong alignments for semicircle- and comma-shaped binding sites. (Reprinted with permission from [6], © 2001 IEEE.)

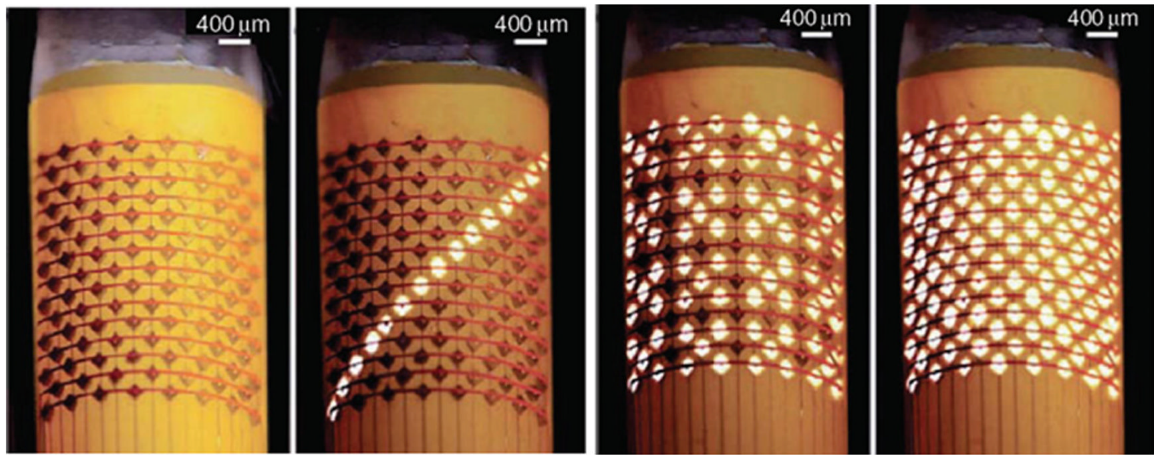

Figure 5.
Optical photographs of tested light-emitting diode (LED) arrays self-assembled on a flexible substrate by capillary forces from low-temperature melting solder. (From [7], reprinted with permission from AAAS.)

NIH-PA Author Manuscript
NIH-PA Author Manuscript
NIH-PA Author Manuscript

NIH-PA Author Manuscript

NIH-PA Author Manuscript

NIH-PA Author Manuscript

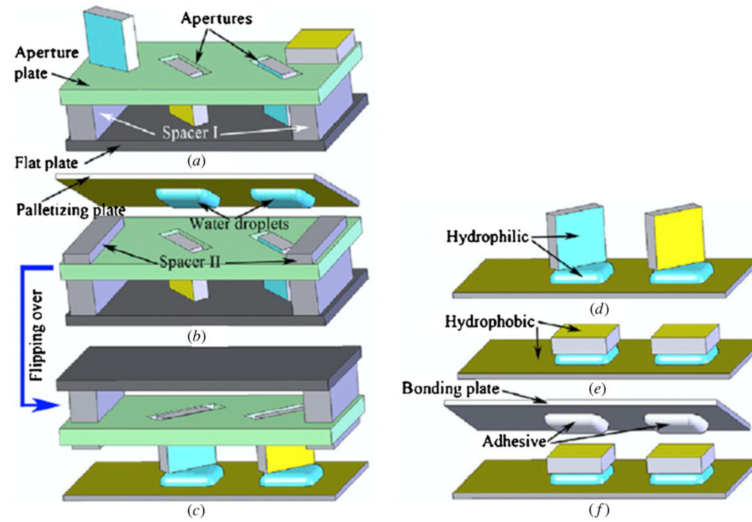

Figure 6.

Schematic overview of the assembly process after Fang *et al*: (*a*) bulk parts fall into apertures vertically; (*b*) a palletizing plate carrying water droplets is aligned with the aperture plate; (*c*) the plates are flipped over to transfer parts onto water droplets; (*d*) parts stand on receptor sites; (*e*) parts rotate to adhere to the palletizing plate with their hydrophilic oxide faces; (*f*) parts are permanently bonded to a bonding plate via wafer level flip-chip bonding. (Reprinted from [37], with permission from IOP.)

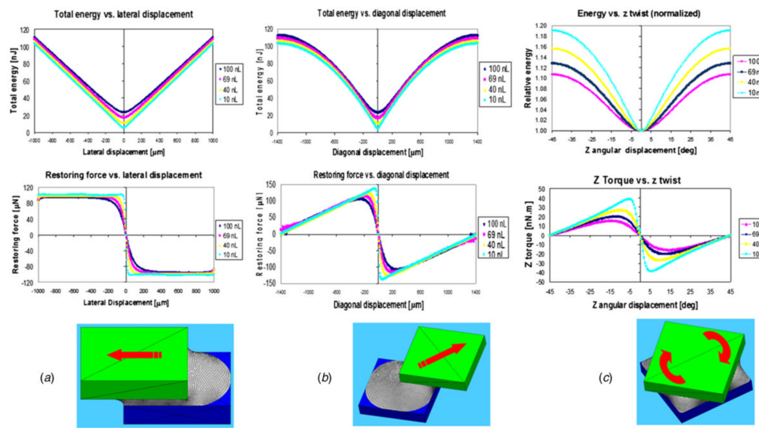

Figure 7.

Results of Surface Evolver simulations of the capillary self-assembly of a square $1 \times 1 mm^2$ part on a binding site of equal size and shape. Energy and force curves versus lateral displacement (*a*), diagonal displacement (*b*) and 90° rotation (*c*) are shown for four values (10, 40, 69 and 100 nL) of the fluid drop volume. The restoring forces are anisotropic, and are inversely proportional to the drop volume.

NIH-PA Author Manuscript

NIH-PA Author Manuscript

NIH-PA Author Manuscript

NIH-PA Author Manuscript

NIH-PA Author Manuscript

NIH-PA Author Manuscript

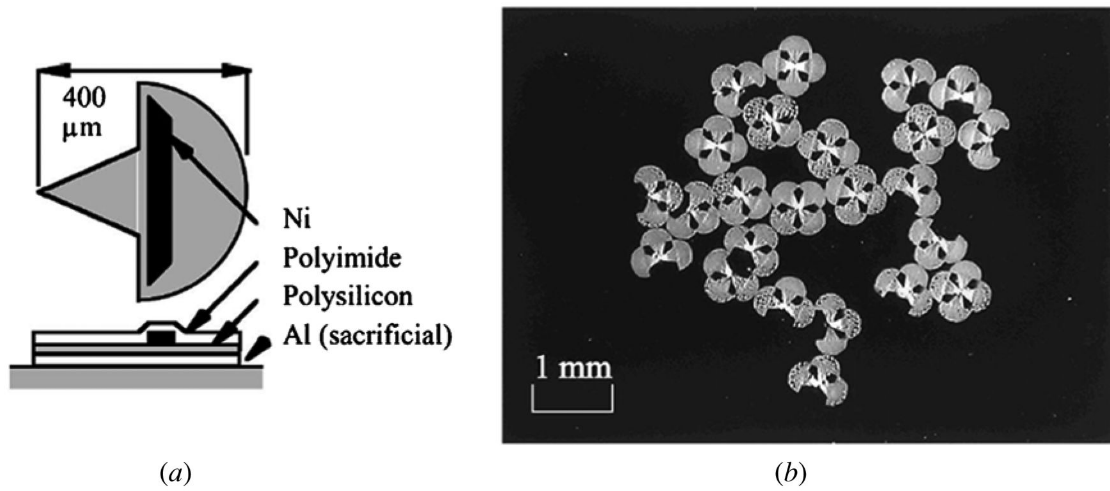

Figure 8.
2D part assembly at the surface of water, after Hosokawa *et al*. (*a*) Part structure. The sharp corner is where the attractive force is maximal, and hence parts preferentially attached to each other at that point. (*b*) Assembled structures on the surface of water. (Reprinted from [51], © 1996 with permission from Elsevier.)

NIH-PA Author Manuscript

NIH-PA Author Manuscript

NIH-PA Author Manuscript

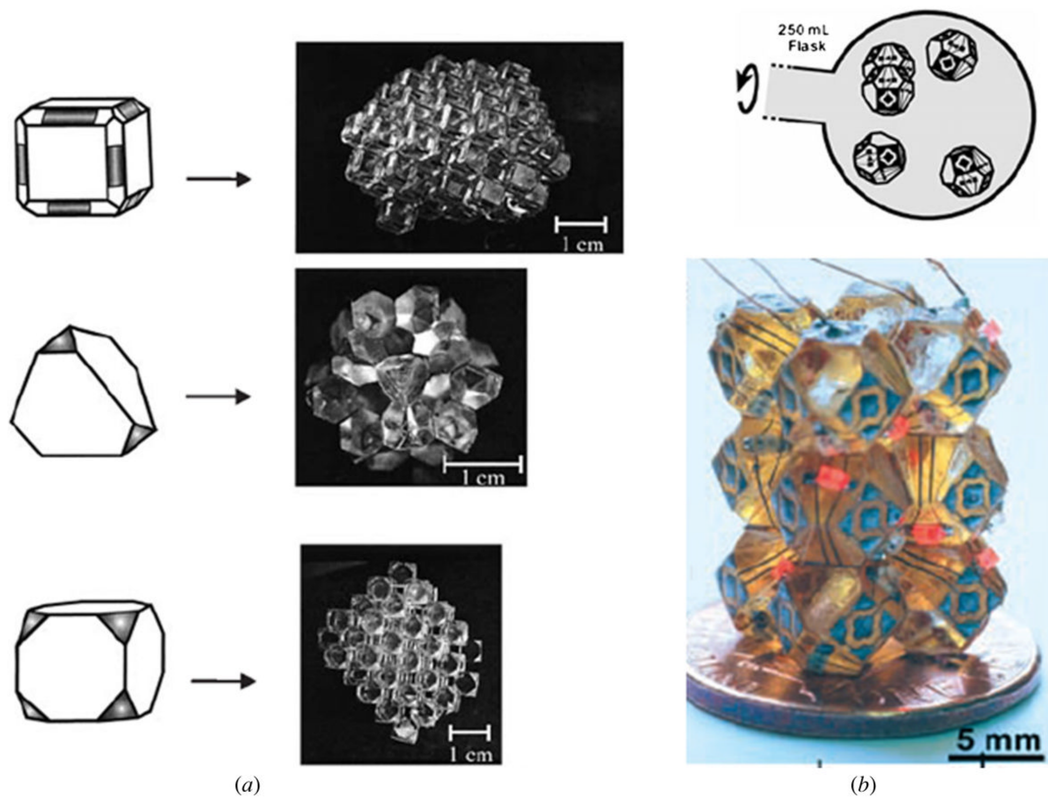

Figure 9.

(*a*) Open lattice structures formed by self-assembly of polyhedra having selected faces coated with liquid alloy by agitation in an aqueous potassium bromide solution. (Reprinted from [57], with permission from AAAS.) (*b*) Self-assembled structure of polyhedra with electronic circuits and LEDs. Two electrically isolated pairs of wires connected to a battery illuminated six LEDs in an electrically continuous loop. (Reprinted from [59], with permission from AAAS.)

NIH-PA Author Manuscript NIH-PA Author Manuscript NIH-PA Author Manuscript

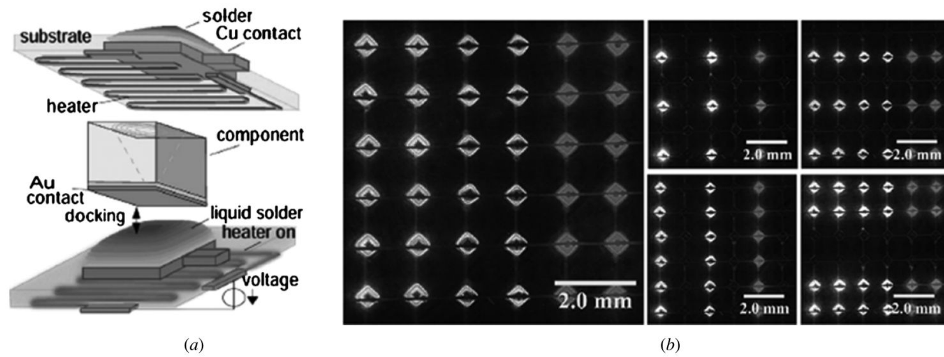

Figure 10.

(*a*) Programmable solder-based self-assembly after Chung *et al*. The solder sites were programmed by applying an external voltage to embedded heaters. (*b*) The operation of the flexible display device fabricated using the process with three different color LEDs. (Reprinted from [9]), © 2006 IEEE.)

NIH-PA Author Manuscript

NIH-PA Author Manuscript

NIH-PA Author Manuscript

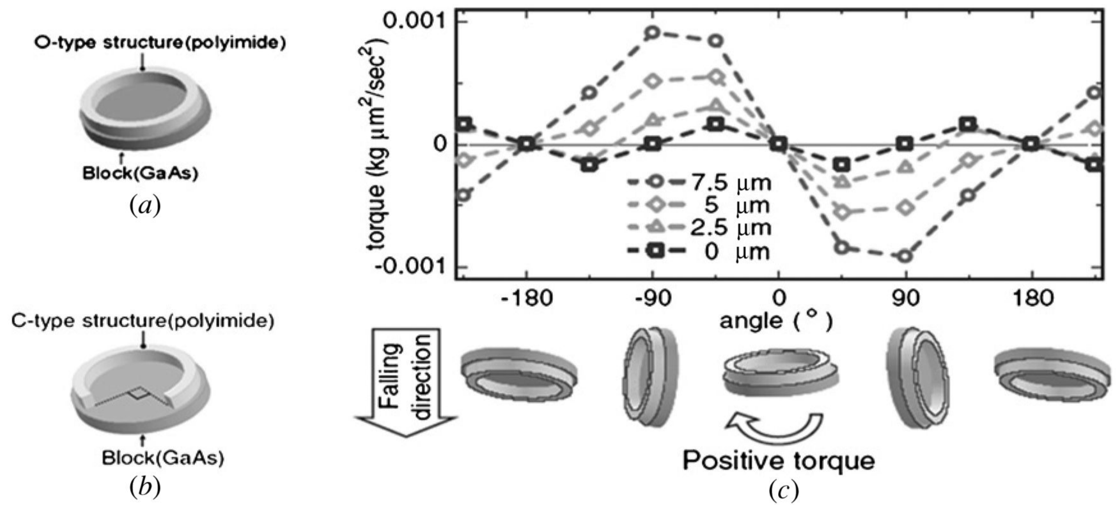

Figure 11.

(*a*) Schematic of blocks with an O-type structure. (*b*) Schematic of blocks with a C-type structure. (*c*) Simulation result of the torque as a function of angle of falling blocks having an O-type structure. The thickness of the structure varied from 0 to 7.5 μm. (Reprinted with permission from [70].)

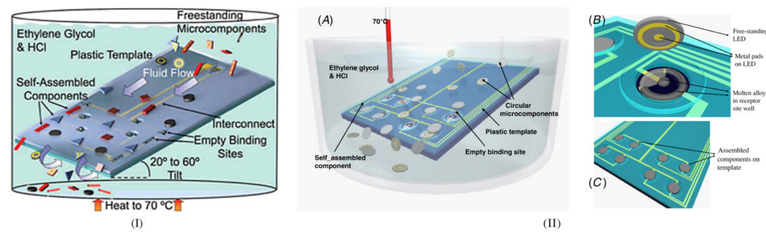

Figure 12.

(I) The heterogeneous self-assembly process with shape matching, after Stauth and Parviz. Microcomponents are introduced over a template submerged in a liquid medium and moved with the fluid flow. Self-assembly occurs as microcomponents first fall into complementarily shaped wells and then become bound by the capillary forces resultant from a molten alloy. (Reprinted from [71], © 2006 National Academy of Sciences, USA.) (II) Another view of the process. (*B*) A microcomponent approaching a binding site with a complementary shape on the template. The molten alloy positioned at the bottom of the binding site on the template wets the metal pads on the microcomponent and forms a mechanical and electrical connection between the microcomponent and the template. (*C*) Assembled circular microcomponents on a template after the fluidic self-assembly is concluded. (Reprinted from [72], with permission from IOP.)

NIH-PA Author Manuscript

NIH-PA Author Manuscript

NIH-PA Author Manuscript

NIH-PA Author Manuscript NIH-PA Author Manuscript NIH-PA Author Manuscript

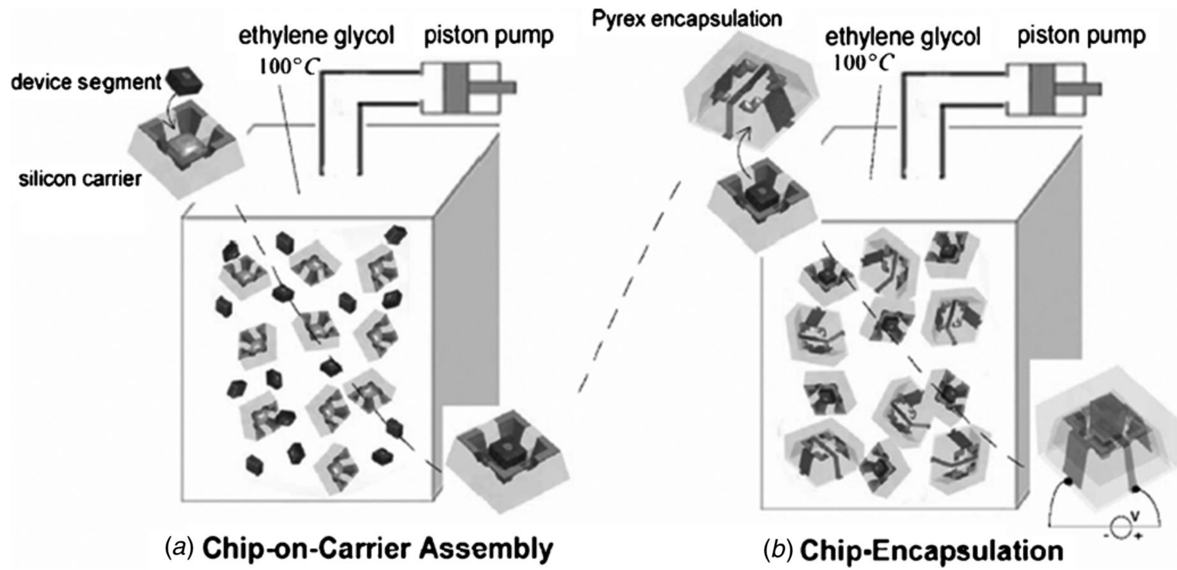

Figure 13.
Fabrication strategy to assemble and package microsystems by shape- and solder-directed self-assembly, after Zheng *et al*. Chip-on-carrier assembly (*a*) and chip encapsulation (*b*) are performed in an ethylene glycol solution at a temperature of 100 °C where the solder is liquid. The illustrated device segment has two contacts: a small circular anode on the front and a large square cathode covering the back. The silicon carrier has a solder-coated area in a tapered opening to host a single semiconductor device segment. The encapsulation unit has five solder-coated copper areas inside a tapered opening to connect to corresponding contact pads on the device and carriers. The agitated components self-assemble in a two-step sequence and form a 3D circuit path between device layers. (*a*) Chip-on-carrier assembly and (*b*) chip–encapsulation. (Reprinted with permission from [76], © 2006 IEEE.)

NIH-PA Author Manuscript

NIH-PA Author Manuscript

NIH-PA Author Manuscript

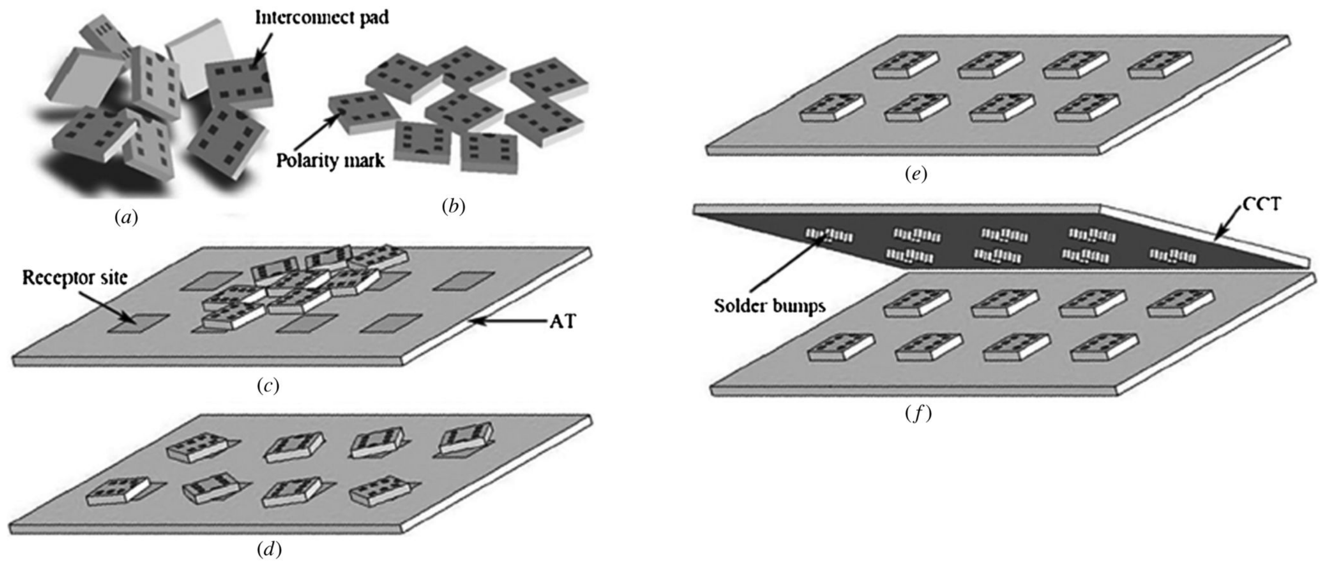

Figure 14.
Wafer-level packaging strategy, after Fang *et al*. (*a*) Randomly oriented bulk parts. (*b*) Bulk parts are uniquely face-oriented and spread in a single layer. (*c*) Parts palletized onto an alignment template (AT). (*d*) Parts are distributed one-to-one to receptor sites. (*e*) Parts are aligned to the receptor sites with unique in-plane orientations. (*f*) Parts are bonded to a chip carrier template (CCT) via wafer-level flip-chip bonding. (Reprinted with permission from [77], © 2006 IEEE.)

NIH-PA Author Manuscript NIH-PA Author Manuscript NIH-PA Author Manuscript

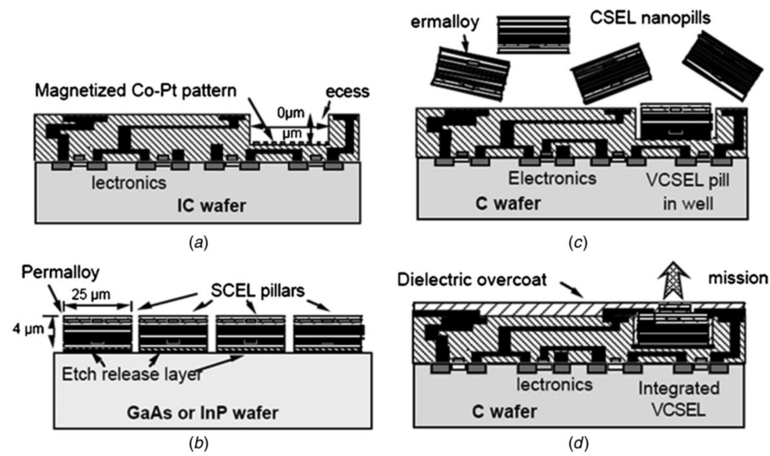

Figure 15.

The MASA process by Fonstad: (*a*) substrate IC wafer with patterned recesses; (*b*) device wafer with fabricated nanopills; (*c*) statistical assembly of the nanopills, coated with magnetic films; (*d*) further processing of substrate to complete the nanopills integration. (Reprinted with permission from [85].)

NIH-PA Author Manuscript

NIH-PA Author Manuscript

NIH-PA Author Manuscript

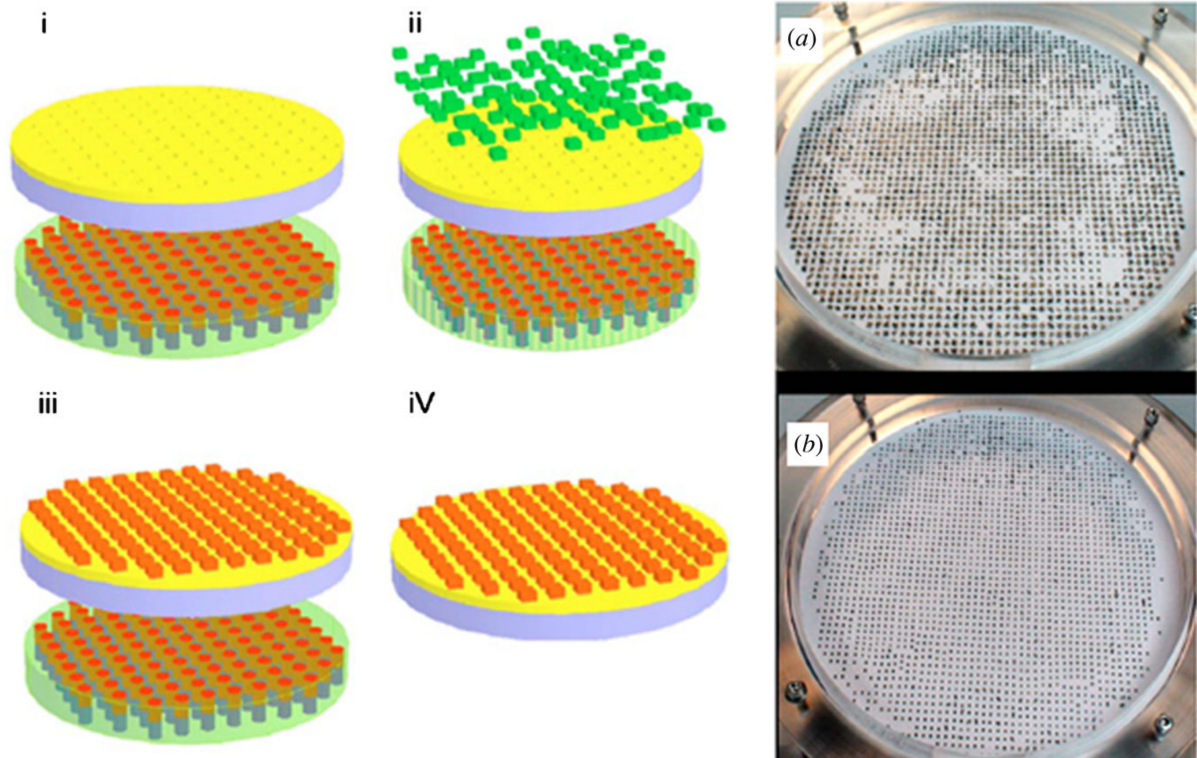

Figure 16.
Dry magnetic assembly over large substrates. (I)–(IV) The patterned substrate was superposed to the magnetic master array, which could be removed after assembly of the chips. (*a*) Assembly of 1 mm^2 chips over 8″ wafer after 2 min, and (*b*) after 5 min. (Reprinted with permission from [89], © 2007 American Institute of Physics.)

NIH-PA Author Manuscript
NIH-PA Author Manuscript
NIH-PA Author Manuscript

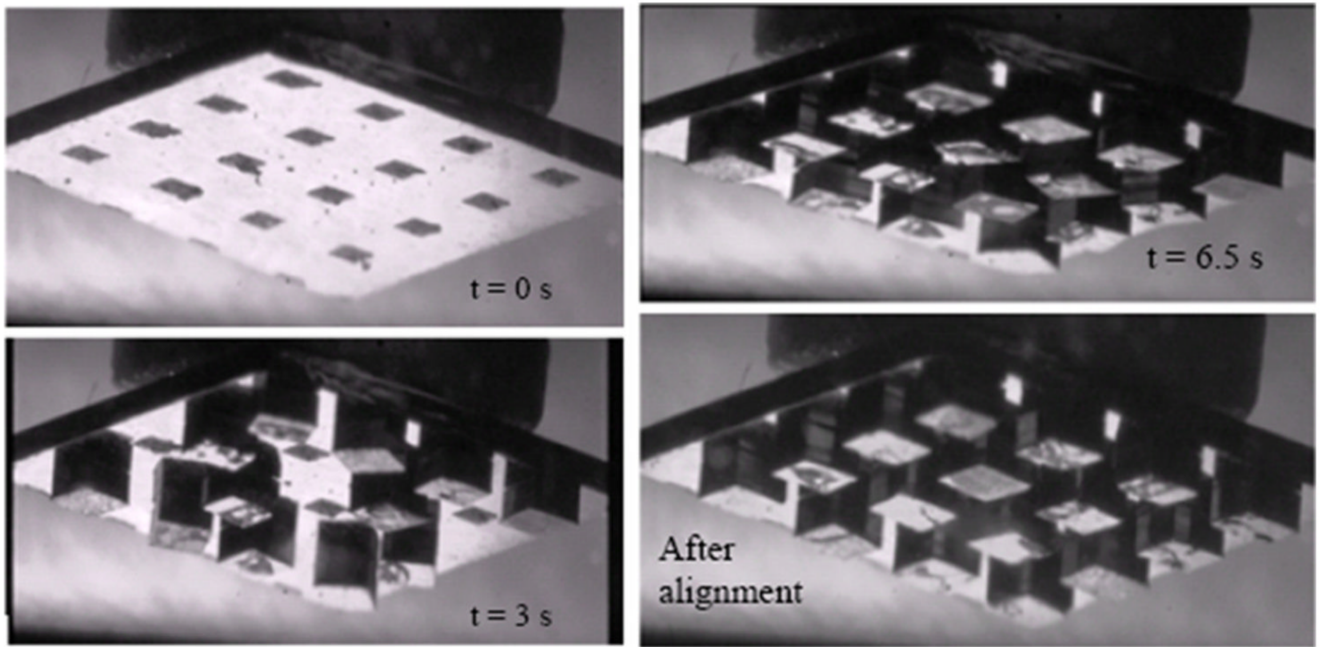

Figure 17.
Dry magnetic part-to-template assembly. Snapshot views of the substrate during self-assembly, and final chips alignment after substrate vibration. (Reprinted with permission from [90], © 2008 IEEE.)

NIH-PA Author Manuscript

NIH-PA Author Manuscript

NIH-PA Author Manuscript

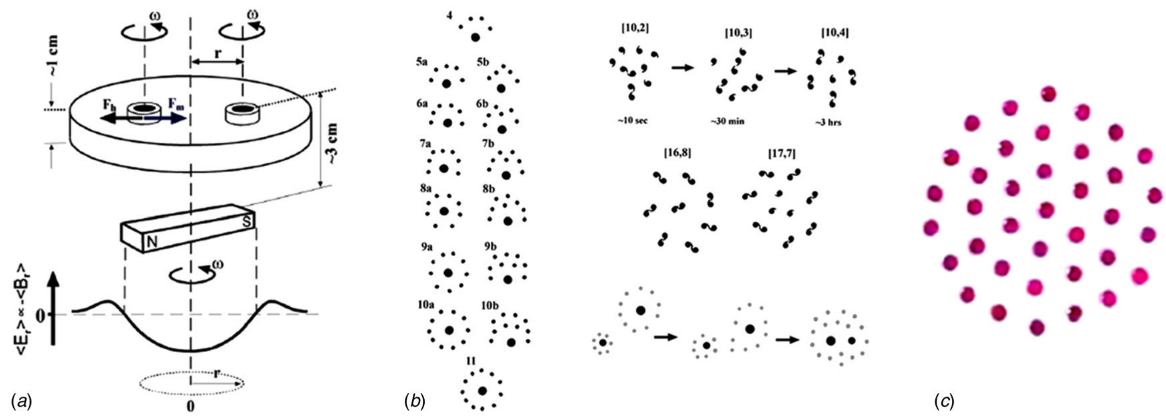

Figure 18.

Dynamic self-assembly of magnetic disks. (*a*) The force F_m attracts the disks toward the rotation axis of the magnet, while the vortices created by the motion of the disks create a pairwise repulsive force F_b between them. (*b*) and (*c*) Photos of various dissipative structures. (Reprinted from [99], with permission from Elsevier.)

NIH-PA Author Manuscript

NIH-PA Author Manuscript

NIH-PA Author Manuscript

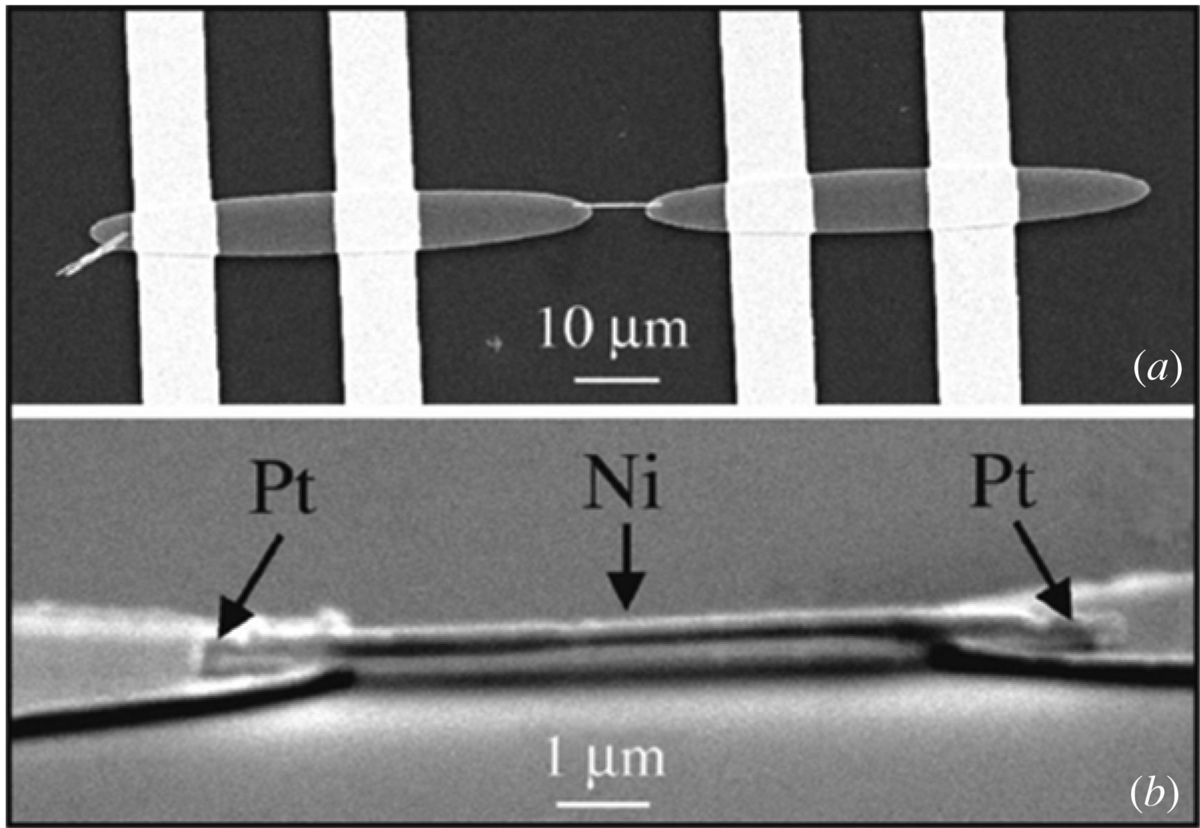

Figure 19.
SEM image of a Pt–Ni–Pt nanowire aligned and trapped between Ni magnetic electrodes. (Reprinted from [102], with permission from American Institute of Physics.)

NIH-PA Author Manuscript

NIH-PA Author Manuscript

NIH-PA Author Manuscript

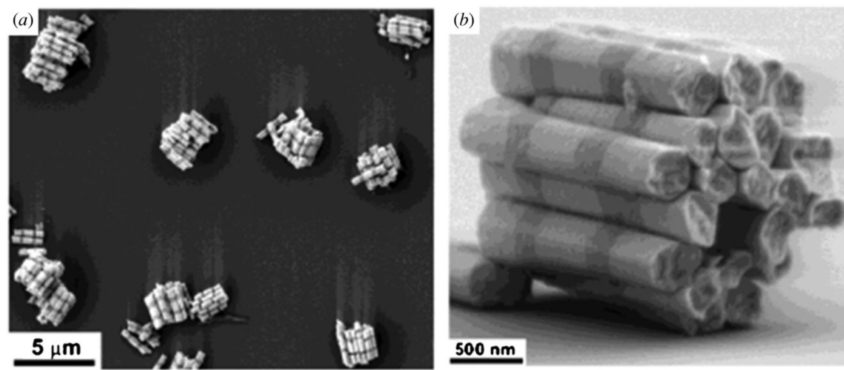

Figure 20.

(*a*) SEM picture of bundles of nanorods self-assembled by lateral magnetic interactions. (*b*) SEM picture of a single bundle, evidencing the alignment of the ferromagnetic sections. (Reprinted from [104], with permission from ACS.)

NIH-PA Author Manuscript
NIH-PA Author Manuscript
NIH-PA Author Manuscript

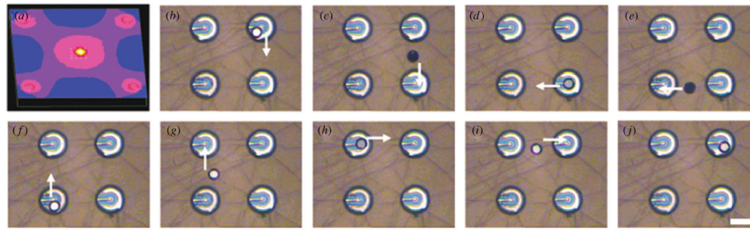

Figure 21.
(*a*) Simulation of electric field distribution across patterned electrodes, after O'Riordan *et al*. (*b*)–(*j*) Programmed placement and transport of a 50 μm diameter, 670 nm wavelength LED around the receptor electrodes in acetonitrile. (Reprinted from [109], with permission from ACS.)

NIH-PA Author Manuscript
NIH-PA Author Manuscript
NIH-PA Author Manuscript

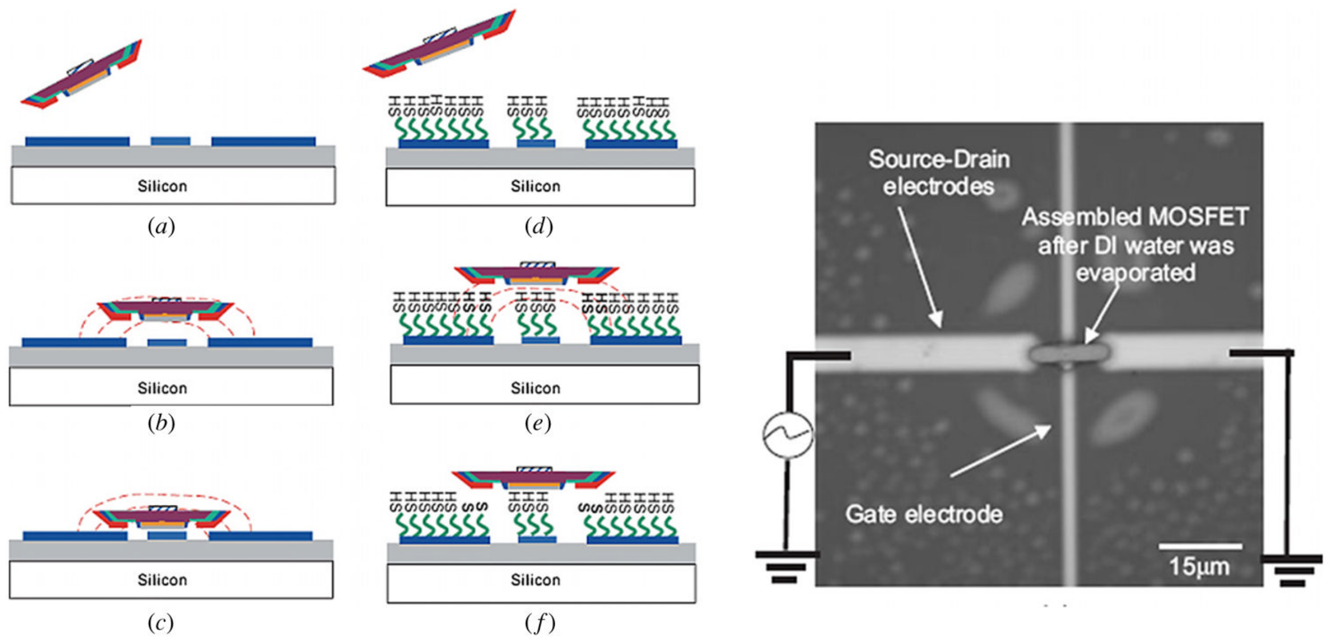

Figure 22.
(*a*)–(*c*) DEP-mediated fluidic assembly, and (*d*)–(*f*) DEP- and chemically-mediated fluidic assembly of 15 μm long, three terminal MOSFETs. Actual assembly is shown in the inset. (Reprinted from [116], with permission from Wiley.)

NIH-PA Author Manuscript
NIH-PA Author Manuscript
NIH-PA Author Manuscript

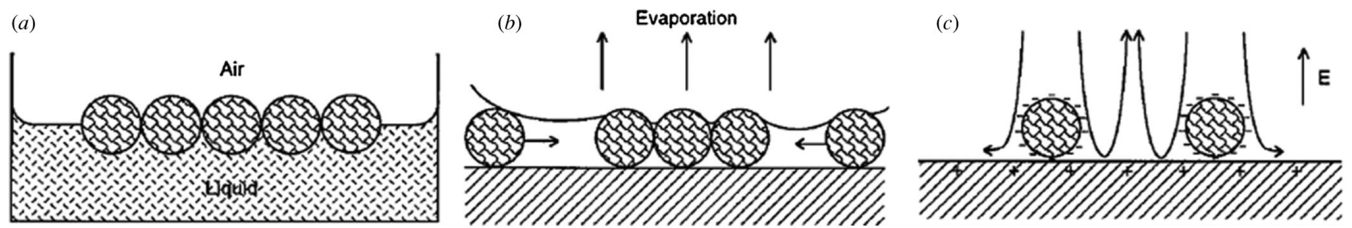

Figure 23.
Schematic representation of three methods for the production of ordered 2D colloidal arrays: (*a*) Langmuir method, (*b*) solvent evaporation (convective assembly) and (*c*) (di) electrophoretic deposition. (Reprinted from [129], with permission from Wiley.)

NIH-PA Author Manuscript

NIH-PA Author Manuscript

NIH-PA Author Manuscript

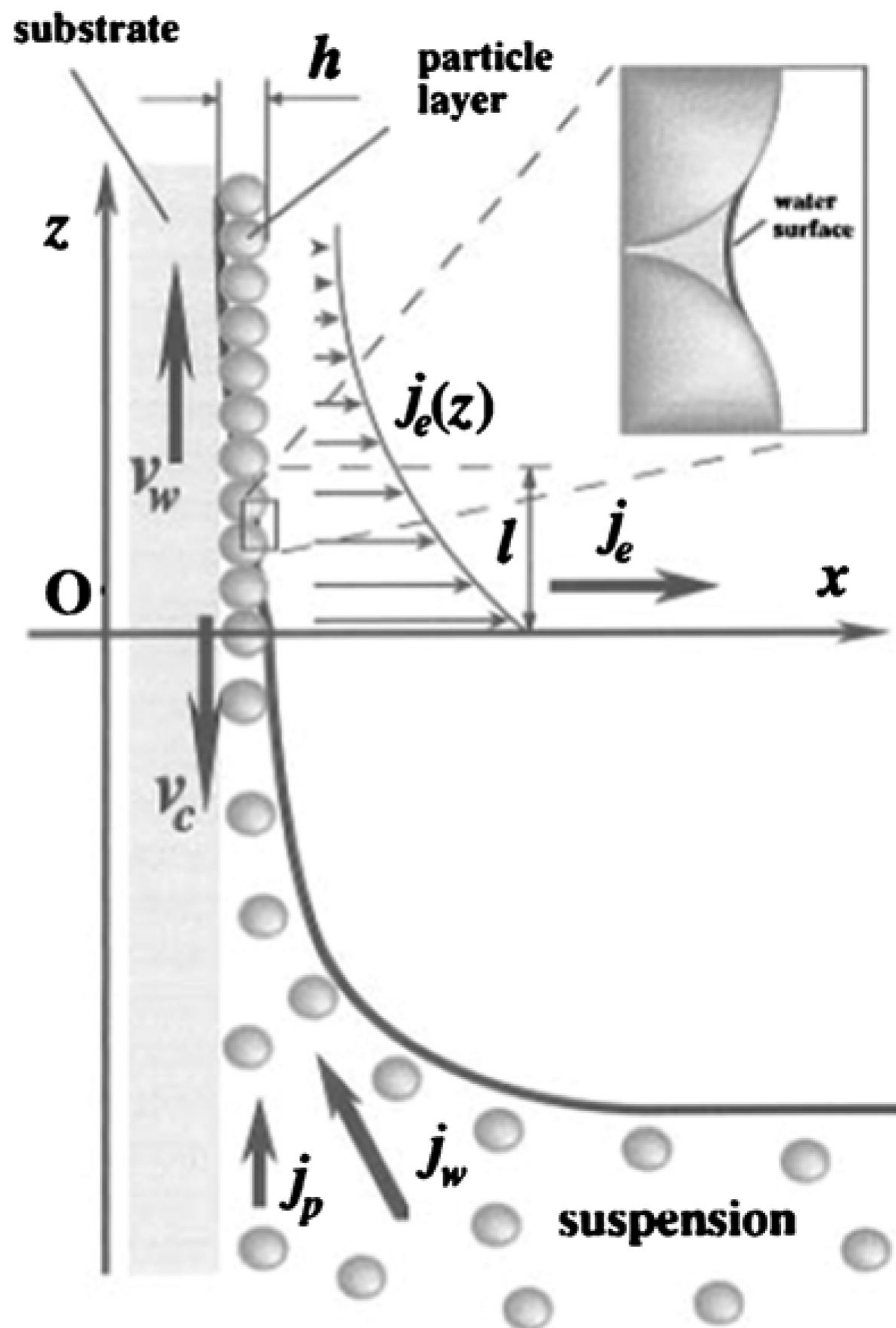

Figure 24.

Schematic dynamics of the controlled plate withdrawal method for assembly of colloidal particles. (Reprinted from [151], with permission from ACS.)

NIH-PA Author Manuscript
NIH-PA Author Manuscript
NIH-PA Author Manuscript

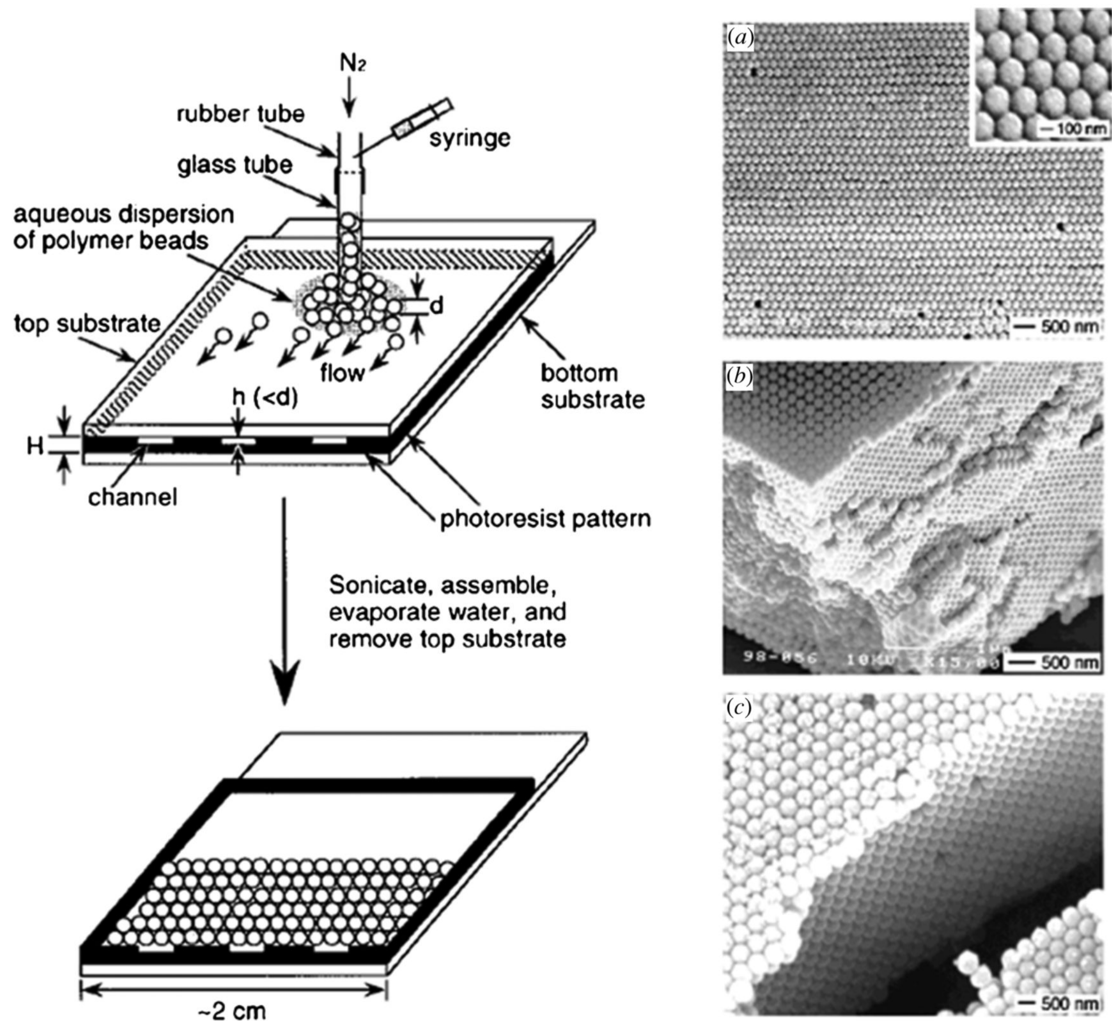

Figure 25.
(*d*) Experimental set-up for the 3D organization of colloidal spheres by the confinement method. (Reprinted from [165], with permission from Wiley.) (*a*)–(*c*) SEM images of 3D crystalline arrays of spheres assembled in a 12 μm thick cell. (Reprinted from [129], with permission from Wiley.)

NIH-PA Author Manuscript
NIH-PA Author Manuscript
NIH-PA Author Manuscript

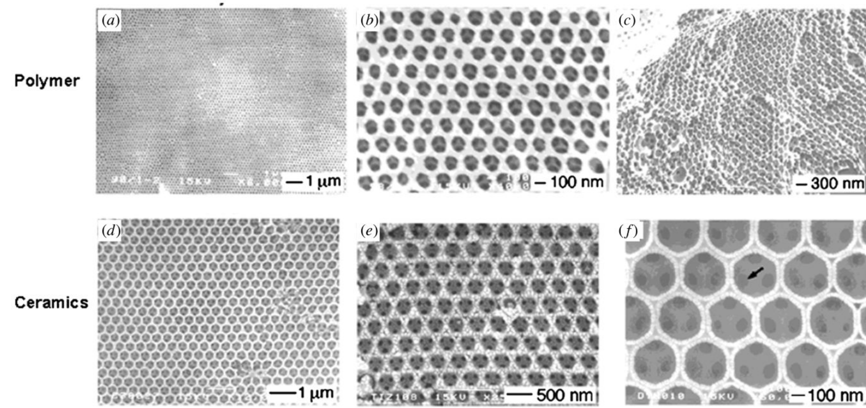

Figure 26.
SEM pictures of 3D porous structures (inverse opals) fabricated using 3D opaline structures. (Reprinted from [129], with permission from Wiley.)

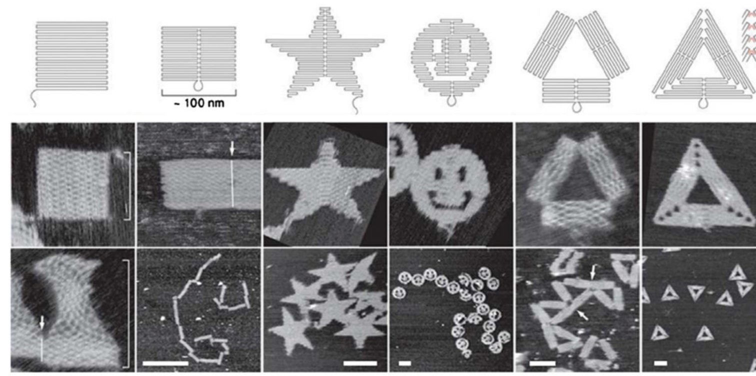

Figure 27.

Geometrical shapes constructed using DNA origami. Top row: folding paths. Last two rows: AFM images of structures. (Reprinted from [184], with permission from the Nature Publishing Group.)

NIH-PA Author Manuscript NIH-PA Author Manuscript NIH-PA Author Manuscript

NIH-PA Author Manuscript
NIH-PA Author Manuscript
NIH-PA Author Manuscript

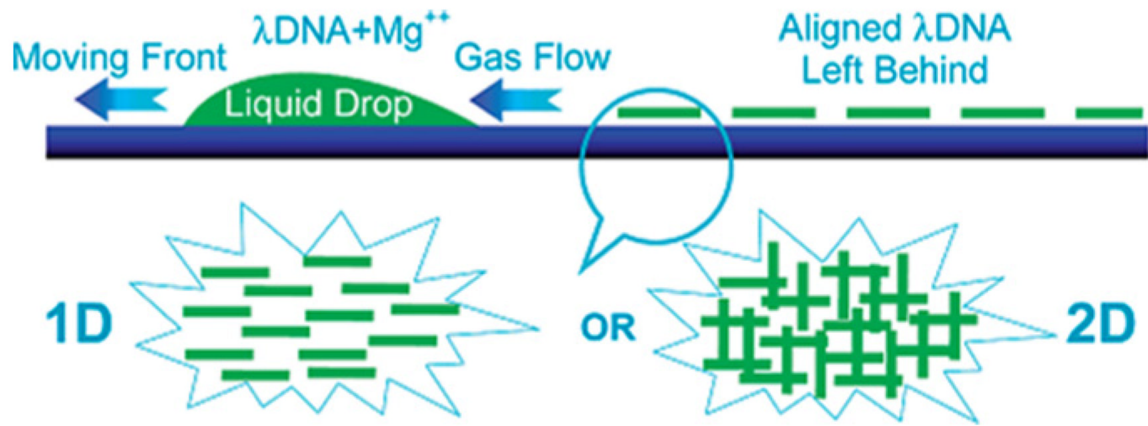

Figure 28.
Schematic representation of unidirectional DNA stretching using a droplet. (Reprinted from [190], with permission from ACS.)

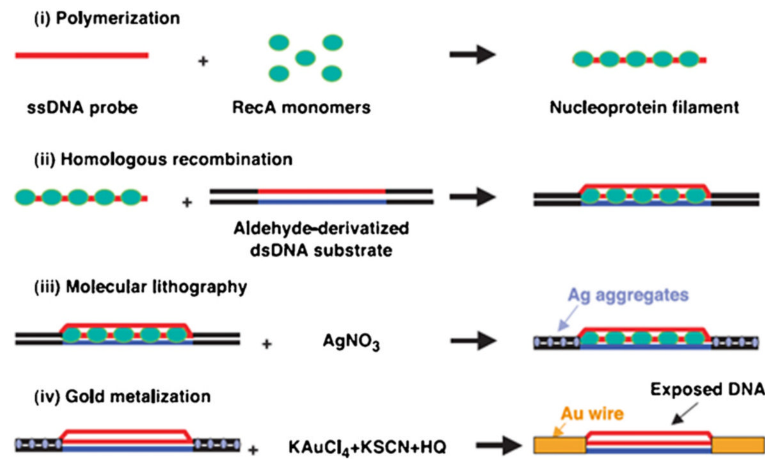

Figure 29.

Steps of molecular lithography. (i) RecA monomers polymerize on a ssDNA forming nucleoprotein filament. (ii) Nucleoprotein filament binds to a dsDNA substrate. (iii) Then it is incubated in a $AgNO_3$ solution and Ag aggregates on unmasked regions. (iv) Ag aggregates promote Au deposition to build conducting wires. (Reprinted from [201], with permission from AAAS.)

NIH-PA Author Manuscript
NIH-PA Author Manuscript
NIH-PA Author Manuscript

NIH-PA Author Manuscript

NIH-PA Author Manuscript

NIH-PA Author Manuscript

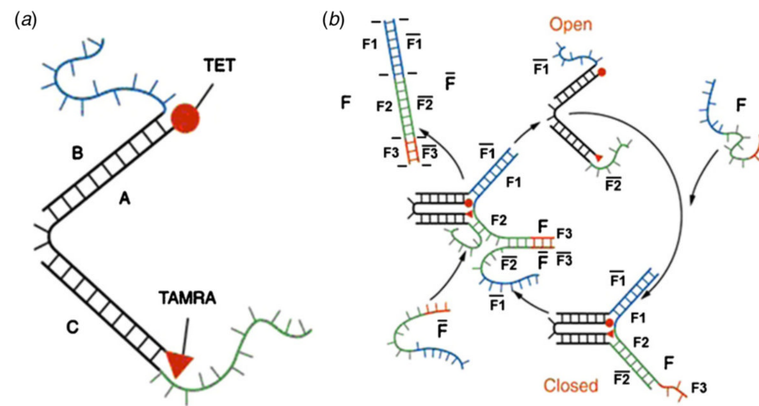

Figure 30.

Operation of molecular tweezers. (*a*) Tweezer structure with labeling groups TET, fluorescent dye with emission peak at 536 nm, and TAMRA, longer-wavelength dye that quenches emission from TET when in proximity. The dyes are used to monitor tweezer motion; when the tweezers are open TET is emitting light at 536 nm and this emission is quenched by TAMRA when the tweezers are closed. (*b*) Opening and closing the tweezers. Strand F hybridizes with free nucleotides on the tweezers, causing them to close. Complementary F strand hybridizes with matching sticky ends (F3) of the F, forming a double helix and removing the F strand from the tweezer, causing it to open. (Reprinted from [218], with permission from the Nature Publishing Group.)

NIH-PA Author Manuscript NIH-PA Author Manuscript NIH-PA Author Manuscript

Table 1

Principal techniques used for milli- to nanoscale self-assembly.

Method	Advantages	Disadvantages	Applications	Remarks
Shape matching	• Efficient use of parts (recycling) • Multibatch	• 3D part shaping required • Physical conditioning of target substrates • Downscaling of gravitational forces unfavorable • Need of further processing for electrical interconnections	Integration of opto-electronic devices (e.g. RFIDs, III/V LEDs [5], VCSELs [67], HEMTs [68]) onto Si substrates	• Claimed overall yield for FSA: ~100% • Claimed overall yield for part-to-part 3D SA: 97% [76] • High parts redundancy required to achieve high throughput
Capillary (fluid driven)	• Self-alignment • High registration accuracy • Programmable and multibatch	• Chemical conditioning of target substrates • Potential disruption of binding sites during assembly affects yield • Contact-based forces	Integration of MEMS (e.g. micromirrors [34], micromachined inductors [35]) and LEDs [8] over pre-processed substrates; computation [55]	• Claimed alignment accuracy (only mechanical bonding): 0.2 μm lateral, 0.3° rotational [6] • High part redundancy required to achieve high throughput
Capillary (molten-solder driven)	• Electrical and mechanical connections at once • Self-alignment • Programmable and multibatch • Efficient use of parts (recycling)	• Consumption of solder material reduces mechanical and electrical yield • Not applicable to temperature-sensitive devices • Contact-based forces	Integration of single-crystal Si FETs [71] and III/V LEDs [72] onto glass and plastic, flexible substrates, 3D electrical networks [59]; folding of planar structures into 3D structures for MEMS [28]	• For conformal part-to-substrate assembly: - Claimed mechanical assembly yield: 97% [71] - Claimed electrical yield: 62% [72] • High part redundancy required to achieve high throughput
Magnetic	• Long-ranged, non-contact forces • Efficient use of parts (recycling)	• Material compatibility with standard IC processing • Need of further processing for electro/	Integration of III/V heterostructures on Si substrates [85]; folding of planar structures into 3D structures for MEMS [22]	• Claimed mechanical assembly yield is up to 98.7% [90] • High part redundancy

NIH-PA Author Manuscript NIH-PA Author Manuscript NIH-PA Author Manuscript

Method	Advantages	Disadvantages	Applications	Remarks
	• Both attractive and repulsive forces	mechanical connections • Small forces in micro- and nanoscale		required to achieve high throughput
Electrophoretic	• Long-ranged, non-contact forces • Charge selective • Favorable force downscaling	• Only charged parts • Need of post-processing for electro/ mechanical connections • Low control over position and quantity of assembled parts	Integration of small devices (e.g. LEDs [108]) onto pre-processed substrates	Low throughput
Dielectrophoretic	• Long-ranged, non-contact forces • Both charged and uncharged parts • Favorable force downscaling	• Non-selective • Need of post-processing for electro/ mechanical connections • Low control over position and quantity of assembled parts	Integration of nanotubes [126] and nanowires [103] onto pre-processed substrates	For nanoparticles assembly, no easy online supervision (e.g. optical) of the process leads to long time to assembly and low throughput